이학박사 학위논문

Determinants of successful gamma entrainment using flickering light stimulation in human

사람에서 점멸광자극을 이용한 성공적인 감마뇌파동조 유도의 결정 요인

2023년 02월

서울대학교 대학원

뇌인지과학과

박 예 승

Determinants of successful gamma entrainment using flickering light stimulation in human

사람에서 점멸광자극을 이용한 성공적인 감마뇌파동조 유도의 결정 요인

지도 교수 김 기 웅

이 논문을 이학박사학위논문으로 제출함

2023년 1월

서울대학교 대학원
뇌인지과학과
박 예 승

박예승의 이학박사 학위논문을 인준함

2023년 1월

위 원 장 권준수 (인)

부위원장 김기웅 (인)

위 원 윤인영 (인)

위 원 김의태 (인)

위 원 박준혁 (인)

Abstract

Determinants of successful gamma entrainment using flickering light stimulation in human

Yeseung Park

Department of Brain and Cognitive Sciences

The Graduate School

Seoul National University

Background and Objectives: Although gamma entrainment using flickering light stimulus (FLS) of 40Hz was effective in reducing pathologies and enhancing cognitive function in mouse models of Alzheimer's disease (AD), its efficacy was controversial in AD patients. The conflicting results in AD patients may be attributable to a couple of key factors. First, the optimal parameters of FLS for gamma entrainment may be different between diurnal humans and nocturnal mice. Second, the response to optimal FLS may be different between AD patients due to inter-individual difference in the microstructural integrity of white matter (WM) tracts. This study aimed to find the optimal parameters (color, luminal intensity and flickering frequency) of FLS for entraining gamma rhythms in diurnal humans and to examine the effect of fractional anisotropy (FA) of WM tracts on the entrainment and propagation of gamma rhythms.

Methods: We first investigated the optimal color (white, red, green, and blue), luminal intensity (10 cd/m^2, 100 cd/m^2, 400 cd/m^2, and 700 cd/m^2), and frequency (32 - 50 Hz) of FLS for entraining gamma rhythms in visual cortex using event-related desynchronization/event-

related synchronization (ERD/ERS) and for propagating gamma rhythm entrained in visual cortex to other brain regions using spectral Granger Causality (sGC) in 16 cognitively normal young adults (24.0 ± 3.7 yrs) and 35 cognitively normal older adults (70.0 ± 2.4 yrs). We also examined the adverse effects of FLS in both younger and older adults. Then we examined the effect of the FA of posterior thalamic radiations on the ERS of gamma rhythms entrained in visual cortex and that of and middle and superior longitudinal fasciculi on the sGC of the connectivity from visual cortex to temporal and frontal regions in 26 cognitively normal older adults using analysis of variance and linear regression analyses.

Results: The FLSs using the lights of longer wavelengths such as white ($p < 0.05$) and red ($p < 0.01$) entrained and propagated gamma rhythms better than those of shorter wavelengths such as green and blue. The FLSs using stronger lights such as 700 cd/m^2 ($p < 0.001$) and 400 cd/m^2 ($p < 0.01$) entrained and propagated gamma rhythms better than weaker lights of 100 cd/m^2 and 10 cd/m^2. The FLSs flickering at 34-38 Hz were best for entraining and propagating gamma rhythm in younger adults (entrainment at Pz: $p < 0.05$, propagation: $p < 0.05$) while those flickering at 32-34 Hz were best for older adults (entrainment at Pz: $p < 0.05$, propagation: $p < 0.001$). In older adults, white FLSs of 700 cd/m^2 flickering at 32–34 Hz entrained the gamma rhythms most strongly at visual cortex ($p < 0.05$) and propagated them most widely to other brain regions ($p < 0.05$).

The FLSs of 700 cd/m^2 flickering at 32 Hz entrained gamma rhythms worse in the visual cortex of the older adults whose FA of left posterior thalamic radiation was low than in those whose FA of left posterior thalamic radiation was not low ($p < 0.05$). In addition, the sGC of gamma rhythms from visual cortex to temporal and frontal regions was significantly associated with the FA of middle and superior longitudinal fasciculi ($p < 0.05$). Younger adults

showed more adverse effects to the FLSs of longer wavelengths (white and red) and stronger luminal intensity (700 cd/m^2) compared to those with shorter wavelengths and weaker lumina intensities respectively ($p < 0.05$ for wavelength and $p < 0.01$ for luminal intensity). However, older adults showed comparable adverse effects between 700 cd/m^2 and 400 cd/m^2 and between white and red FLSs ($p > 0.05$), and their severity of adverse effects was milder than that in younger adults.

Conclusion: In diurnal human, optimal flickering frequency for gamma entrainment was about 20% lower than that in nocturnal mice. Although the FLSs of stronger luminal intensity and the longer wavelength may entrain gamma rhythms better, they may result in more and severe adverse effects. In older adults, white or red FLSs of 700 cd/m^2 flickering at 32-34 Hz may be optimal for entraining and propagating gamma rhythms. Since gamma rhythms were not properly entrained by optimal FLS in the older adults whose microstructural integrity of the white matter tracts was impaired, the integrity of the white matter tracts involved in the entrainment and propagation of gamma rhythm should be measured and considered in determining the indication of gamma entrainment using visual stimulation.

Keywords: gamma rhythm, entrainment, propagation, flickering light stimulation, white matter microstructural integrity, human, older adults

Student number: 2017-26326

Part of this works were previously published on:

- Lee, K., Park, Y et al. “Optimal flickering light stimulation for entraining gamma waves in the human brain.” *Scientific Reports* (2021) 11, 16206.

- Park, Y et al. “Optimal flickering light stimulation for entraining gamma rhythms in older adults.” *Scientific Reports* (2022) 12, 15550.

69

Contents

70

71

List of Tables

72

73

List of Figures

74

List of Abbreviations

AD	Alzheimer's disease
Aβ	Amyloid beta
ASSR	Auditory Steady State Response
BR	Break
CSF	cerebrospinal fluid
CT	Click train
DTI	Diffusion tensor image
DMN	Default mode network
EEG	Electroencephalography
EMG	Electromyogram
EPSPs	Excitatory post synaptic potentials
ERD	Event-related desynchronization
ERS	Event-related synchronization
ERSP	Event-related spectral perturbation
EXP-1	Experiment1
EXP-2	Experiment2
FA	Fractional anisotropy
FLS	Flickering light stimulation
fMRI	functional magnetic resonance image
GABA	Gamma-aminobutyric acid
GABAR	Gamma-aminobutyric acid receptor
GAD	Glutamate decarboxylase
GAT	Gamma-aminobutyric acid transporters
GDS	Geriatric Depression Scale

HC	Healthy control
HFA	Second-to-highest quartile group of the fractional anisotropy values
LFA	The lowest quartile group of the fractional anisotropy values
LGN	Lateral geniculate nucleus
M	Mid aged adults
MCI	Mild cognitive impairment
MLF	Middle longitudinal fasciculus
MMSE	Mini Mental Status Exam
MRI	Magnetic resonance image
O	Older adults
O-LC	Occipito-left central
OLED	Organic light-emitting diode
O-LF1	Occipito-left frontal1
O-LF2	Occipito-left frontal2
O-LT	Occipito-left temporal
O-RC	Occipito-right central
O-RF1	Occipito-right frontal1
O-RF2	Occipito-right frontal2
O-RT	Occipito-right temporal;
PiB SUVR	Pittsburgh compound B standard uptake value ratio
PTR	Posterior thalamic radiation
rmANOVA	Repeated measures analysis of variance
ROI	Regions of interest
rsEEG	Resting state electroencephalography
SF	Spatial frequency
sGC	Spectral Granger Causality

SLF2	Superior longitudinal fasciculus 2
SLF3	Superior longitudinal fasciculus 3
SNR	Signal to noise ratio
SS-1	Sub-study 1
SS-2	Sub-study 2
SSVEP	Steady-state visually evoked potentials
SZ	Schizophrenia patient
tACS	transcranial alternating current stimulation
TMS	Transcranial magnetic stimulation
WM	White matter
Y	Young adults

76

1. Introduction

1.1 Background

Electroencephalography (EEG) provides important information about neurobiological phenomena by reflecting the summation of excitatory and inhibitory postsynaptic electrical potential in cerebral cortex [1, 2]. EEG is known to produce when pyramidal neurons form a synchronous polarization by laminar arrangement in perpendicular to the cortical surface [1, 3]. The range of EEG is generally characterized by delta (1-4Hz), theta (4-7Hz), alpha (8-12Hz), beta (13-30Hz), and gamma (30-100Hz) [4]. Each EEG range is known to reflect the general functions of the brain. Delta waves are known to relate to decision making, relaxation, and sleep [5, 6]; theta waves to REM sleep, attention, emotion, awareness, and creativity [6, 7]; alpha waves to resting, visual input, awakeness, and memory maintenance [8-12]; beta waves to decision making, awakeness, and logical thinking [6, 13]; and gamma waves to sensory processing, attention object perception, word encoding, the maintenance of relevant items in working memory, cross-modal semantic matching and short-term memory retention [14-21].

Resting state and evoked EEG are known to change with advancing age. With advancing age, the powers of resting delta and theta waves decrease [22-26], those of resting alpha and beta waves remained stable [23, 26, 27], and that of resting gamma wave increases [27-29]. In contrast, the powers of evoked potential decrease with advancing age in all frequency bands including alpha, beta and gamma as well as delta and theta [28, 30-33](Table1).

Resting state and evoked EEG are known to change in neurodegenerative diseases [22]. Alzheimer disease (AD) is a neurodegenerative disease with widespread neuronal and synaptic losses and functional decline [34, 35]. In AD, with advancing disease severity, the powers of resting delta and theta waves increase while those of resting alpha, beta and gamma waves decrease [36-38]. These changes start earlier in the theta, beta and gamma waves in AD [36, 37, 39, 40]. The powers of evoked potential decrease in AD in all frequency bands[31, 41-44](Table2). In AD patients, the gamma waves

power were well correlated with the level of AD pathologies including amyloid beta accumulation and neurodegeneration [45, 46] as well as the scores of various cognitive tests including the California Verbal Learning Test, the Alzheimer's Disease Assessment Scale–Cognitive Subscale, the Mini Mental Status Examination (MMSE) and the Montreal Cognitive Assessment [47, 48]. In contrast to other mental disorders like schizophrenia in which the power of auditory evoked potential of low gamma band centered around 40 Hz was selectively reduced [49-51], the powers of evoked potential decrease in AD in all frequency bands including gamma band [41, 42]. AD patients showed delayed gamma rhythm response and reduced power and connectivity of the gamma rhythm response than healthy controls [52, 53], although such changes in evoked gamma rhythm were not replicated in some studies [45, 54] probably due to the unstable behavior of AD patients [45]. Most importantly, only evoked gamma waves were found to change the pathologies in animal models. Entrainment of gamma waves reduced amyloid beta accumulation and improved cognitive function [55-57] whereas entrainment of alpha and beta waves did not influence the level of amyloid beta accumulation or cognitive function [55, 58, 59]. Furthermore, entrained gamma waves were well propagated to other brain regions whereas entrained alpha and beta waves were not [60-62]. These are why gamma entrainment is proposed as a promising intervention for preventing AD and/or modifying the course of AD that may directly eliminate neuropathologies by modulating regional immune responses, not just improve symptoms by restoring functional connectivities between regions.

In several exploratory trials, however, the therapeutic efficacy of gamma entrainment on cognitive function and/or amyloid beta accumulation has not been consistently replicated in humans with AD [63-65]. In a trial on six AD patients, 552–577 cd/m^2 light flickering at 40 Hz for 120 minutes a day at home for 10 consecutive days failed to reduce amyloid burden in the primary visual cortex, visual association cortex, lateral parietal cortex, precuneus, and posterior cingulate [63]. However, this study did not examine whether their FLS properly entrained gamma rhythms in the participants, leaving it for future research to find whether FLS failed to entrain gamma rhythms or gamma entrainment failed to reduce the amyloid burden in humans. In the another trial on eight AD patients, 40 Hz mixed sensory

stimulation (~700 cd/m^2 visual pulses and ~80 dB auditory pulses) administered for 60 minutes per day for three months succeeded in entraining gamma rhythm. However, this study did not examine the changes of amyloid beta deposition [65], leaving it for future research to find whether entrained gamma rhythms by sensory stimuli can reduce amyloid burden in human brain. In other trial on ten AD patients, 40 Hz mixed sensory stimulation (197-200 cd/m^2 visual pulses and 68 dB auditory pulses) administered for 60 minutes per day for two months succeeded in entraining gamma rhythm but failed to reduce cerebral amyloid deposition [64](Table3), leaving it for future research to find whether the characteristics and/or dosage of sensory stimulation were proper for entraining gamma rhythm strong and wide enough for reducing cerebral amyloid burden in humans.

These conflicting results in the humans with AD may be attributable to a couple of key factors in addition to the limited sample sizes of the trials. First, the parameters of sensory stimulation employed in these trials may not be optimal for entraining gamma waves in human. For example, optimal frequency for entraining gamma waves in visual cortex was 30-50 Hz in cats [66], 45-55 Hz in monkeys [67, 68], and 35-45Hz [69, 70] in mice but 30-40Hz in humans [71, 72]. The frequency of higher than 60Hz could not properly entrain gamma waves in humans [71, 73, 74]. In addition, the gamma range frequency that shows the strongest SSVEP response decreases by 0.1Hz every year in human [28], and the power of gamma waves entrained by a given visual stimulus in older adults was lower than that in younger adults [75]. Therefore, 40Hz that was optimal for entraining gamma waves in mice may not work properly in older humans. Likewise, the sensitivity and adverse responses to the intensity and color of visual stimuli may be different between diurnal animal like human and nocturnal animal like mouse [76-78]. Within humans, the sensitivity and adverse responses to the intensity and color of visual stimuli may also change with advancing age due to the age-associated changes in pupil, lens and retina [79, 80]. Second, even though the parameters of visual stimuli are optimized for entraining gamma waves in older adults, the entrainment and propagation of gamma waves may not be uniform between individuals because the structural integrity of brain may vary significantly between individuals particularly in late life. With advancing age, microstructural integrity of white matter (WM) decreases

[81-83]. White matter hyperintensity (WMH) which increases with advancing age [84] and is more prevalent in AD compared to normal controls [85] may impair the microstructural integrity of WM tract differentially between individuals. The WM integrity influences not only the coherence of resting gamma waves [86, 87] but also the entrainment and propagation of gamma waves [40, 88-90].

Gamma waves can be entrained by both visual or auditory stimuli and the central gamma frequency is different between visual and auditory cortices. In humans, auditory stimuli evoked the gamma waves of approximately 40Hz in the temporal cortex [49-51, 91-95]while visual stimuli evoked the gamma waves of 32-40Hz in visual cortex [96, 97]. Although gamma waves entrained by auditory stimuli propagated to frontal and central regions [49, 98] those entrained by visual stimuli propagated to the wider brain regions [62]. The duration of evoked potentials induced by 40Hz visual stimuli was also twice as long as that induced by 40Hz auditory stimuli in humans [99](Table4). The gamma entrainment by visual stimuli reduced synaptic loss and amyloid beta accumulation broadly from posterior to frontal cortices while that entrained by auditory stimuli only did locally in the auditory cortex in mice [56, 57]. Furthermore, hearing loss is quite prevalent in AD patients [100, 101], which may considerably limit the applicability of gamma entrainment using auditory stimuli. Therefore, in AD patients, it may be better to use visual stimuli than auditory stimuli for entraining gamma waves.

1.2. Purposes

We conducted this study under two purposes. First, we investigated the optimal parameters (color, intensity, and frequency) of visual stimuli for entraining gamma waves in visual cortex and propagating them to other target brain regions such as temporal and frontal corticies in older adults. Second, we investigated the influence of WM microstructural integrity on the entrainment and propagation of gamma waves using visual stimuli in older adults. To achieve these two purposes, we conducted two studies as below.

1) In the study 1, we investigated the optimal parameters of flickering light stimulation (FLS) for

gamma entrainment in healthy younger adults (sub-study 1) and older adults (sub-study 2).

2) In the study 2, we investigated the association of the fractional anisotropy (FA) of WM tracts with the event-related synchronization of gamma waves entrained in visual cortex and the spectral Granger causality of the gamma wave connectivity from visual cortex to temporal and frontal corticies.

2. Methods

2.1. Study design

The study 1 consisted of two sub-studies (the sub-study 1 [SS-1] and the sub-study 2 [SS-2]). The SS-1 consisted of two experiments (the experiment 1 [EXP-1] and the experiment 2 [EXP-2]). We examined the optimal color, intensity, and frequency of FLS for entraining gamma rhythms in younger and older adults in the study 1 (Figure 2 and Figure 3), and the effect of WM microstructural integrity on the gamma entrainment by the FLS with optimal parameters in the older adults in the study 2. We instructed participants not to drink alcohol 24 hours before all experiments and fast for at least two hours before all experiments.

2.1.1. Study 1. Investigation on the optimal parameters of FLS for gamma entrainment in humans

The SS-1 on younger adults consisted of two separate experiments and the SS-2 consisted of one experiment. In both sub-studies, each experiment consisted of a 5-minute resting phase for recording resting-state EEG (rsEEG) and four experimental sessions for recording steady-state visually evoked potentials (SSVEP). Considering the washout between stimuli, we set the break between sessions to 180s [102-104]. All intervals between the resting phase and the four experimental sessions were three minutes. Each session consisted of 10 blocks, and each block consisted of 10 FLS trials of a given color, intensity, and frequency. A 10-second break was placed before and after each block. Each FLS was presented for 2 s, and the inter-FLS interval was randomly given from 3–6 s (4.5 ± 1.5 s). After each session, we asked participants to rate the severity of six adverse effects of FLS (fatigue, headache, dizziness, dazzling, asthenopia, and ocular pain) using a 7-point Likert-type scale from 0 (not at all) to 6 (extremely severe).

In the SS-1, the FLS frequencies in each block were one of the ten frequencies from 32 to 50 Hz with a 2-Hz interval, and the order of FLS frequency of the 10 blocks was random. In the EXP-1,

the color of 10 cd/m^2 FLS in the first session was always white, and those of the following sessions were randomly assigned among other colors (red, green, blue). In the EXP-2, the intensity of white FLS in the first session was always 10 cd/m^2, and those of the following sessions were randomly assigned among other intensities (100, 400, 700 cd/m^2). Considering the washout between stimuli, we set the break between sessions to 180s. Experiments were separately conducted twice for each participant, and the inter-experiment intervals were 7–10 days.

In the SS-2, the flickering frequencies of FLS in each block were one of the five frequencies from 32 to 40 Hz with a 2-Hz interval, and five randomly ordered frequencies were assigned twice. We simultaneously investigated FLS color and intensity. Each session had one of four FLS sources: 400 cd/m^2 white FLS, 700 cd/m^2 white FLS, 400 cd/m^2 red FLS, and 700 cd/m^2 red FLS. Considering the washout between sessions, we set the break between sessions to 180s.

2.1.2. Study 2. Investigation on the effect of WM microstructural integrity on the gamma entrainment by FLS in humans

We obtained the fractional anisotropy (FA) of WM of the older participants in the SS-2 from the diffusion tensor images (DTI) acquired using a 3.0 Tesla Achieva Scanner (Philips Medical Systems; Eindhoven, NL). We employed a DTI-DwiSE sequence (echo time = 49 ms; repetition time = 5165 ms; axial-plane acquisition matrix size = 112 × 112 mm; slice thickness = 2 mm; acquired voxel size = 2.00 × 2.00 × 2.00 mm; and flip angle = 90°), and acquired a baseline image (b = 0) and 14 different diffusion orientations with a b-value of 1000 s/mm^2. Then we investigated the associations of FA of WM with the strength and propagation of gamma rhythms entrained by FLS.

2.2. Participants

2.2.1. Study 1. Investigation on the optimal parameters of FLS for gamma

entrainment in humans

In the SS-1, we enrolled 19 young healthy and cognitively normal volunteers (11 men and eight women) aged 19 – 31 years old (24.1 ± 3.6 years old) to investigate the optimal FLS parameters for gamma entrainment in healthy younger adults. Among them, we included 16 participants (nine men and seven women; 24.0 ± 3.7 years old) in the final analysis after excluding three participants (one due to severe glare and other two due to excessive electromyogram [EMG] noise in their EEG). In the SS-2, we enrolled 46 healthy and cognitively normal volunteers (22 men and 24 women aged 65 – 76 years old (69.9 ± 2.3 years old) to investigate the optimal FLS parameters for gamma entrainment in healthy older adults. Among them, we included 35 participants (17 men and 18 women; 70.0 ± 2.4 years old) in the final analysis after excluding 11 participants (three due to withdrawal of their consents and eight due to excessive EMG noise in their EEG).

All participants of the two experiments had a normal or corrected-to-normal vision and normal hearing. They had no current or previous history of major psychiatric or neurological disorders. The characteristics of the participants are summarized in Table 5.

2.2.2. Study 2. Investigation on the effect of WM microstructural integrity on the gamma entrainment by FLS in humans

Among the 35 older adults who were included in the final analysis of the SS-2 of the Study 1, we included 26 participants (11 men and 15 women; 69.8 ± 2.3 years old) who completed diffusion weighted magnetic resonance imaging and showed the signal to noise ratio (SNR) at occipital region (POz, Oz, O1, O2) of above 1.5 at the occipital region. We defined SNR as the ratio of power of the SSVEP at the stimulated frequency to the mean power of the background noise ranging from 1~60Hz from 501 ms to 2000 ms after FLS onset [105, 106]. Their characteristics are summarized in Table 5.

2.2.3. Clinical evaluation of the participants

In the SS-1 of the Study 1, we evaluated the presence of psychiatric or neurologic disorders in the younger participants by history taking only. In the SS-2 of the study 1 and the study 2, geriatric psychiatrists evaluated the presence of psychiatric or neurologic disorders in the older participants through face-to-face standardized diagnostic interviews, physical and neurologic examinations, and laboratory tests using the Korean version of the Consortium to Establish a Registry for Alzheimer's Disease Assessment Packet [107] and the Korean version of the Mini International Neuropsychiatric Interview [108]. Ophthalmologists confirmed that all participants were free from eye diseases to be excluded from this study by the forced visual activity test, slit lamp examination, fundoscopy and optical coherence tomography.

2.3. Research ethics

All participants provided written informed consent to participate in each study by themselves. The protocols of the substudies were approved by the Institutional Review Board of the Seoul National University of Bundang Hospital (B-1904-534-303, B-1809-493-004, and B-1809-493-004).

2.4. FLS

We delivered the FLS to each participant using a pair of white organic light-emitting diode (OLED) panels (4.7 cm × 4.7 cm; color temperature 3000K; LG Display Co., Ltd., Seoul, Korea) attached to an eyeglass. We measured the voltage-luminance (light intensity) characteristics of OLED panels using a calibrated spectroradiometer (CS2000, Konica-Minolta Inc. Tokyo, Japan) at voltage-controlled mode using a precise source measurement unit (Keithley 2400, Tektronix Inc., Beaverton, OR, USA). The distance between OLED panel and the cornea was assumed to be about 2 cm. The subtended angle seen by the center point of cornea for the middle points of edges and the vertex point of OLED panel were 1.73 and 2.06 radians, respectively.

We drove the OLED panels with a square rhythm using a function generator (TG 5012A, Aim & Thurlby Thandar Instruments, Huntingdon, Cambridgeshire, UK) with 100% modulation depth and

50% duty cycle. We controlled the error of voltage fluctuation under 5 mV. The corresponding error of luminance was estimated to be less than 5%.

We changed the color of FLS by placing an optical color filter (KODAK WRATTEN 2, Eastman Kodak Company; No. 25 for red, No. 58 for green, and No. 47 for blue). White, red, green, blue, and white colors had their peak wavelengths at 610 nm, 700 nm, 530 nm, and 440 nm, respectively.

We changed the intensity and frequency of FLS by modulating the amplitude and frequency of the square rhythm using an in-house LabVIEW program (National Instruments Corporation, Austin, TX, USA). We changed the intensity of FLS by modulating the supply voltage of the OLED. In the sub-study 1 of the study 1, we achieved the intensity of 10 cd/m^2 by supplying 7.19 V, 7.25 V, 7.99 V, and 7.04 V in red, green, blue, and white FLS, respectively. In the SS-1 of the study 1, we achieved the intensities of 100 cd/m^2, 400 cd/m^2, and 700 cd/m^2 by supplying 7.38 V, 7.71 V, and 7.91 V respectively in white FLS. In the SS-2 of the study 1 and the study 2, we achieved the intensities of 400 cd/m^2 and 700 cd m^2 by supplying 7.71 V, and 7.91 V respectively in white FLS and 8.31 V and 8.72 V respectively in red FLS.

We provided the FLS of 10 distinctive flickering frequencies (32 Hz, 34 Hz, 36 Hz, 38 Hz, 40 Hz, 42 Hz, 44 Hz, 46 Hz, 48 Hz, and 50 Hz) in the SS-1 of the study 1, and five distinctive flickering frequencies (32 Hz, 34 Hz, 36 Hz, 38 Hz, and 40 Hz) in the SS-2 of the study 1 and the study 2.

2.5. Recording, preprocessing and analysis of EEG

We recorded EEG with 64 Ag-AgCl electrodes on elastic caps (Easycap, EASYCAP GmbH, Munich, Germany) according to the extended International 10–20 System. FCz was the reference electrode. We used the forehead for the ground electrode, and below and above the left eye to record an EMG by attaching a pair of electrodes. We maintained electrodes at an impedance of 10 kΩ or less during the entire recording. A 24-bit ActiCHamp DC amplifier and BrainVision Recorder (Brain Products Gmbh, Gliching, Germany) amplified and stored the recorded EEG signal. The sampling rate was 1,000 Hz.

EEG recording did not apply online filters. We delivered the stimulus markers from the FLS control system and synchronized with the recording rsEEG

We preprocessed and analyzed procedures using MATLAB (The MathWorks Inc., Natick, MA, USA), EEGLAB [109], and BSMART [110] toolbox. We filtered recorded signals with a 1-Hz high-pass finite impulse response filter and a 60-Hz notch filter and then applied it to a common average reference. We did an independent component analysis to remove eye blinks and other ocular artifacts from the EEG signal.

After preprocessing, we segmented 5-min resting state EEG (rsEEG) recordings into 1,500-ms epochs, and then randomly selected 20 artifact-free epochs from them. We obtained a 4,000-ms epoch from 1,000 ms before each FLS onset to 1,000 ms after each FLS offset, resulting in twenty 4,000-ms epochs of each frequency. For the spectral Granger Causality (sGC) analysis, we obtained 1500 ms from 501 ms to 2000 ms from each 4000-ms epoch.

We calculated frequency spectrums of each rsEEG epochs using the fast Fourier transform algorithm. We accumulated and averaged over time for each epoch with the estimated frequency spectrums. We measured the absolute and relative rsEEG powers of all frequency bands from delta to high gamma at each electrode.

To find the optimal color, intensity, and frequency of FLS for entraining gamma rhythms in human, we analyzed the spectral power change of EEG induced by FLS using event-related spectral perturbation (ERSP) in each block. We calculated the time-frequency spectrum in each epoch and normalized the spectrum by dividing the average power of pre-stimulus intervals. We calculated the ratio of the spectral power of EEG during FLS to the spectral power during the pre-FLS interval for each FLS. To get a normalized averaged spectral power change induced by a given color, intensity, and frequency of FLS, we calculated the event-related desynchronization/event-related synchronization (ERD/ERS) value by averaging the ratios of the spectral power of EEG of a given FLS frequency from 20 FLS trials (SS-1: 10 FLS per session*2 visit, SS-2: 20 FLS per session; total 400trials). We also calculated the time-associated change of power spectrum by averaging ERSP of 11 successive, non-

overlapping, 250- ms subwindows from 250 ms before FLS onset to 2,500 ms after FLS onset in each block (T0-T10). T0 (-250-0 ms) represents the time windows right before FLS onset, and T9 (2,000-2,250 ms) and T10 (2,250-2,500 ms) represent the time windows right after FLS offset. Then, we compared ERS between these 11 blocks to confirm FLS entrained gamma rhythm. We used the average ERS during FLS (T1-T8) in the analyses on the effects of FLS intensity, color, and frequency on gamma entrainment. We chose Pz as the representative channel of the posterior region and chose Fz as the representative channel of the anterior region to be Fz for examining the universal SSVEP response [74, 111].

To examine whether gamma rhythms entrained in the occipital cortex propagate to other brain areas, we compared the sGC of gamma rhythms during FLS to that in the resting state. We calculated sGC for all possible electrode pairs and averaged each FLS frequency in each session. We set the time lags to 75 samples for calculating sGC [112]. We compared the mean sGC of the 20 1,500-ms epochs from rsEEG with that of 20 1,500-ms epochs from SSVEP during FLS. Since EEG of each FLS condition had different pairs of significant connections between electrodes, we employed graph theory measures to compare the network structures quantitatively between conditions of FLS intensity, color, and frequency [113, 114]. We compared the number of edges where sGC of parietooccipital to frontotemporal connection significantly increased after FLS compared to rsEEG.

We investigated the propagation of entrainment with sGC by designating the following regions: occipital (POz, Oz, O1, O2), temporal (left, FT7, T7, TP7, TP9; right, FT8, T8, TP8, TP10), central (left, FC5, FC3, C5, C3, CP5, CP3; right, FC4, FC6, C4, C6, CP4, CP6), frontal regions (left1-left fore of middle to inferior frontal region : AF7, AF3, F7, F5; left2-left rear of middle to inferior frontal region : F7, F5, FC5, FC3; right1-right fore of middle to inferior frontal region AF4, AF8, F6, F8; right2-right rear of middle to inferior frontal region F6, F8, FC4, FC6) [115-117]. We calculated connectivity from occipital to temporal, central, or frontal regions using these regions. Then we chose Oz as the representative channel of the occipital region to investigate the association of WM tract microstructural

integrity and entrainment, since Oz is considered a direct entrainment signal from the occipital region [118, 119].

2.6. Acquisition, preprocessing and analysis of DTI

We conducted DTI parameter acquisition using FMRIB Software Library (FSL 6.0)[120] to acquire fractional anisotropy (FA) of the white matter tracts of desired region of interests (ROIs). First, we converted DTI Digital Imaging and Communication in Medicine (DICOM) volumes to NIfTI format and extracted the brain using 'bet' function and the baseline image using 'fslroi' function on FSL. We then corrected the inhomogeneity using eddy current function to arrange the distortion and movement. We created subject's FA map using ‘dtifit’ function on FSL. We registered subject's FA map into the FMRIB58_FA standard-space and used this transformation to register regions of interest (ROI) defined in that standard space [121, 122] back to each subject's space. Finally, we transformed the ROIs into diffusion space of each subject with 20 % of probability threshold applied. Then we acquired mean value of FA within each ROIs.

Using the FSL atlas tool, we defined four ROIs that may play key roles in the entrainment and propagation of gamma rhythms. Using ‘JHU DTI-based white-matter atlases’ [123] , we defined the posterior thalamic radiation (PTR) which are distributed from the lateral geniculate nucleus (LGN) to primary visual cortex. PTR may play a key role in entraining gamma rhythms in visual cortex. Using ‘XTRACT HCP tract atlases’ [124], we defined left and right middle longitudinal fasciculus (l-MLF and r-MLF), which are distributed from the occipital area to the temporal area. MLF may play a key role in propagating gamma rhythms entrained in visual cortex to temporal lobe. In addition, we defined left and right superior longitudinal fasciculus (l-SLF 2 and r-SLF 2; l-SLF 3 and r-SLF 3). SLF 2 is distributed from the parietooccipital area to the middle frontal area, and SLF 3 is distributed from the parietooccipital area to the inferior frontal area. SLF may play a key role in propagating gamma rhythms entrained in visual cortex to frontal lobe (Figure 4).

2.7. Statistical analyses

We examined the mean and standard deviation of the continuous variables of demographics of subject groups in the study 1 and the study 2.

In the study 1, we analyzed the effect of FLS parameters on entrainment and propagation. In the EXP-1 of the SS-1 on the younger adults, we examined the effect of the time window of ERS, FLS color, and FLS frequency on the changes of gamma rhythm associated with FLS using repeated measures analysis of variance (rmANOVA) with the Greenhouse-Geisser non-sphericity correction and Bonferroni post hoc comparisons in Pz and Fz. In the EXP-2 of the SS-1 on the younger adults, we examined the effect of the time window of ERS, FLS intensity, and FLS frequency on the changes of gamma rhythm associated with FLS using rmANOVA with the Greenhouse-Geisser non-sphericity correction and Bonferroni post hoc comparisons in Pz and Fz. Additionally, in the EXP-2 of the SS-1 on the younger adults, we performed a paired t-test on twenty 1,500-ms epochs to compare the sGC of SSVEP during FLS and sGC of rsEEG, and to specify thresholds for constructing an adjacency matrix of a given FLS intensity and frequency using the edges that were found to be significantly different between rsEEG and SSVEP with false discovery rate (FDR) corrected $p < 0.05$. We then examined the effects of FLS intensity and frequency on the connection strengths during FLS using rmANOVA with the Greenhouse-Geisser non-sphericity correction and Bonferroni post hoc comparisons. In the SS-2 on the older adults, we examined the effect of the time window on ERS, FLS color, FLS intensity, and FLS frequency on the changes of gamma rhythm associated with FLS using rmANOVA with the Greenhouse-Geisser non-sphericity correction and Bonferroni post hoc comparisons in Pz and Fz. Additionally, in the SS-2 on the older adults, we performed a paired t-test of twenty 1,500-ms epochs to compare the sGC of SSVEP during FLS and sGC of rsEEG, and to specify thresholds for constructing an adjacency matrix of a given FLS intensity and frequency using the edges that were found to be significantly different between rsEEG and SSVEP with false discovery rate (FDR) corrected $p < 0.05$. We then examined the effects of FLS color, intensity and frequency on the connection strengths during FLS using rmANOVA with the Greenhouse-Geisser non-sphericity correction and Bonferroni post hoc

comparisons. Both the SS-1 and the SS-2, we examined adverse effects (fatigue, headache, dizziness, dazzling, asthenopia, ocular pain) according to FLS color and intensity using repeated measures rmANOVA with the Greenhouse-Geisser non-sphericity correction and Bonferroni post hoc comparisons.

In the SS-2 on the older adults, we examined the association between the rsEEG powers of all frequency bands with MMSE score using linear regression analyses adjusting for age.

In the study 2, we compared the age and the SNR between the included and excluded participants using Student t-test. We examined the effect of the FA values of PTRs on the ERS of gamma rhythms entrained at Oz using multiple linear regression analysis with enter method. Then we compared the ERS of gamma rhythms entrained at Oz between the lowest quartile group of the PTR FA values with the rest quartile group of the PTR FA values using Student t-tests. In the current analyses, we employed the ERS at Oz for measuring the strength of gamma rhythms entrained by FLS because PTR fiber projects more to V1 than other visual cortex sub-regions [125] and Oz is right above the V1 region [118, 119].

We examined the effect of the FA values of MLFs and SLFs on the sGC of gamma rhythms connectivity from occipital (POz, Oz, O1, O2) to temporal (left, FT7, T7, TP7, TP9; right, FT8, T8, TP8, TP10), central (left, FC5, FC3, C5, C3, CP5, CP3; right, FC4, FC6, C4, C6, CP4, CP6) and frontal regions (left1, AF7, AF3, F7, F5; left2, F7, F5, FC5, FC3; right1, AF4, AF8, F6, F8; right2 F6, F8, FC4, FC6) using multiple linear regression analysis with enter method adjusting for the ERS at Oz. We also compared the sGCs of gamma rhythm connectivity between the lowest quartile group of the FA values of MLFs and SLFs with the rest quartile group of the FA values of MLFs and SLFs using Student t-tests.

For all analyses, we used SPSS in Windows version 20.0 (IBM Co., Armonk, NY, USA) and MATLAB (The MathWorks Inc., Natick, MA, USA) and considered 2-sided p value below 0.05 as statistically significant.

3. Results

3.1. Effects of the rsEEG band powers on cognitive function

As summarized in Table 6, the relative power of resting low-low gamma (30 – 38Hz) was reversely associated with the MMSE score at Pz, Cz and Fz in older adults (β = -0.418, p = 0.014 at Pz; β = -0.473, p = 0.007 at Cz; β = -0.404, p = 0.023 at Fz). However, the relative powers of rsEEG of other frequency bands were not associated with the MMSE scores. The absolute powers of rsEEG were not associated with MMSE scores at all frequency bands (Table 7).

3.2. Entrainment and propagation of the gamma rhythms by FLS

Spectral power of the SSVEP increased in fundamental and harmonic frequencies of FLS after FLS onset, lasted during the FLS, and diminished after FLS offset at both Pz and Fz in both the SS1 on younger adults (Figure 5) and the SS-2 on older adults (Figure 6). The averages of ERD/ERS in each time window after FLS onset were positive (ERS), indicating that the spectral power of SSVEP increased after FLS. During FLS, alpha band brain rhythms of 9 Hz ~ 13 Hz decreased both Pz and Fz ($p < 0.001$), but theta and beta band rhythms were not changed ($p > 0.1$).

In the SS-1 on the younger adults, the main effect of the time window on ERS was significant in both experiments ($F_{10, 150} = 31.145$, $p < 0.001$ at Pz and $F_{10, 150} = 12.731$, $p < 0.001$ at Fz, in the EXP-1, Figure 7A; $F_{10, 150} = 134.172$, $p < 0.001$ at Pz and $F_{10, 150} = 50.869$, $p < 0.001$ at Fz in the EXP 2, Figure 7B). In response to FLS, high gamma band of 64 Hz ~ 100 Hz, which are harmonic frequencies of 32 Hz ~ 50 Hz, also increased in response to the light stimulation of 32 Hz ~ 50 Hz at both Pz and Fz ($p < 0.001$). In the SS-2 on the older adults, the main effect of the FLS time window on ERS was significant at both Pz and Fz ($F_{10, 340} = 170.699$, $p < 0.001$ at Pz and $F_{10, 340} = 96.205$, $p < 0.001$ at Fz, Figure 7C). ERS during FLS (T1 - T9) was higher than ERS before FLS (T0) and that after FLS (T10) at both Pz

and Fz.

Since the spectral power of gamma rhythms was increased at both Pz and Fz, gamma rhythms entrained in primary visual cortex by FLS may be propagated to other brain regions including frontal lobe. The gamma rhythm entrained in the parietooccipital region was found to successfully propagate to the frontotemporal region. In the sGC analysis on the data from the EXP-2 of the SS-1 on younger adults (Figure 8A), parietooccipital-to-frontotemporal connectivity at 32–38 Hz for 400 cd/m^2 FLS and at 34–40 Hz for 700 cd/m^2 FLS showed significantly increased number of edges compared to rsEEG. In the sGC analysis on the data from SS-2 on older adults (Figure 8B), parietooccipital-to-frontotemporal connectivity also showed significantly increased number of edges compared to rsEEG at all FLS frequencies, intensities, and colors. The connectivity of gamma rhythm increases significantly after FLS in parietooccipital-to-frontotemporal-connection edges (FDR corrected $p < 0.05$).

3.3. Effects of the FLS color on gamma entrainment and propagation

In the EXP-1 of the SS-1 on the younger adults, the main effect of the FLS color on ERS was significant at the low FLS intensity of 10 cd/m^2 ($F_{3, 45} = 12.599$, $p < 0.001$ at Pz and $F_{3, 45} = 6.736$, $p < 0.01$ at Fz, Figure 9A). ERS of gamma rhythms entrained by red or white FLS was higher than that entrained by green or blue FLS ($p < 0.05$ for white FLS; $p < 0.01$ for red FLS at Pz; $p < 0.05$ for both white and red FLS at Fz). ERS entrained by red or white FLS were comparable at both Pz and Fz ($p = 0.117$ at Pz; $p = 1.000$ at Fz).

In the SS-2 on the older adults, ERS entrained by red or white FLS were comparable at both Pz and Fz at the high FLS intensity of 400 or 700 cd/m^2 ($F_{1, 34} = 0.003$, $p = 0.955$ at Pz and $F_{1, 34} = 1.306$, $p = 0.261$ at Fz, Figure 9B). In addition, in the sGC analysis, the strengths of parietoocciptial-to-frontotemporal connectivity was also comparable between red and white FLS with high FLS intensity of 400 or 700 cd/m^2 ($F_{1, 34} = 0.163$, $p = 0.689$).

3.4. Effects of the FLS intensity on gamma entrainment and propagation

In the EXP-2 of the SS-1 on younger adults, the main effect of the FLS intensity on ERS was significant ($F_{3, 45} = 49.156$, $p < 0.001$ at Pz and $F_{3, 45} = 17.742$, $p < 0.001$ at Fz, Figure 10A). The ERS entrained by 700 cd/m^2 and 400 cd/m^2 FLS was higher than that entrained by 100 cd/m^2 and 10 cd/m^2 FLS ($p < 0.01$ for 400 cd/m^2 FLS, $p < 0.001$ in 700 cd/m^2 FLS at Pz; $p < 0.001$ in 400 cd/m^2 FLS, $p < 0.05$ in 700 cd/m^2 FLS at Fz). However, the ERSs entrained by 700 cd/m^2 and 400 cd/m^2 FLS were comparable at both Pz and Fz ($p = 0.970$ at Pz; $p = 1.000$ at Fz). On the other hand, in the SS-2 on older adults, the ERS entrained by 700 cd/m^2 was comparable to that entrained by 400 cd/m^2 FLS at Fz but higher at Pz ($F_{1, 34} = 0.773$, $p = 0.385$ at Fz and $F_{1, 34} = 10.536$, $p = 0.003$ at Pz, Figure 10B).

In the sGC analysis on the data from the EXP-2 of the SS-1 on younger adults, the main effect of the FLS intensity on the strength of the parietooccipital-to-frontotemporal connectivity was significant ($F_{1, 15} = 10.306$, $p < 0.001$, Figure. 11A). The strength of connectivity entrained by 700 cd/m^2 FLS was higher than that entrained by 400 cd/m^2 FLS. In the sGC analysis on the data from the SS-2 on older adults, the main effect of the FLS intensity on the strength of the parietooccipital-to-frontotemporal connectivity was also significant ($F_{1, 34} = 15.903$, $p < 0.001$; Figure. 11B) The strength of connectivity entrained by 700 cd/m^2 FLS was stronger than that entrained by 400 cd/m^2 FLS ($p < 0.001$).

3.5. Effects of the FLS frequency on gamma entrainment and propagation

In the SS-1 on younger adults, the fundamental and harmonic responses became weaker as the FLS frequency increased over 40 Hz in all colors (EXP-1) and intensities (EXP-2). In the EXP-2, the main effect of the FLS frequency was significant at both Pz and Fz ($F_{9, 135} = 9.042$, $p < 0.001$ at Pz and $F_{9, 135} = 6.492$ $p < 0.001$ at Fz, Figure 12B). ERS was highest at 38 Hz, followed by 36 Hz and 34 Hz at Pz;

and was highest at 36 Hz, followed by 38 Hz and 34 Hz at Fz. Moreover, the interaction between the FLS frequency and intensity was also significant ($F_{27, 405} = 5.514$, $p < 0.001$ at Pz and $F_{27, 405} = 1.794$, $p = 0.78$ at Fz). ERS was highest at 36 Hz, followed by 38 Hz and 34 Hz for 400 cd/m^2 FLS; and was highest at 38 Hz, followed by 36 Hz and 40 Hz for 700 cd/m^2 FLS. However, in the EXP-1 with a low luminance intensity of 10 cd/m^2 FLS, the main effect of FLS frequency ($F_{9, 135} = 1.998$, $p = 0.131$ at Pz and $F_{9, 135} = 1.606$, $p = 0.154$ at Fz, Figure 12A) and its interaction with the FLS color on ERS ($F_{27, 405} = 1.261$ $p = 0.269$ at Pz and $F_{27, 405} = 1.061$, $p = 0.396$ at Fz) were not statistically significant.

In the SS-2 on older adults, the main effect of the FLS frequency on ERS was significant at both Pz and Fz ($F_{4, 136} = 9.584$, $p < 0.001$ at Pz and $F_{4, 136} = 17.453$ $p < 0.001$ at Fz, Figure 12C). ERS of fundamental and harmonic responses became weaker as the FLS frequency increased from 32 Hz to 40 Hz at both Pz and Fz. ERS was higher at 32 Hz and 34 Hz FLS than 38 Hz and 40 Hz at both Pz and Fz ($p < 0.05$ at Pz and $p < 0.01$ at Fz). The interaction between the FLS frequency and the FLS color was significant at Pz ($F_{4, 136} = 3.383$, $p < 0.05$). At Pz, under red FLS, ERS entrained by 32 Hz was higher than those entrained by 36 Hz or higher flickering frequencies ($p < 0.05$). However, under white FLS, ERS was comparably entrained at all flickering frequencies at Pz ($p > 0.05$). Such interaction was not found at Fz ($F_{4, 136} = 0.692$, $p = 0.545$). In addition, the interaction between the FLS frequency with the FLS intensity was not significant at both Pz and Fz ($F_{4, 136} = 0.427$, $p = 0.781$ at Pz and $F_{4, 136} = 0.226$, $p = 0.907$ at Fz).

In the sGC analysis on the data from the EXP-2 of the SS-1 on younger adults, the main effect of FLS frequency on the strength of the parietooccipital-to-frontotemporal connectivity was significant ($F_{9, 135} = 34.982$, $p < 0.001$, Figure 13A). The strength of connectivity entrained by 34–38 Hz FLS was significantly stronger than that entrained by FLS of other frequencies ($p < 0.05$). In addition, its interaction with FLS intensity was also significant ($F_{9, 135} = 20.591$, $p < 0.001$). The strength of connectivity was strongest at 34 Hz, followed by 38 Hz and 36 Hz under 400 cd/m^2 FLS ($p < 0.05$, Figure 13C) while strongest at 38 Hz, followed by 36 Hz and 40 Hz under 700 cd/m^2 FLS ($p < 0.01$,

Figure 13D).

In the sGC analysis on the data from the SS-2 on older adults, the main effect of FLS frequency on the strength of the parietooccipital-to-frontotemporal connectivity were significant ($F_{4, 136} = 58.469$, $p < 0.001$ for main effect, Figure 13B). The strength of connectivity entrained by 32 Hz FLS or 34 Hz FLS was-stronger than that entrained by FLS of 36 Hz or higher ($p < 0.001$). However, in the older adults, the interaction between the FLS frequency and FLS intensity on the strength of connectivity was not significant ($F_{4, 136} = 0.847$, $p = 0.479$). In addition, the interaction between the FLS frequency and the FLS color on the strength of connectivity was not significant ($F_{4, 136} = 3.106$, $p = 0.059$), and the three-way interaction between FLS frequency, FLS intensity and FLS color was not significant either ($F_{4, 136} = 1.042$, $p = 0.374$).

3.6. Effects of the microstructural integrity of WM tracts on the gamma entrainment and propagation

The characteristics of the 26 participants are summarized in Table 5. The six participants excluded from the analyses on the effect of the WM microstructural integrity on the entrainment and propagation of gamma rhythms were all men and their ages were comparable to those of the 26 included participants (69.6 ± 2.65 years old versus 69.81 ± 2.39 years old, $p = 0.868$). The mean SNR of the included participants was (5.65 ± 3.08). However, the mean SNR of the excluded participants was below 0 (-3.33 ± 2.59), indicating that gamma rhythms were not entrained at all by FLS in them.

In the linear regression analyses, the effects of the FA values of PTRs on the ERSs of gamma rhythms entrained at Oz were not significant in both hemispheres ($p > 0.05$, Figure 14). As Figure 14 illustrates, the standardized regression coefficient between FA values of l-PTR and ERS at Oz was not statistically significant ($\beta = 0.142$, $p > 0.05$) and neither did the standardized regression coefficient between FA values of r-PTR and ERS at Oz ($\beta = 0.016$, $p > 0.05$).However, the lowest quartile group

of the FA value of l-PTR showed significantly lower ERS of gamma rhythms at Oz than the second-to-highest quartile group of the FA value of l-PTR ($t = 2.301$, $p < 0.05$, Table 10), indicating that the microstructural integrity of PTRs may be important in proper entrainment of gamma rhythms in visual cortex.

As shown in Figure 15 and Table 12, the higher the FA values of MLFs and SLFs, the more strongly the gamma rhythms entrained in occipital cortex were propagated to other brain regions. In the multiple linear regression analyses, the sGCs of occipital to temporal, central and frontal connectivities increased as the FA of the MLFs and SLFs increased after adjusting the ERS at Oz in both hemispheres (Table 11). In all multiple linear regression models, the sGCs of occipital to temporal, central and frontal connectivities significantly increased as the ERS of entrained gamma rhythms at Oz increased ($p < 0.001$). In addition, in all multiple linear regression models, the standardized coefficient of the ERS of entrained gamma rhythms at Oz was higher than those of the FA values of MLFs and SLFs, indicating that the stronger entrainment of gamma rhythms at visual cortex may be also critical for propagating the entrained gamma rhythms to target brain regions. When the sGC values of the connectivities were compared between the lowest quartile group of the FA value of MLFs and SLFs and the second-to-highest quartile group of the FA value of MLFs and SLFs, the lowest quartile group showed the lower sGC values than the second-to-highest quartile group in all connectivities and the differences were statistically significant in all connectivities in left hemisphere and occipito-frontal connectivities in right hemisphere (Table 12). These results indicate that microstructural integrity of the MLFs and SLFs may be important in proper propagation of gamma rhythms entrained in visual cortex to other target brain regions.

3.7. Adverse effects

In the EXP-1 of the SS-1 on younger adults, the severities of all adverse effects induced by low luminance intensity FLS of 10 cd/m^2 were mild (< 3) under all FLS colors. However, the frequencies

of dazzling and asthenopia were different between the colors of FLS ($F_{3,45} = 3.115$, $p < 0.05$ for dazzling; $F_{3,45} = 5.433$, $p < 0.05$ for asthenopia, Table 8). Asthenopia was more common under the red and white FLS the than under the green FLS ($p < 0.05$). Dazzling was more common under red FLS and blue FLS with 2.6 and 2.3, respectively, than under white and green FLS with 1.9 and 1.4, respectively.

In the EXP-2 of the SS-1 on younger adults, the severities of most adverse effects induced by white FLS was mild (< 3) under all FLS intensities. However, under 700 cd/m^2 FLS the severities of dazzling and asthenopia were moderate to severe (> 3). The frequencies of fatigue, dazzling, asthenopia, and ocular pain were different between the FLS intensities ($F_{3,45} = 47.003$, $p < 0.001$ for dazzling; $F_{3,45} = 15.657$, $p < 0.001$ for asthenopia; $F_{3,45} = 7.847$, $p < 0.01$ for fatigue; $F_{3,45} = 9.226$, $p < 0.01$ for ocular pain, Table 8). Dazzling, asthenopia, fatigue and ocular pain were more common under the FLS of 700 cd/m^2 than under the FLSs of other intensities ($p < 0.05$). Dazzling and asthenopia were more common under the FLS of 400 cd/m^2 than under the FLS of 10 cd/m^2 ($p < 0.05$).

In the SS-2 on older adults, the severities of all adverse were mild (< 3) and comparable between colors and intensities (Table 9).

4. Discussions

This study demonstrated that gamma entrainment and propagation are considerably influenced by the FLS color, intensity, frequency, and WM microstructural integrity in humans. FLS with the longer wavelengths such as white and red entrained and propagated gamma rhythms better than those with the shorter wavelengths such as green and blue. FLS with the stronger FLS intensity such as 700 cd/m^2 and 400 cd/m^2 entrained and propagated gamma rhythms better than those with the weaker FLS intensity such as 100 cd/m^2 and 10 cd/m^2. White FLS of 700 cd/m^2 best entrained and propagated gamma rhythm in both younger and older adults. Flickering at 34–38 Hz white FLS entrained stronger and spread gamma oscillations more widely than other FLS frequencies in younger adults, while FLS of 32 and 34 Hz entrained stronger and spread gamma rhythm more widely than that of other higher FLS frequencies in older adults. In summary, White FLS of 700 cd/m^2 flickering at 32–38 Hz entrained the gamma rhythms more strongly at visual cortex and propagated them more widely to other brain regions than those flickering at 40Hz or higher in humans. The older adults whose FA of left PTR was low showed higher ERS at the left visual cortex than those whose FA of left PTR was not low. The older adults with the higher FA of MLF and SLF showed higher sGC from visual cortex to temporal and frontal regions respectively. Adverse effects in younger adults were more common under the white and red FLS than under the green FLS, and with 700 cd/m^2 intensity than other FLS intensity. However, in older adults, adverse effects on both FLS color and FLS intensity were comparable.

In previous research, the powers of resting and evoked beta and gamma waves decrease in the early stage of AD [31, 36-43]. However, when entrained, only gamma waves could clear AD pathologies and improve cognitive function in AD-modeled mice [55-57]. Entrainment of alpha, beta and high gamma waves did not influence the level of amyloid beta accumulation or cognitive function [55, 58, 59, 126]. Furthermore, entrained alpha and beta waves were not properly propagated to other target brain regions [60-62] While the correlation of resting gamma power/synchrony in healthy old adults with cognitive tests are yet to be known, in AD patients, the power of gamma waves was well correlated

with the level of AD pathologies [45, 46] and the scores of various cognitive tests [47, 48]. In line with these previous studies, MMSE score was associated with the relative power of resting gamma waves but not with those of other frequency bands (Table 6). These results indicate that in AD patients, not just by strengthening functional connectivity between brain regions, the decrease in the power of resting gamma may be involved in the decrease of cognitive function in AD and the restoration of gamma waves may improve cognitive function by directly clearing AD pathologies. Resting low gamma band power of frontal to parietal region seems to be related to higher-order cognitive functions [127-130]. The power of resting gamma waves of cognitively normal older adults whose Aβ standardized uptake value ratio (SUVR) is below threshold value [46] increases with advancing age. Therefore, the relative power of resting gamma waves showed a negative correlation with MMSE score in cognitively normal older adults in the current study. Nevertheless, in AD patients, the power and/or synchrony to external stimuli of gamma waves decreased with advancing amyloid beta deposition in AD patients [44-46, 53, 65, 131, 132]. These are why entrainment of gamma, not that of other frequency bands, is employed as a potential therapeutic intervention for AD.

Gamma entrainment using FLS consistently cleared AD pathologies in AD-modeled mice. [55-57, 126] However, its effect was not consistently observed in AD patients [63-65]. This discrepancy in the effect of gamma entrainment using FLS between mice and humans may be attributable, at least in part, to the potential differences in optimal stimulation for gamma entrainment between mice and human. Sensitivity to visual stimuli may be considerably different between diurnal human and nocturnal mice. For example, visual contrast sensitivity decreased rapidly after 32Hz in humans while after 42Hz in mice [133-135]. Since the dim light of 150 cd/m^2 for just one hour was enough to induce retinal neurodegeneration in mice [76, 77], the FLS applied to the AD-modeled mice in previous research may be relatively stronger than those applied to AD patients in previous clinical trials. Humans perceive visible long-wavelength light well, while mice are more sensitive to light with shorter wavelengths like ultraviolet, blue, and green [78]. Therefore, in humans, it may be more efficient to use lower flickering light frequency, longer wavelength light, and stronger light intensity than the light stimulus used in the

mice study. Previous research also found that low gamma waves can be more strongly entrained than high gamma waves in humans. The gamma waves entrained by the FLS of 30-40Hz were stronger and more widely propagated to frontal regions than the of 47-60Hz [61, 73, 74]. However, there was no previous study that compared the gamma entrainment between low-low gamma waves of 30-38Hz and low-high gamma waves of 40-48Hz. The current study clearly demonstrated that optimal frequency for gamma entrainment may be different between them. Previous research found that optimal frequency of visual stimuli for entraining gamma waves in humans was lower than those in other mammals [66-72]. In addition, the center frequency of gamma waves decrease by 0.1Hz every year in humans [28]. In line with these studies, in the current study, 32 - 34Hz was found to be optimal for gamma entrainment using FLS in older adults, which is about 15% - 20% lower than the frequency that was effective in mice. However, all previous clinical trials on AD patients employed a 40Hz FLS as an intervention. In our study, 40Hz FLS failed to entrain gamma waves in 39% of the older adults. All previous clinical trials on gamma entrainment were subject to limited statistical power due to small sample sizes (6 - 10 participants). Employment of 40Hz FLS might have further reduced the power of the studies because gamma waves might not have been entrained in about only 4 - 6 participants.

In our study on young adults, when the difference of FLS intensity of 400 cd/m^2 and 700 cd/m^2 is disregarded and only frequency effect is considered, the numbers of nodes where the gamma rhythms in the occipital region were entrained by 34 Hz, 36 Hz, and 38 Hz FLS had 170%, 160%, and 210% more nodes and their strengths of connections were 220%, 230%, and 280% higher than those entrained by 40 Hz FLS, respectively. These results indicate that the visual SSVEP entrained by 34 - 38 Hz FLS may spread more strongly and widely than that by 40 Hz FLS when the intensity is ≥400 cd/m^2. The 40 Hz sensory modulations, which were employed in previous clinical studies on MCI and AD patients [63-65], failed to reduce AD pathologies. However, the failure could be attributed to them failing to entrain and propagate gamma rhythms to the frontal and temporal areas, or their lack of research on optimal conditions (light frequencies, light intensities, color, length of treatment period) to best entrain

and propagate gamma rhythm. Indeed, in our older adults study, the optimal frequency for inducing and propagating gamma entrainment was different from that in young adults.

In older adults, 32 Hz or 34 Hz FLS entrained gamma rhythms were approximately 120% stronger at Pz and 140% stronger at Fz than 40 Hz FLS. In addition, 32 Hz and 34 Hz FLS entrained gamma rhythms at approximately 125% more nodes with approximately two times higher strength than 40 Hz FLS. While in our study on young adults, 32 Hz FLS comparably entrained gamma rhythm to 40 Hz FLS and 38 Hz FLS entrained gamma rhythms approximately 120% stronger at both Pz and Fz and at 210% more nodes with 280% higher strength than 40 Hz FLS. In short, the FLS frequency that entrained the strongest and most widely spread gamma rhythm was 32 Hz or 34 Hz in the older adults, while it was 36 Hz or 38 Hz in younger adults. Showing that the optimal FLS frequencies for entraining gamma rhythm in older adults were a bit lower than those in younger adults. Even within older adults, the optimal FLS frequency for entraining gamma rhythm of the older participants (> 70 yrs.) was found to be approximately 1.5 Hz lower than that of the younger (≤ 70 yrs.) participants in older adults study. These results indicate that optimal FLS frequency for entraining gamma rhythm may decrease with advancing age in humans.

This age-associated decrease in the optimal FLS frequency for gamma entrainment may be attributable to the age-associated decrease in the center frequency of gamma rhythms in humans [28] [97]. According to Murty et al., center frequency gradually decreased with advancing age (0.16 Hz per year in high gamma range of 36 Hz or higher and 0.08 Hz per year in low gamma range below 36 Hz) [28]. If we employ these results to estimate the difference in the center frequency of gamma rhythm between the older adults study and the young adult study (69.9 ± 2.3 years versus 24.1 ± 3.6 years), and that between the older participants and younger participants of the older adults study (71.6 ± 1.8 years versus 67.9 ± 1.0 years), differences are 7.4 Hz and 0.5 Hz, respectively, in high gamma rhythm (≥ 36Hz) and 3.7 Hz and 0.2 Hz, respectively, in low gamma rhythm (< 36Hz). Center frequency is the frequency where the power changes most in response to external visual stimulation [28, 68]. It increases

monotonically with increasing intensity of visual input such as visual contrast [136-139]and motion velocity [140, 141]. Contrast sensitivity to medium and high contrast and spatial frequencies seems to decrease with advancing age [142] which the lower contrast sensitivity may influence cortical excitation and consequently lower center frequency in the older population [143]. Center frequency is also positively correlated with GABA level in the visual cortex [97, 144] and increases with the increase of the tonic excitability of GABAergic inhibitory interneurons [145, 146], which is believed to generate gamma rhythms by regulating global excitatory-inhibitory balance in cortex (e.g. visual cortex) [147-150]. Age-associated decrease in center frequency may be attributable to the age-associated decrease in the excitability of GABAergic inhibitory interneurons [97, 151]. According to related studies, with increasing age, glutamate decarboxylase (GAD) [152] and gamma-aminobutyric acid transporters (GAT) [153] decreases, could result in decrease in gamma-aminobutyric acid receptor (GABAR) [154] and functional degeneration of GABAergic neuron [155] . In addition, the level of GABA decreased in visual, sensory motor, frontal, and prefrontal cortices areas with advancing age in humans [156, 157], which may represent degradation of GABA inhibitory intracortical circuits [158-161], and may be the result of age-associated motion velocity and contrast sensitivity change. In short, GABAergic inhibitory neurons are seemingly affected by advancing age that likely leads to decrease in center frequency.

In addition to the frequency of FLS, the color and the luminal intensity of FLS may also influence the entrainment of gamma waves in human, particularly in older adults. FLS with longer wavelengths induced stronger SSVEP than FLS with shorter wavelengths in humans [162, 163]. In humans, retinal cones are responsible for color vision, and long-wavelength sensitive cones are denser than medium and short-wavelength sensitive cones. The ratio of red, green, and blue cones in the retina is 11:5:1 [164, 165]. Therefore, lights with longer wavelengths reach a wider primary visual cortex area and may entrain gamma rhythms stronger than those with shorter wavelengths. In the current study, young adults that are ERS entrained by white FLS was comparable to that entrained by red FLS at Fz and Pz. However, Bieger and colleagues [166] reported that white FLS using white-black contrast showed a faster information transfer rate of SSVEP-based brain-computer interface than FLS using red,

green, or blue colors. Therefore, white FLS may entrain gamma rhythms as strong as or even better than red FLS if its contrast is optimized. In addition, as age increases, miosis and lenticular senescence [167, 168] increase, and becomes difficult to distinguish between short-wavelength colors such as green and blue [169]. There is also a risk of stereotyped discomfort [166] or epileptic seizures [170] given by the red color. Therefore, since there was no statistical difference in the adverse effects felt by white and red FLS in both young and old adults, it is reasonable to choose white FLS as an optimal color condition for an effective entrainment in humans. Since all previous clinical trials employed white light, the lack of consistent results between them might have not been attributable to the color of FLS.

FLS with high intensity or contrast was also found to induce stronger SSVEP than FLS with low intensity or contrast in humans [171-173]. In our study on young adults, the amplitudes of SSVEP entrained by 100 cd/m^2, 400 cd/m^2, and 700 cd/m^2 FLS were 182%, 261%, and 278% higher than those entrained by 10 cd/m^2 FLS at Pz and 204%, 312%, and 351% at Fz, respectively. Compared with the ERS entrained by 400 cd/m^2 FLS, ERS entrained by 700 cd/m^2 FLS was 107% and 112% stronger at Pz and Fz, respectively. The current study also demonstrated that stronger FLS could also entrain gamma rhythm more strongly and widely in older adults. Compared with the ERS entrained by 400 cd/m^2 FLS, ERS entrained by 700 cd/m^2 FLS was 107% and 103% stronger at Pz and Fz, respectively. In addition, ERS entrained by 700 cd/m^2 FLS was spread to 105% more nodes from the parieto-occipital region to frontotemporal region with 114% stronger connections than that entrained by 400 cd/m^2 FLS. In addition, ERS entrained by 700 cd/m^2 FLS was spread to 107% more nodes from the parieto-occipital region to frontotemporal region with 125% stronger connections than that entrained by 400 cd/m^2 FLS. In line with our study, previous studies had shown that 1,000 cd/m^2 FLS entrained 130% stronger SSVEP than 400 cd/m^2 FLS [174] and 1,400 cd/m^2 FLS entrained gamma rhythms more strongly and widely than 700 cd/m^2 FLS [175] in younger adults, and 377 cd/m^2 FLS entrained stronger gamma rhythm at both occipital and frontal electrodes than 192 cd/m^2 FLS in healthy older adults [175]. Although it is not fully understood yet how stronger light entrains stronger SSVEP, higher-amplitude light energy may induce more changes in the electrochemical properties of retinal photoreceptors and

673 nerve conduction of visual pathways to induce stronger SSVEP [176].

674 Even though the parameters of visual stimuli are optimized for entraining gamma waves in
675 older adults, the entrainment and propagation of gamma waves may not be uniform between individuals
676 because the impairment in the microstructural integrity of WM may be considerably different between
677 AD patients [81-85]. Although microstructural integrity of WM influences not only the coherence of
678 resting gamma waves [86, 87] but also the entrainment and propagation of gamma waves [40, 88-90],
679 none of the previous clinical trials included the presence or severity of WMH in their
680 inclusion/exclusion criteria for selecting participants nor adjusted them in their analysis on the effect of
681 FLS on AD pathologies and/or cognitive function.

682 EEG is known to be a measured superimposed dipole [177], and many consider pyramidal
683 neurons in cortical layers to be a major part of measured EEG [178]; however many studies show
684 functional connectivity of the brain is not only related to the cortical part of the brain, but also related
685 to the white matter integrity [86, 87, 89, 179-184]. According to Pamela Douglas et al., white matter
686 integrity can affect measured EEG through white matter axonal conduction [90]. In white matter
687 neuronal axon bundles that are aligned parallel to the scalp are likely to affect measured EEG. The
688 difference in intra and extracellular charge in the aligned axon allows dipoles to be formed. Another
689 thing to take note of is the existence of myelination of axonal bundles [185]. Myelinated neurons' fast
690 transduction speed (~2msec) [186] makes dipoles difficult to be superimposed, making reasonable un-
691 myelination a necessary condition [187]. It seems cortical U-fiber [188] and long distance cross fissural
692 fascicles [189] are the likeliest candidates. These arguments are yet to be proven, but the connection
693 between measured EEG and white matter integrity seem to be shown in a number of studies. Therefore,
694 change in EEG is related to the alternation of white matter microstructural integrity.

695 In particular, with aging, as the microstructural integrity of white matter fascicles and white
696 matter in the frontal lobe, temporal lobe, parietal lobe, and occipital lobe decreases, [81-83] the power
697 or synchronization of EEG decreased [86, 87, 89]. In the normal older adults group, FA, a measurement

used to determine the degree of neurodegeneration [190], of inferior fronto-occipital fasciculus, gamma/alpha EEG connectivity, and cognitive function performance have stronger positive correlations compared to younger adults [86, 87]. As a result, the relationship between FA and irrelevant information suppression function is mediated by gamma and alpha synchronization, explaining that reduced integrity leads to reduced synchrony between brain regions.

Therefore, the entrainment and propagation of gamma rhythms may be also influenced by the microstructural integrity of related WM tracts. The PTR, one of the projected branches from thalamocortical radiations to primary visual cortex [191], plays a key role in delivering information from retina to visual cortex, and thus their microstructural integrity may be a prerequisite for entraining gamma rhythms in visual cortex using FLS. Most branches of the PTR project to the primary visual cortex [125, 192, 193], and neuronal activation of the terminal branches of the thalamocortical radiation that project to primary sensory cortex affects excitatory post synaptic potentials (EPSPs) and involves in EEG responses [194]. In previous research, FA values of the PTRs were associated with the visual fixation score [195] and visual processing speed [196]. In the current study, although the FA values of PTRs were not linearly associated with the ERS entrained by FLS, the lowest quartile group of the FA value of PTR showed significantly lower ERS than the second-to-highest quartile group of the FA value of PTR in left hemisphere, indicating that the microstructural integrity of PTR may influence the entrainment of gamma using visual stimuli. However, such difference was not observed in right hemisphere in the current study, suggesting that gamma entrainment by visual stimuli may be lateralized due to the structural lateralization of the PTR. It is not statistically significant that FA value of PTR left is larger than that of PTR right ($t=0.241$, $p=0.812$), but the difference seems to be reflected. Postnatal maturation based on ocular dominance reinforces the hemisphere asymmetry of the PTR [197]. Right handedness has been shown to accompany left lateralized language function [198, 199] and left ocular dominance [200, 201], and the 26 participants in the study 2 were all right handed. In human, left PTR showed larger volume [192, 198, 202], higher number of fibers, higher FA, and lower mean diffusivity [200] than right PTR. Leftward asymmetry of PTRs was also found in postmortem human brains [202].

In addition, functional lateralization also could have influenced the gamma entrainment by FLS. Left visual cortex processes the visual stimuli of high frequency (approximately above 15Hz) faster than those of low frequency [203-205] Compared to right visual cortex, left visual cortex perceives high frequency stimuli more frequently in right handed people [206].

The MLFs and SLFs may play a key role in delivering information from visual cortex to other brain regions, and thus their microstructural integrity may be a prerequisite for propagating gamma rhythms in visual cortex entrained by FLS to other target brain regions such as temporal and frontal corticies. The MLFs that project from occipital area to temporal area [207] and SLFs that projects from parietooccipital area to middle frontal and inferior frontal area respectively [208] may influence brain rhythm propagated to the temporal/central and frontal area that was entrained by gamma rhythm [209]. In the current study, the FA values of MLFs and SLFs were significantly associated with the sGC values of the connectivities between corresponding brain regions after adjusting for ERS at Oz, and the lowest quartile groups of FA values of MLFs and SLFs showed significantly lower sGC values in all connectivities in left hemisphere. Gamma rhythm forms long-distance connectivity [209] and related to structural connectivity [210, 211]. Therefore, understanding the importance of microstructural integrity in propagation of gamma rhythm entrainment from posterior region to frontal or temporal region could be a pivotal role in developing a treatment using gamma rhythm entrainment. We believe our study has shown the relation between white matter integrity and visual entrainment and propagation. Optimal FLS did work, but lower white matter integrity was related to less entrainment and propagation. This could mean that patients with damaged white matter will have less effect from the FLS treatment. In the older adults whose WM microstructural integrity is impaired, it is required to entrain gamma waves directly in target brain regions using transcranial magnetic stimulation, transcranial direct current stimulation, transcranial alternating current stimulation, or transcranial ultrasound stimulation

SSVEP deficit is a failure of SSVEP induction, resulting in low SSVEP value [105, 106]. Thus, in order to use FLS as a treatment, it is necessary to first determine whether there is an SSVEP deficit

and present an optimized stimulus accordingly. Between the optimal and non-optimal conditions, optimal condition (White 700cd/m^2 32Hz: 16%) has shown less SSVEP deficit compared to non-optimal conditions (White 700cd/m^2 40Hz: 39%). Considering normal populations (18~55 years) have shown ~35% of SSVEP deficit in gamma rhythm (34-40 Hz) [212], optimal conditions did effectively reduce the number of SSVEP deficits. Additionally, SSVEP deficit increases with age [30], while WM integrity decreases with age [84]; and since SNR, a determinant for SSVEP deficit, also increases as the FA of the PTR increases [213], the information on the level of WM integrity may be useful for FLS treatment by estimating the amount of SSVEP deficit from targeted patients. Therefore, the result from our study suggests that the use of optimal FLS conditions and individual white matter integrity information can be applied for AD patients in clinical application to determine and increase the effectiveness of the FLS treatment.

For clinical application with FLS, determining and measuring adverse effects from FLS is an important step. In young adults, 700 cd/m^2 FLS showed more adverse effects than 400 cd/m^2 FLS, and some of their adverse effects were moderate to severe. Although 400 cd/m^2 entrained gamma rhythm slightly less than FLS 700 cd/m^2 FLS, it was more tolerable and still able to propagate strong gamma rhythm beyond visual cortex. To ensure that gamma rhythm is properly entrained in target brain regions with tolerable adverse effects, it is important to choose an appropriate light intensity. In older adults, adverse effects on 700 cd/m^2 FLS and 400 cd/m^2 FLS were mild and comparable between different intensities, and in a previous study with 10 patients with AD, patients only experienced mild adverse effects with light intensity of approximately 700 cd/m^2 FLS [64]. On the other hand, unlike older adults, our study on younger adults had more common and severe adverse effects in 700 cd/m^2 FLS compared with those in 400 cd/m^2 FLS. Older adults being more tolerable to stronger light than younger adults may be the reason for this difference, and their tolerance may be due to an age-associated increase of miosis and lenticular senescence [167, 168]. In both younger and older subjects, adverse effect for white and red color, which strongly

774 entrained gamma rhythm, were comparable. Therefore, considering all the adverse effect, 700 cd/m^2
775 with white color seems to be the optimal stimulus conditions for clinical application. Furthermore, we
776 were able to investigate the gamma entrainment by FLS of 32, 34 Hz and successfully propagated
777 gamma rhythm to the frontal and temporal areas, using optimized FLS without any additional sensory
778 stimulus may be effective to reduce AD pathologies.

779 Several previous studies employed auditory stimulation alone or in combination with visual
780 stimulation to entrain gamma waves [57, 64, 65]. However, they failed to clear AD pathologies the
781 brain regions other than auditory cortex using auditory stimulus alone [49, 51, 57]. In contrast, visual
782 stimuli could clear AD pathologies in frontal and temporal cortices as well as visual cortex [56, 59].
783 Gamma waves entrained by visual stimuli lasted twice as long as those entrained by auditory stimuli
784 [99]. Moreover, senile deafness increased in the adults aged 70 years or older [214] and central auditory
785 processing disorder that interferes the recognition of complex sounds was more prevalent in MCI [100,
786 101, 214]. Therefore, visual stimuli are far more effective and widely applicable than auditory stimuli
787 in entraining gamma waves in older adults, particularly in those with AD.

788 This study has several limitations. First, as mentioned above, the participants were healthy
789 volunteers. Optimal FLS intensity or frequency in patients with AD may be different from those in
790 healthy older adults. For instance, patients with AD showed smaller pupillary diameter than healthy
791 older controls [215, 216], and Aβ microaggregates in the lens may induce fluctuation of refractive index
792 increasing light scattering effect [217, 218]. In addition, comparing microstructural integrity between
793 healthy subjects may be not enough in finding the relationship of entrainment, propagation and
794 microstructural integrity as their difference in integrity value is miniscule to find a comparison. Second,
795 optimal FLS intensity and frequency for entraining gamma rhythm might be different between
796 individuals since the center frequency of gamma rhythm [28, 219] and the degree of miosis [220] and
797 lens senescence [221] could be different between individuals. Third, the effects of FLS on cognitive
798 performance or cerebral amyloid deposition were not examined. Fourth, the change of spontaneous

gamma by gamma entrainment and its relation with cognitive improvement are yet to be found; therefore, further research should study the effect of gamma entrainment on spontaneous gamma and the relation of changed spontaneous gamma with cognitive function. Fifth, due to volume conduction, the source signal will be spread out in the scalp making measured EEG not a direct measurement of the microstructural change of selected white matter ROI. In order to accurately determine the degree and effect of lateralization of microstructural integrity, it is necessary to conduct functional brain imaging studies in a follow-up study. Sixth, the sample size was small and subject to limited statistical power. Lastly, the long term effect of FLS was not examined in this study. Gamma entrainment by short duration FLS is believed to build up to eventually induce pathophysiological change in AD patients. Therefore, future study should apply these optimal parameters to find the pre post pathophysiological change and the effect of prolonged entrainment by the long term FLS stimuli for AD patients.

For further research, the limitation of individual difference needs to be addressed using customized sensory stimulation based on their white matter and center frequency. In addition, patients with enough microstructural brain damage is needed for elaborating a relationship between connectivity, functionality, and brain integrity. Gathering amyloid deposition and cognitive performance pre-post experiment should also be considered. Our study also cannot confidently relate ROI's with measured EEG due to the innate volume conduction property of EEG, therefore, doing a source analysis could solidify future arguments.

Despite these limitations, the current study reported the optimal visual stimulation parameters for gamma entrainment and the effect of WM microstructural integrity on the entrainment and propagation of gamma rhythms in older humans for the first time. We believe these results may contribute to improving efficacy of gamma entrainment using sensory stimuli and to specifying optimal therapeutic indications of gamma entrainment.

5. Conclusions

This study provides the optimal FLS conditions to most effectively induce gamma entrainment in humans. In human, gamma rhythms were more strongly entrained and widely propagated by FLSs with the higher luminal intensity and the longer wavelengths, which has never been investigated in animals. Compared to mice, gamma rhythms were more strongly entrained and widely propagated by FLSs with lower flickering frequency in humans. In addition, microstructural integrity of WM tracts played a pivotal role in delivering gamma rhythms entrained at visual cortex by FLS to other brain regions. These results are significant in that they provide the key evidence for developing gamma entrainment using visual stimulation as a new non-invasive intervention for preventing AD or modifying the course of AD and for designing clinical trials on the efficacy of gamma entrainment on AD properly.

Table 1. Summary of studies of EEG spontaneous/evoked power changes in aging

	Frequency band	Measured EEG	Power(μV^2)	Reference
Aging	Delta (1-4Hz),	spontaneous	Decrease	Jeong, J.,2004 [22] Jelic, V., et al., 2000[23]
		evoked	Decrease	Rossini, P.M., et al.,2007[31] Güntekin, B. and E. Başar, 2016 [32]
	Theta (4-7Hz),	spontaneous	Decrease	Adler, G., et al. 2004[24] Onofrj, M., et al.,2003[25]
		evoked	Decrease	Sridhar and Manian, 2019[30] Rossini, P.M., et al.,2007[31]
	Alpha (8-12Hz),	spontaneous	-	Onofrj, M., et al.,2003[31] Özbek, Y., E. Fide, and G. Yener, 2021[26]
		evoked	Decrease	Sridhar and Manian, 2019[30]
	Beta (13-30Hz),	spontaneous	-	Ko, J., et al., 2021[27]
		evoked	Decrease	Sridhar and Manian, 2019[30]
	Gamma (30-100Hz)	spontaneous	Increase	Ko, J., et al., 2021[27] Murty, D.V.P.S., et al.,2020[28] Jabès, A., et al.,2021[29]
		evoked	Decrease	Murty, D.V.P.S., et al.,2020[28] Griskova-Bulanova, I.,2013[33]

Table 2. Summary of studies of EEG spontaneous/evoked power changes in Alzheimer's disease

	Frequency band	Measured EEG	Power(μV^2)	Reference
Alzheimer's disease	Delta (1-4Hz),	spontaneous	Decrease	Soininen, H., et al., 1991[36] Jelic, V., et al., 1996[37]
		evoked	Decrease	Rossini, P.M., et al., 2007[31] Basar, E. and B 2013[41] Başar, E., 2013[42]
	Theta (4-7Hz),	spontaneous	Decrease	Soininen, H., et al., 1991[36] Jelic, V., et al., 1996[37]
		evoked	Decrease	Koenig, T.,et al., [44] Rossini, P.M., et al., 2007[31]
	Alpha (8-12Hz),	spontaneous	-	Dierks, T., et al., 1991[38] Pozzi, D., et al., 1995[39]
		evoked	Decrease	Rossini, P.M., et al., 2007[31]
	Beta (13-30Hz),	spontaneous	-	Pozzi, D., et al., 1995[39]
		evoked	Decrease	Koenig, T.,et al., [44] Basar, E. and B 2013[42]
	Gamma (30-100Hz)	spontaneous	Increase	Babiloni, C., et al., 2021[40]
		evoked	Decrease	Basar, E. and B, 2013[41] Rossini, P.M., et al., 2006[43]

Table 3. Summary of studies of gamma entrainment on Alzheimer's disease patients

Stimuli type	Treatment	Control	N	Measurement	Result	Reference
FLS (40Hz)	2hour/days *10days		AD 6	[11C]PiB PET ,PiB SUVR values	After 10 days treatment, no significant decrease of PiB SUVR values in V1, V2, parietal region, and precuneus	Ismail, R., et al. 2018 [63]
tACS (40 Hz)	30min/days *5days/weeks *4weeks	no-tACS	AD 17	Wechsler memory scale, Montgomery-Asberg depression rating scale	Memory improvement in the active and sham group which maintained in the active group after 1 month	Kehler, L., et al., 2020[222]
FLS + CT (40 Hz)	1hour/days *32days		MCI 10	CSF immune factors, CSF Aβ42, CSF t-tau, CSF p-tau, functional connectivity (fMRI), EEG, adverse effect	Altered cytokines and immune factors in the CSF and increased functional connectivity in the DMN with mild adverse effects	He, Q., et al., 2021 [64]
FLS + CT (40 Hz)	1hour/days *90days	White noise+ contrast light	AD 8 treatment /AD 7 control	EEG, MRI, connectivity (fMRI), actigraphy, cognitive assessments	The 40Hz sensory stimuli improved visuospatial task accuracy , connectivity, circadian rhythmicity, brain atrophy increase.	Chan,D., et al., 2021 [65]
tACS (40 Hz)	1hour tACS over Pz	Sham stimulation	MCI 20	Cognitive assessments and indirect measures of cholinergic transmission	Memory performance and restoration of intracortical connectivity improved comparison to sham therapy	Benussi, A., et al., 2021[223]
TMS (40 Hz)	30 rTMS trials/days * 3days/weeks * 4weeks	Sham stimulation	AD37,NC41	Neuropsychological assessments, MRI, EEG	Neuropsychological assessment score, spontaneous gamma-band power, connectivity within the brain increased in AD patients.	Liu, C., et al.,2021 [48]

FLS, flickering light stimuli; CT, click train; tACS, transcranial alternating current stimulation; TMS, transcranial magnetic stimulation; MCI, mild cognitive impairment; fMRI, functional magnetic resonance imaging; PiB SUVR, Pittsburgh compound B standard uptake value ratio; CSF, cerebrospinal fluid; DMN, default mode network.

Table 4. Summary of studies of gamma entrainment with sensory stimuli listed chronologically within each section

Stimuli type	Stimulus frequency	N	Measure	Result	Reference
Gamma entrainment with visual stimuli					
FLS	1-100 Hz, 1-Hz steps	Y10	Power spectrum density	The steady-state potentials exhibited clear resonance phenomena around 10, 20, 40 and 80 Hz, while above 60 Hz elicited small amplitude responses.	Herrmann, C. 2001[73]
FLS	5, 10, 12, 15, 17, 20, 22, 25, 27, 30, 35, 40, 47, and 60 Hz	Y16	Power spectrum density	Stimulation at frequencies of >30 Hz activated only the primary and association cortex representing the macular region of the retina	Pastor, M., et al. 2004[71]
FLS	13, 32Hz	Y1	Coherence	32Hz synchronized wider than 16Hz in the whole brain area.	Vialatte FB.,et al. 2009[62]
SF	3cycles per degree	Y30	Evoked field peak latency and Evoked field amplitude	Gamma frequency tends to decline with age and is positively correlated with the thickness of the pericalcarine cortex.	Muthukumaraswamy, S.D., et al. 2010[97]
FLS	40-60 Hz, 2- Hz steps	Y32	Event-related synchronization/	SSVEP was more localized around the parieto-occipital sites for higher frequencies (>54 Hz) and spread to frontocentral locations for lower frequencies	Tsoneva, T., G. Garcia-Molina, and P. Desain 2015[74]
FLS	40Hz, 60Hz, and 80 Hz	Y3	Power spectrum density	Largest amplitudes for the high intensity 40Hz stimulus were consistently found at the primary FLS cortex.	Jones, M., et al. 2019[175]
FLS	40–60 Hz	Y32	Event related synchronization, Source localization, Phase synchrony analysis	Lower frequency conditions are characterized by a broader response compared to higher frequencies, which propagated to fronto-central sites.	Tsoneva, T., G. Garcia-Molina, and P. Desain 2021[111]
FLS	40Hz	Y20	Power spectrum density	Peak amplitude of VEP with 40 Hz violet light was smaller than that of 40 Hz white light in occipital area.	Noda Y., et al. 2021 [224]

FLS	40Hz	Y13	Power spectrum density	The 40 Hz neural activity were significantly higher in signal-to-noise ratio during exposure to spectral flicker compared to continuous light.	Agger MP., et al. 2022 [225]
SF	1.5 cycle/deg	Y30	Magnetoencephalography , evoked power, Source localization	Red stimuli induced stronger gamma power above 30 Hz versus non-red colors, while Blue stimuli showed no or very weak increase in gamma-power at V1.	Benjamin, J S., et al. 2022 [226]
FLS	Flickering image 'Rubin's vase' 8 Hz, 36 Hz	Y10 O54	Power spectrum density	The difference in cerebral rhythmic activity between the alpha and gamma bands is associated with age and cognitive status	Horwitz, A., et al. 2017[75]
SF	1, 2, and 4 cycle/deg, 16 cycles/s	Y47 O227	Power spectrum density	Power and center frequency of slow and fast gamma decreased with age	Murty, D.V.P.S., et al. 2020[28]
FLS	22, 25, 40, 60Hz	Y, M, O 1464	Amplitude	Age affects induced gamma activity, but advanced age does not fundamentally change the behavior of the response in either magnitude or spatial distribution.	Zibrandtsen IC, Agger M, Kjaer TW. 2020 [227]
Gamma entrainment with auditory stimuli					
CT	3.3, 10, 20 and 40Hz	Y20	Amplitude	Latency and amplitude measurements on the 40-Hz ERP indicates that it may contain useful information on the number and basilar membrane location of the auditory nerve fibers. Adequate processing of sensory information may require cyclical brain events in the 30- to 50-Hz range	Galambos, R., S. Makeig, and P.J. Talmachoff, 1981[50]
CT	20, 30 and 40 Hz	Y, M30 (HC15,SZ15)	Power spectra, Phase delay	In normal subjects, the 40Hz ASSR response is bigger than the schizophrenia patients. There was no phase delay in normal subjects unlike schizophrenia patients.	Kwon, J.S., et al., 1999[49]
CT	12, 20, 30, 32, 35, 37.5, 40, 42.5, 45, 47.5, 50, and 60 Hz	Y28	Amplitude	40 Hz selectively activated the auditory region of the pontocerebellum, a brain structure with important roles in cortical inhibition and timing.	Pastor, M.A., et al., 2002[95]
CT	32, 40 and 48 Hz	Y20	Evoked power, Phase-locking	Frequency main effect indicated that the 40 and 48 Hz	Rojas, D.C., et al.,

			factor	modulators had significantly greater induced power reductions than the 32 Hz condition	2011[91]
CT	20, 30, and 40 Hz.	Y21	Intertrial phase coherence, Event-related spectral perturbation	The 40 Hz most powerfully activated the auditory and in frontal region	Tada, M., et al., 2016[51]
CT	40 Hz	Y28	Phase-locking index, Event-related power perturbation	The 40-Hz ASSR has positive correlation with late-latency gamma and planning and problem-solving abilities.	Parciauskaite, V., et al., 2019[94]
CT	25 Hz, 40 Hz and 100 Hz	Y9	-	Improvement in remembering a sentence, solving a mathematical problem scores within gamma 40 Hz entrainment frequency population	Sharpe RLS., et al., 2020 [228]
CT	40Hz	Y14	Evoked power, Source localizations	The time courses of 40Hz ASSR amplitude and phase during recovery from the decrement resembled those after stimulus onset, indicating that a new ASSR was built up after the resetting stimulus.	Ross, B., A.T. Herdman, and C. Pantev,, 2005[92]
CT	40Hz	Y12 M11 O10	Amplitude, Phase delay	The ASSRs were interpreted in relation to oscillatory gamma-band activity representing auditory object representation.	Ross, B., 2008[93]
CT	40Hz	Y, M 46	Amplitude, Phase-locking index	The ability to synchronize to high frequency external stimulation diminishes with age.	Griskova-Bulanova, I., K. Dapšys, and V. Maciulis, 2013 [33]
Gamma entrainment with visual/ auditory stimuli					
FLS/ CT	40Hz	Y15	Wavelet coefficients	The FLS evoked response of gamma oscillations lasts longer than the auditory evoked response.	Sakowitz, O.W., et al., 2001[99]
FLS/ CT	40Hz	Y13 O12	Global coherence	The evoked potential power of young adults is greater than that of the elderly, and the evoked potential power of FLS stimuli is greater than that of auditory, at 40 Hz.	Chan, D., et al., 2021[65]

FLS, flickering light stimuli; SF, spatial frequency; CT, click train Y, young adults; M, mid aged adults; O, older adults; HC, healthy control; SZ, schizophrenia patient;

Table 5. Demographic and clinical characteristics of the participants

	SS-1 of the Study-1	SS-2 of the Study-1	Study 2
Numbers	16	35	26
Age, years*	24.0 ± 3.7	70.0 ± 2.4	69.81 ± 2.39
Women, %	43.8	51.4	48.4
Education, years*	14.9 ± 2.2	11.43 ± 4.91	11.68 ± 4.51
MMSE*	-	28.17 ± 2.05	28.26 ± 1.87
GDS*	-	7.06 ± 4.97	7.52 ± 5.06

MMSE, Mini Mental Status Exam; GDS, Geriatric Depression Scale; SS, sub-study

*Presented as mean ± stand

Table 6. Effects of the relative powers of resting electroencephalography on the Mini Mental Status Examination scores *

	B	SE	β	t	*p*	R^2	adjusted R^2
At Fz							
Delta	-1.105	9.235	-0.023	-0.120	0.905	0.001	-0.062
Theta	20.764	16.452	0.219	1.262	0.216	0.048	-0.012
Alpha	8.433	6.833	0.215	1.234	0.226	0.046	-0.014
Beta	-13.592	11.998	-0.203	-1.133	0.266	0.039	-0.021
Low-low gamma	-57.322	23.943	-0.404	-2.394	**0.023**	0.152	0.099
Low-high gamma	-61.039	40.328	-0.259	-1.514	0.140	0.067	0.009
High gamma	-35.486	39.724	-0.160	-0.893	0.378	0.024	-0.037
At Cz							
Delta	-5.954	7.882	-0.144	-0.755	0.456	0.018	-0.044
Theta	23.614	13.261	0.302	1.781	0.084	0.090	0.033
Alpha	10.205	7.314	0.242	1.395	0.173	0.057	-0.001
Beta	-2.807	11.755	-0.044	-0.239	0.813	0.002	-0.060
Low-low gamma	-57.116	19.959	-0.473	-2.862	**0.007**	0.204	0.154
Low-high gamma	-64.953	37.173	-0.299	-1.747	0.090	0.087	0.030
High gamma	-63.582	44.232	-0.250	-1.437	0.160	0.061	0.002
At Pz							
Delta	-5.826	7.644	-0.134	-0.762	0.452	0.018	-0.043
Theta	18.159	11.914	0.260	1.524	0.137	0.068	0.010
Alpha	11.601	6.582	0.300	1.762	0.088	0.089	0.032
Beta	-17.060	14.138	-0.211	-1.207	0.236	0.044	-0.016
Low-low gamma	-64.922	25.060	-0.418	-2.591	**0.014**	0.173	0.122
Low-high gamma	-58.052	32.434	-0.308	-1.790	0.083	0.091	0.034
High gamma	-49.987	30.982	-0.286	-1.613	0.116	0.075	0.018

SE, standard error; Delta = 1-4 Hz; Theta = 4-7 Hz; Alpha = 8-12 Hz; Beta = 13-30Hz; Low-low gamma = 30-38 Hz; Low-high gamma = 40-48 Hz; High gamma ≥ 50 Hz

*Linear regression analyses adjusting for age

Table 7. Effects of the absolute powers of resting electroencephalography on the Mini Mental Status Examination scores *

	B	SE	β	t	*p*	R^2	adjusted R^2
At Fz							
Delta	0.713	0.941	0.135	0.758	0.454	0.018	-0.044
Theta	1.391	1.245	0.194	1.118	0.272	0.038	-0.022
Alpha	1.316	1.010	0.225	1.304	0.202	0.051	-0.009
Beta	-1.062	2.886	-0.067	-0.368	0.715	0.004	-0.058
Low-low gamma	-5.881	5.205	-0.204	-1.130	0.267	0.038	-0.022
Low-high gamma	-11.206	14.044	-0.142	-0.798	0.431	0.020	-0.042
High gamma	-12.317	22.752	-0.095	-0.541	0.592	0.009	-0.053
At Cz							
Delta	0.451	0.687	0.118	0.656	0.517	0.013	-0.048
Theta	1.067	0.890	0.208	1.199	0.239	0.043	-0.017
Alpha	1.425	0.981	0.250	1.453	0.156	0.062	0.003
Beta	0.760	2.508	0.055	0.303	0.764	0.003	-0.059
Low-low gamma	-6.285	4.243	-0.267	-1.481	0.148	0.064	0.006
Low-high gamma	-6.918	9.975	-0.129	-0.694	0.493	0.015	-0.047
High gamma	-40.269	23.781	-0.288	-1.693	0.100	0.082	0.025
At Pz							
Delta	0.746	1.082	0.121	0.689	0.496	0.015	-0.047
Theta	1.413	1.031	0.236	1.371	0.180	0.056	-0.003
Alpha	1.124	0.772	0.250	1.456	0.155	0.062	0.004
Beta	0.578	3.307	0.032	0.175	0.862	0.001	-0.061
Low-low gamma	-6.953	8.234	-0.149	-0.844	0.405	0.022	-0.039
Low-high gamma	-8.600	14.704	-0.103	-0.585	0.563	0.011	-0.051
High gamma	-21.738	19.390	-0.196	-1.121	0.271	0.038	-0.022

SE, standard error; Delta = 1-4 Hz; Theta = 4-7 Hz; Alpha = 8-12 Hz; Beta = 13-30Hz; Low-low gamma = 30-38 Hz; Low-high gamma = 40-48 Hz; High gamma ≥ 50 Hz

*Linear regression analyses adjusting for age

Table 8. Self-reported adverse effects of flickering light stimulation in the sub-study 1 of the study 1 on younger adults

	Color						Intensity					
	White[a]	Red[b]	Green[c]	Blue[d]	F	Post hoc	10 cd/m^2 [a]	100 cd/m^2 [b]	400 cd/m^2 [c]	700 cd/m^2 [d]	F	Post hoc
Fatigue	2.1 (1.8)	2.1 (1.8)	1.3 (1.9)	1.7 (1.9)	1.84	-	1.2 (1.3)	2.0 (1.7)	2.1 (1.8)	2.8 (2.0)	**7.85****	d > a, c
Headache	0.1 (0.3)	0.1 (0.3)	0.2 (0.5)	0 (0)	1.00	-	0 (0)	0.1 (0.3)	0.3 (0.9)	0.6 (1.1)	3.02	
Dizziness	2.3 (2.0)	1.3 (1.4)	1.6 (1.5)	1.4 (1.6)	2.75		1.4 (1.3)	1.6 (1.1)	1.2 (1.2)	1.2 (1.2)	1.37	
Dazzling	1.9 (1.7)	2.6 (1.8)	1.4 (1.2)	2.3 (2.1)	**3.12***		1.4 (1.0)	2.7 (1.4)	3.6 (1.5)	4.7 (1.3)	**47.00*****	d > c > b > a
Asthenopia	2.3 (1.3)	2.6 (1.6)	1.4 (1.2)	2.4 (1.9)	**5.43***	a, b>c	1.6 (1.1)	2.2 (1.6)	2.7 (1.7)	3.6 (1.9)	**15.66*****	d > a, b, c > a
Ocular pain	0.4 (0.7)	0.6 (1.25)	0.1 (0.3)	0.6 (1.2)	1.78	-	0.3 (0.8)	0.6 (1.0)	1.0 (1.4)	1.7 (1.8)	**9.23****	d > a, b, c

$^{*}p < 0.05$, $^{**}p < 0.01$, $^{***}p < 0.001$ by repeated measures analysis of variance.

Table 9. Self-reported adverse effects of flickering light stimulation in in the sub-study 2 of the study 1 on older adults

	White and 400 cd/m^2	White and 700 cd/m^2	Red and 400 cd/m^2	Red and 700 cd/m^2	F*	*p*
Fatigue	1.3 (2.0)	1.3 (1.8)	1.0 (1.7)	1.0 (1.8)	0.01	1.000
Headache	0.4 (1.2)	0.5 (1.2)	0.4 (1.2)	0.3 (1.2)	0.09	0.761
Dizziness	1.1 (1.8)	1.1 (1.6)	1.1 (1.8)	0.9 (1.6)	0.13	0.726
Dazzling	2.0 (1.8)	2.1 (2.0)	2.0 (2.0)	2.2 (1.9)	0.57	0.454
Asthenopia	1.6 (1.8)	1.3 (1.9)	1.4 (1.6)	1.6 (1.9)	2.96	0.094
Ocular pain	0.1 (0.7)	0.0 (0.2)	0.1 (0.3)	1.1 (0.7)	0.67	0.419

*repeated measures analysis of variance

Table 10. Comparison of the event-related synchronization of gamma rhythms at Oz entrained by flickering light stimulation between the groups with the low and high fractional anisotropy of posterior thalamic radiations

	Left posterior thalamic radiation				Right posterior thalamic radiation			
	HFA (n = 20)	LFA (n = 6)	Statistics*		HFA (n = 20)	LFA (n = 6)	Statistics*	
			t	*p*			t	*p*
Fractional anisotropy	0.567 ± 0.024	0.519 ± 0.031	3.505	**0.010**	0.567 ± 0.029	0.514 ± 0.018	5.436	**<0.001**
Event-related synchronization	13.689 ± 4.390	9.486 ± 3.753	2.310	**0.045**	12.552 ± 4.922	13.277 ± 3.329	-0.415	0.685

HFA, second-to-highest quartile group of the fractional anisotropy values of posterior thalamic radiations; LFA, the lowest quartile group of the fractional anisotropy values of posterior thalamic radiations

All values are presented as mean ± standard deviation

*Student t-test

Table 11. Effects of the fractional anisotropy of middle and superior longitudinal fasciculi on the spectral Granger Causality of the connectivities from visual cortex to other brain regions*

	B	SE	β	t	*p*	R^2	adjusted R^2
FA of left MLF							
sGC from occipital to left temporal	5.166	2.203	0.294	2.345	**0.028**	0.641	0.610
sGC from occipital to left central	5.262	1.191	0.349	4.418	**< 0.001**	0.854	0.845
FA of right MLF							
sGC from occipital to right temporal	4.082	1.782	0.253	2.290	**0.032**	0.721	0.697
sGC from occipital to right central	6.033	1.671	0.363	3.611	**0.001**	0.768	0.748
FA of left SLF 2							
sGC from occipital to left frontal 1	3.688	2.557	0.131	1.442	0.163	0.813	0.796
sGC from occipital to left frontal 2	4.670	2.271	0.183	2.057	0.051	0.821	0.805
FA of right SLF 2							
sGC from occipital to right frontal 1	4.831	2.139	0.175	2.259	**0.034**	0.862	0.850
sGC from occipital to right frontal 2	7.233	2.425	0.263	2.982	**0.007**	0.821	0.806
FA of left SLF 3							
sGC from occipital to left frontal 1	5.811	2.811	0.180	2.067	**0.050**	0.828	0.813
sGC from occipital to left frontal 2	7.087	2.416	0.241	2.933	**0.007**	0.846	0.832
FA of right SLF 3							
sGC from occipital to right frontal 1	8.180	2.432	0.236	3.363	**0.003**	0.887	0.877
sGC from occipital to right frontal 2	10.352	2.867	0.300	3.611	**0.001**	0.842	0.828

SE, standard error; FA, fractional anisotropy; MLF, middle longitudinal fasciculus; sGC; spectral Granger Causality; SLF, superior longitudinal fasciculus; frontal 1, fore of middle to inferior frontal area; frontal 2, rear of middle to inferior frontal area;

*Multiple linear regression analyses adjusting for the event-related synchronization values of entrained gamma rhythms at Oz

Table 12. Comparison of the spectral Granger Causality of the connectivities from visual cortex to other brain regions between the groups with the low and high fractional anisotropy of middle and superior longitudinal fasciculi

	Left				Right			
	HFA (n = 20)	LFA (n = 6)	Statistics*		HFA (n = 20)	LFA (n = 6)	Statistics*	
			t	*p*			t	*p*
FA of MLF	0.47 ± 0.13	0.43 ± 0.14	5.704	**<0.001**	0.48 ± 0.17	0.44 ± 0.11	6.206	**<0.001**
sGC from occipital to temporal	0.56 ± 0.36	0.22 ± 0.15	3.419	**0.008**	0.51 ± 0.36	0.37 ± 0.34	0.906	0.389
sGC from occipital to central	0.54 ± 0.31	0.23 ± 0.16	3.306	**0.008**	0.56 ± 0.38	0.30 ± 0.25	1.903	0.080
FA of SLF 2	0.37 ± 0.12	0.34 ± 0.01	7.014	**<0.001**	0.36 ± 0.01	0.33 ± 0.16	4.448	**0.004**
sGC from occipital to frontal 1	0.76 ± 0.52	0.38 ± 0.26	2.417	**0.027**	0.75 ± 0.49	0.55 ± 0.48	0.862	0.413
sGC from occipital to frontal 2	0.75 ± 0.47	0.35 ± 0.23	2.841	**0.011**	0.77 ± 0.49	0.50 ± 0.40	1.372	0.200
FA of SLF 3	0.36 ± 0.12	0.33 ± 0.01	6.326	**<0.001**	0.36 ± 0.01	0.34 ± 0.01	4.927	**0.001**
sGC from occipital to frontal 1	0.78 ± 0.52	0.35 ± 0.21	2.955	**0.007**	0.79 ± 0.50	0.39 ± 0.26	2.593	**0.019**
sGC from occipital to frontal 2	0.76 ± 0.46	0.31 ± 0.17	2.267	**0.033**	0.80 ± 0.49	0.37 ± 0.26	2.817	**0.012**

HFA, the second-to-highest quartile group of the fractional anisotropy values of middle longitudinal fasciculus or superior longitudinal fasciculus; LFA, the lowest quartile group of the fractional anisotropy values of middle longitudinal fasciculus or superior longitudinal fasciculus; FA, fractional anisotropy; FA, fractional anisotropy; MLF, middle longitudinal fasciculus; sGC; spectral Granger Causality; SLF, superior longitudinal fasciculus; frontal 1, fore of middle to inferior frontal area; frontal 2, rear of middle to inferior frontal area;

All values are presented as mean ± standard deviation

*Student t-test

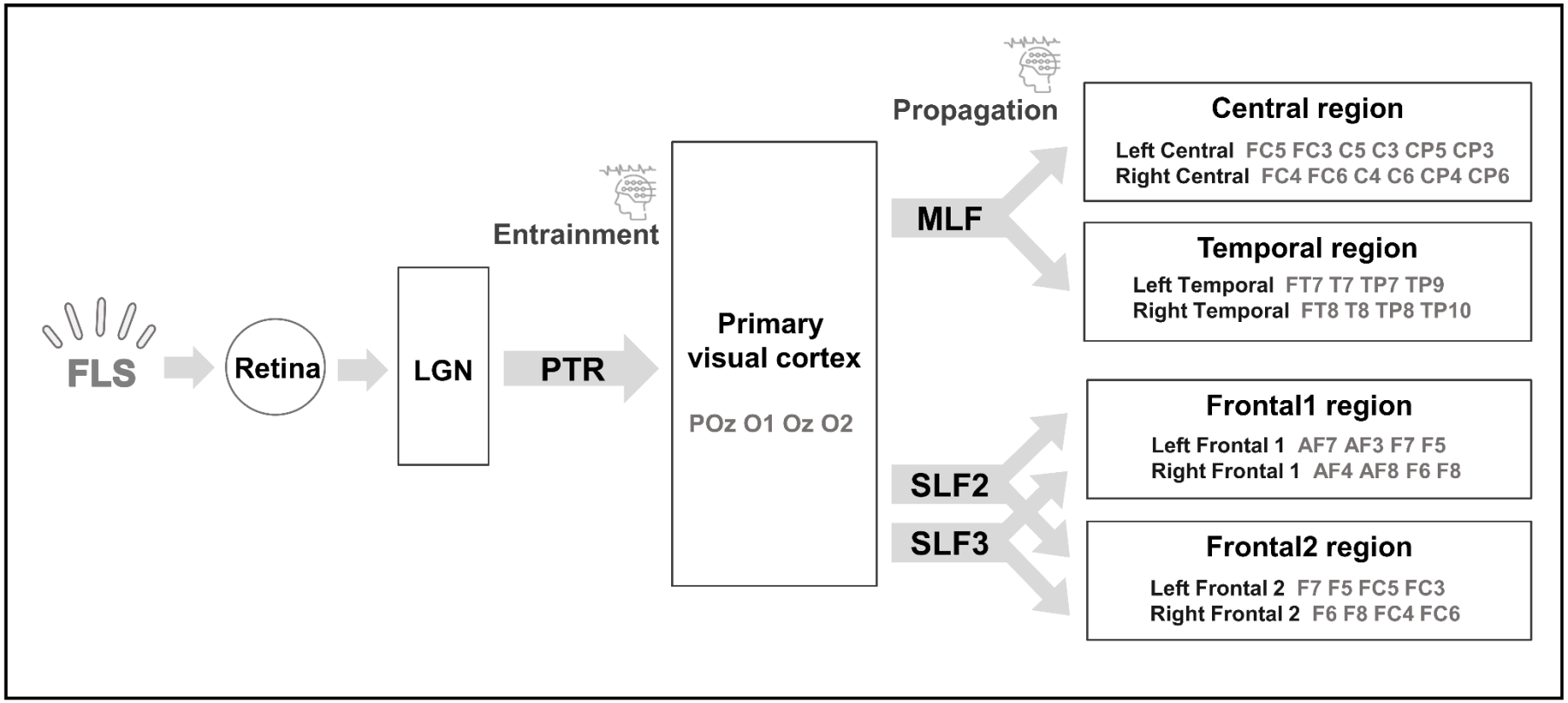

Figure 1. White matter tracts involved in the entrainment of gamma rhythms at visual cortex by flickering light stimulation and the propagation of entrained gamma rhythms from visual cortex to other target brain regions

FLS, flickering light stimulation; PTR, right posterior thalamic radiation; SLF 2, superior longitudinal fasciculus 2; SLF 3, superior longitudinal fasciculus 3; Frontal 1, fore of middle to inferior frontal area; Frontal 2, rear of middle to inferior frontal area;

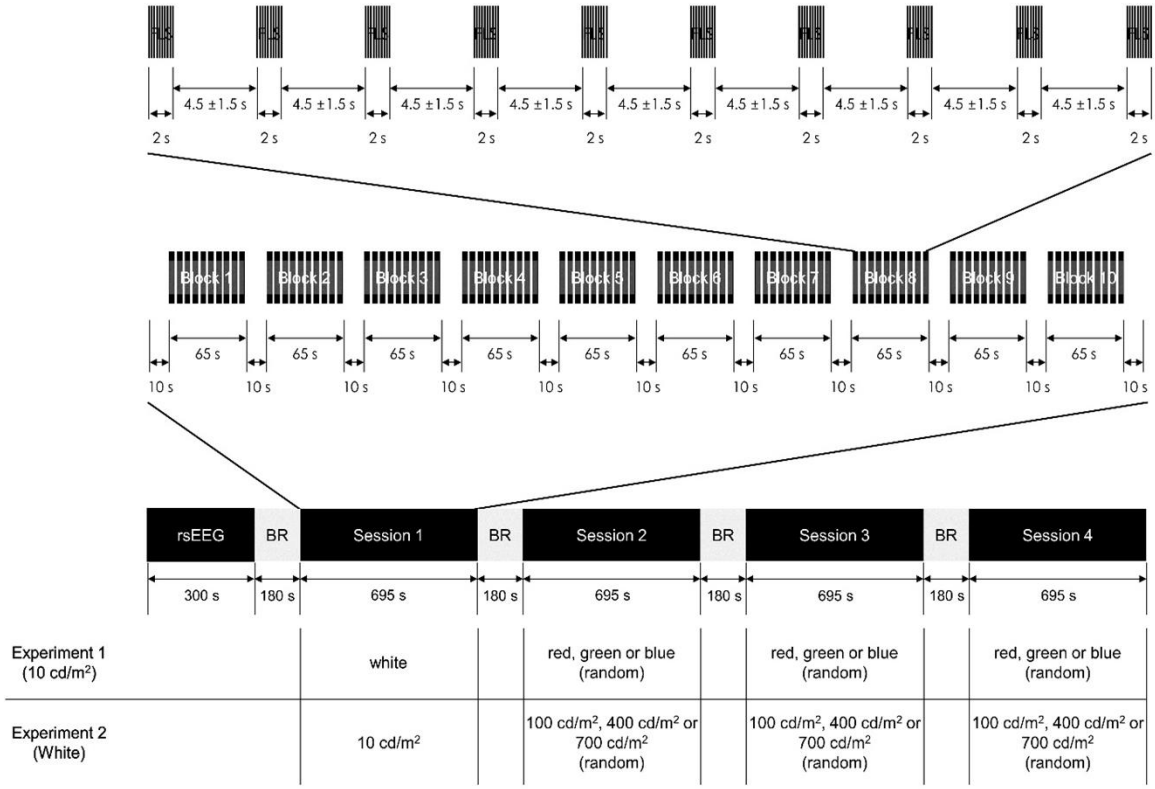

Figure 2. Experimental procedures of the sub-study 1 of the study 1

FLS, flickering light stimulation; rsEEG, resting-state electroencephalogram; BR, break

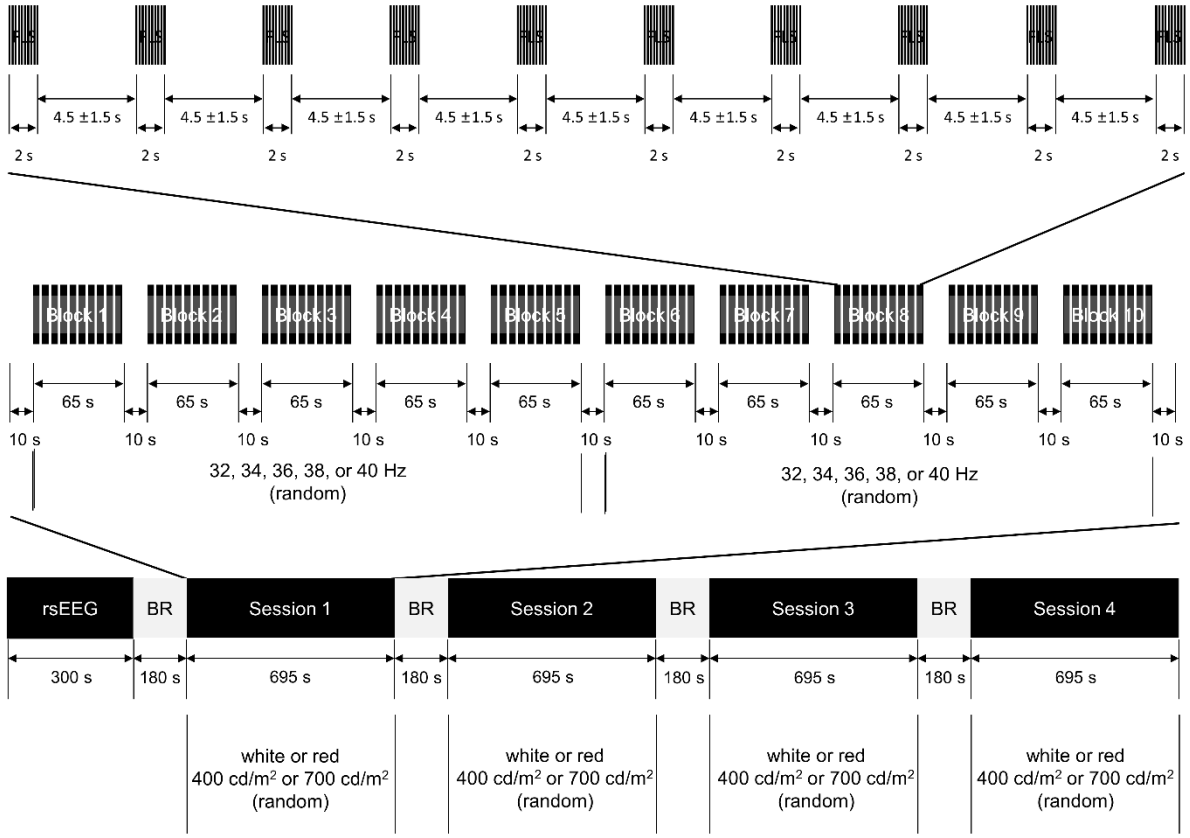

Figure 3. Experimental procedures of the sub-study 2 of the study 1

FLS, flickering light stimulation; rsEEG, resting-state electroencephalogram; BR, break

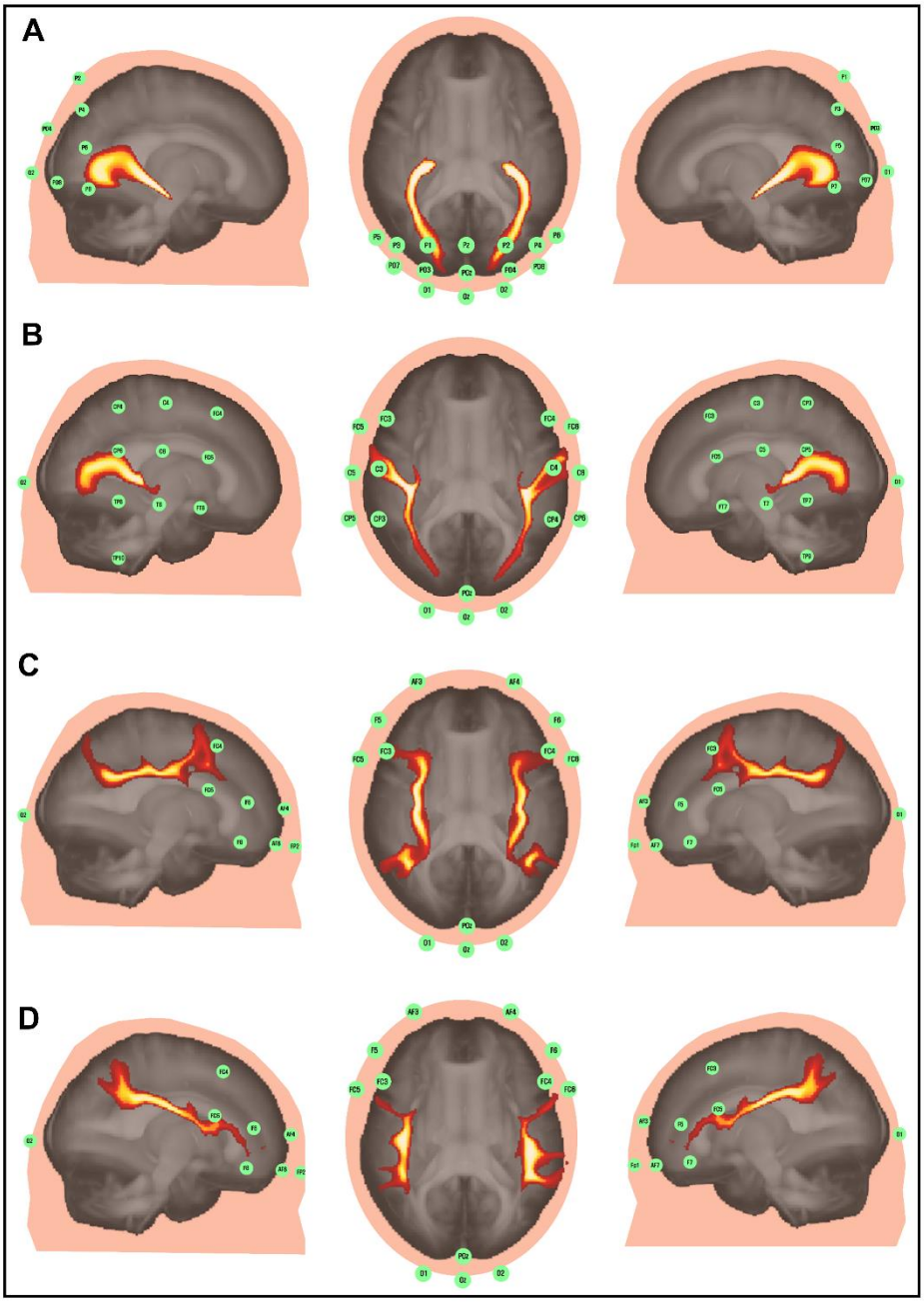

Figure 4. Electroencephalography channels over posterior thalamic radiation and white matter tracts of occipital-temporal, central direction and parietooccipital- frontal direction. (A) EEG channels for PTR: Oz (B) EEG channels for MLF: left temporal FT7, T7, TP7, TP9; left central FC5, FC3, C5, C3, CP5, CP3; right temporal FT8, T8, TP8, TP10; right central FC4, FC6, C4, C6, CP4, CP6; occipital POz, O1, Oz, O2 (C) EEG channels for SLF 2: left frontal 1 AF7, AF3, F7, F5; left frontal 2

F7, F5, FC5, FC3; right frontal 1 AF4, AF8, F6, F8; right frontal 2 F6, F8, FC4, FC6; occipital POz, O1, Oz, O2 ; (D) EEG channels for SLF 3: left frontal 1 AF7, AF3, F7, F5; left frontal 2 F7, F5, FC5, FC3; right frontal 1 AF4, AF8, F6, F8; right frontal 2 F6, F8, FC4, FC6; occipital POz, O1, Oz, O2

PTR, posterior thalamic radiation; MLF, middle longitudinal fasciculus; SLF 2, superior longitudinal fasciculus 2; SLF 3, superior longitudinal fasciculus 3

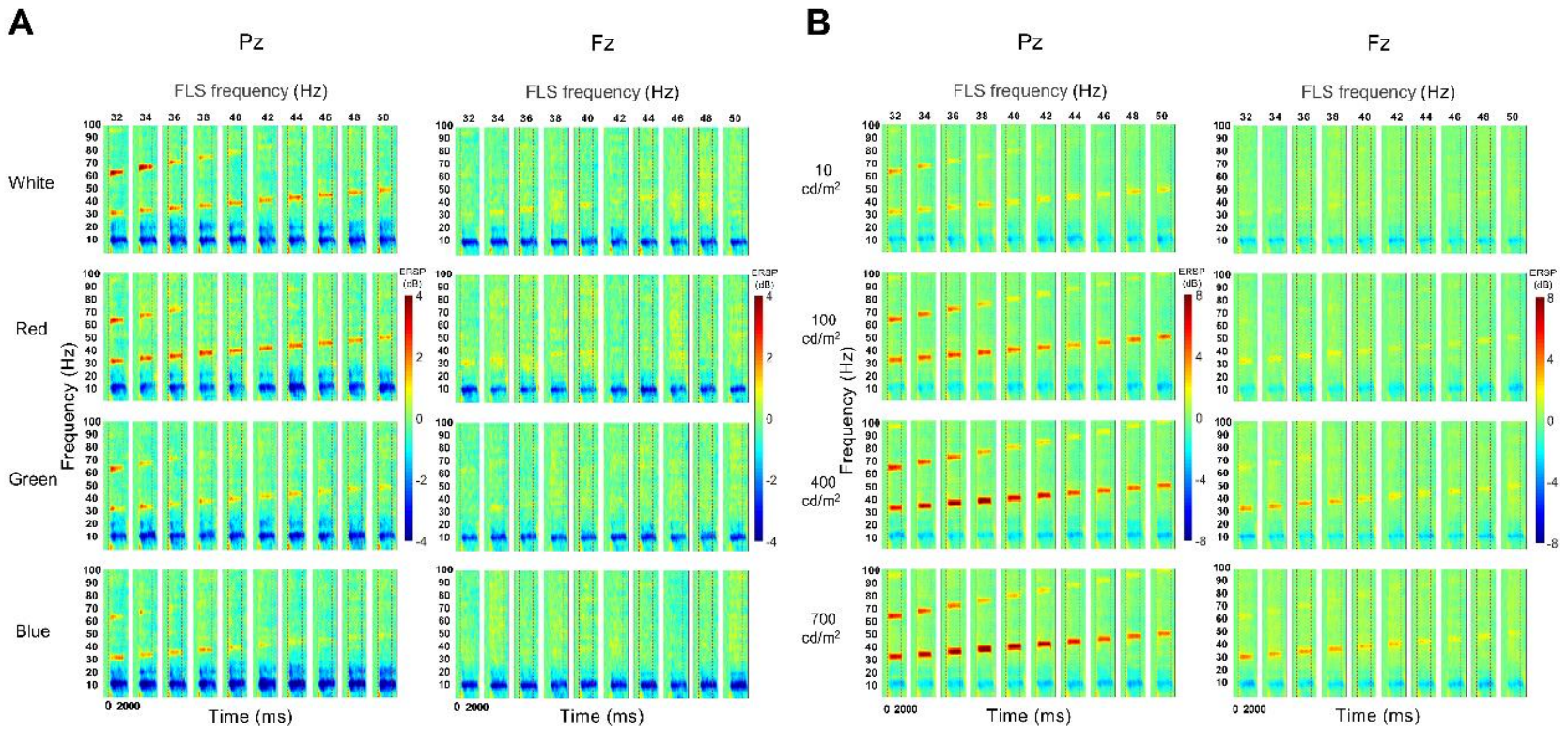

Figure 5. Comparisons of the grand-average event-related spectral perturbation of steady-state visually evoked potentials induced by flickering light stimulus in younger adults between different parameters of the flickering light stimulation in the sub-study 1 of the study 1

Each column shows ERSP from 750 ms before the onset of FLS to 750 ms after the offset of flickering light stimulation

(A) Comparison between colors in the experiment 1 of the sub-study 1 of the study 1

(B) Comparison between intensities in the experiment 2 of the sub-study 1 of the study 1

FLS, flickering light stimulation; ERSP, event-related spectral perturbation

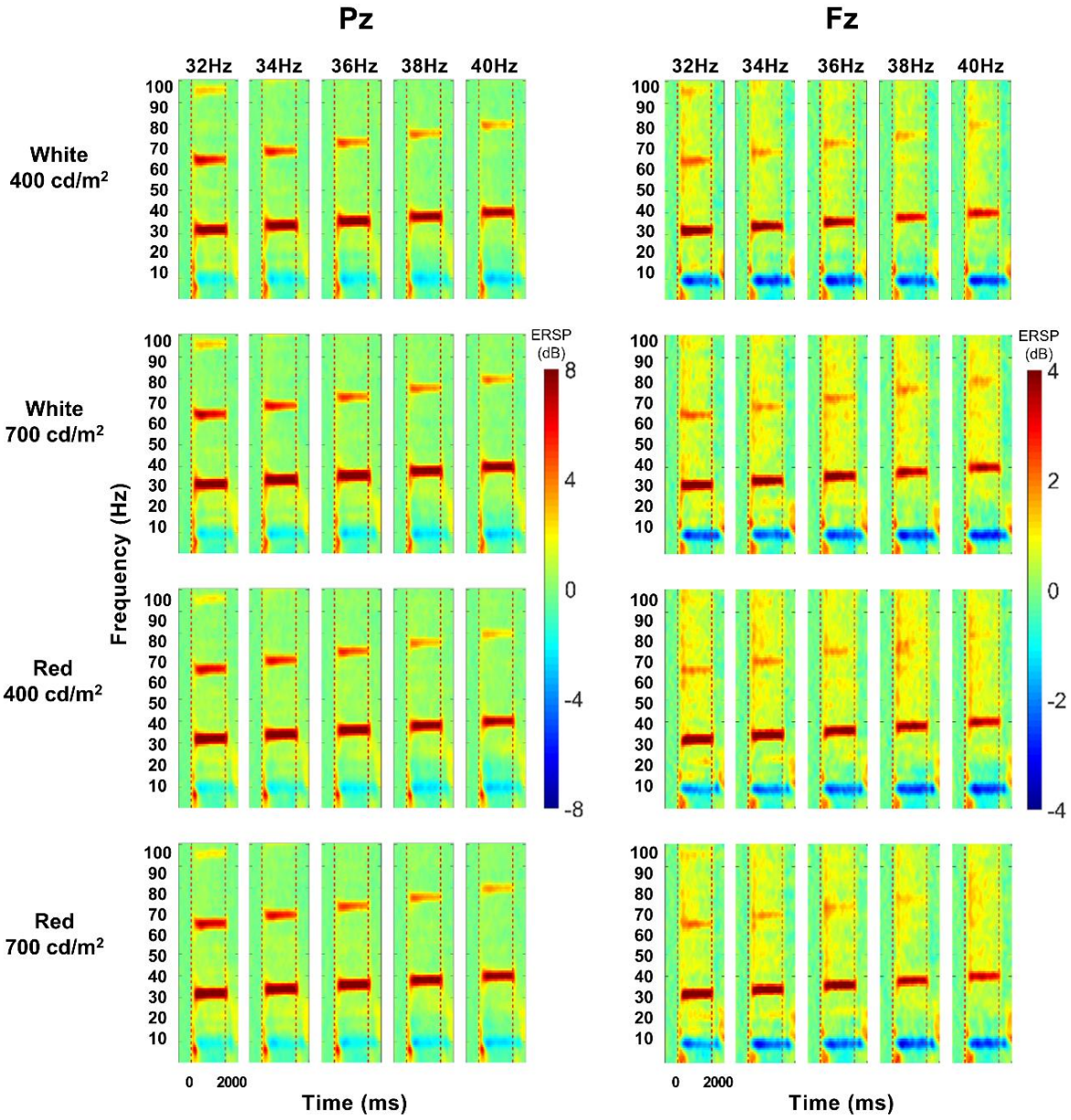

Figure 6. Comparisons of the grand-average event-related spectral perturbation of steady-state visually evoked potentials induced by flickering light stimulus in older adults between different parameters of the flickering light stimulation in the sub-study 2 of the study 1

Each column shows ERSP from 750 ms before the onset of FLS to 750 ms after the offset of flickering light stimulation

FLS, flickering light stimulation; ERSP, event-related spectral perturbation

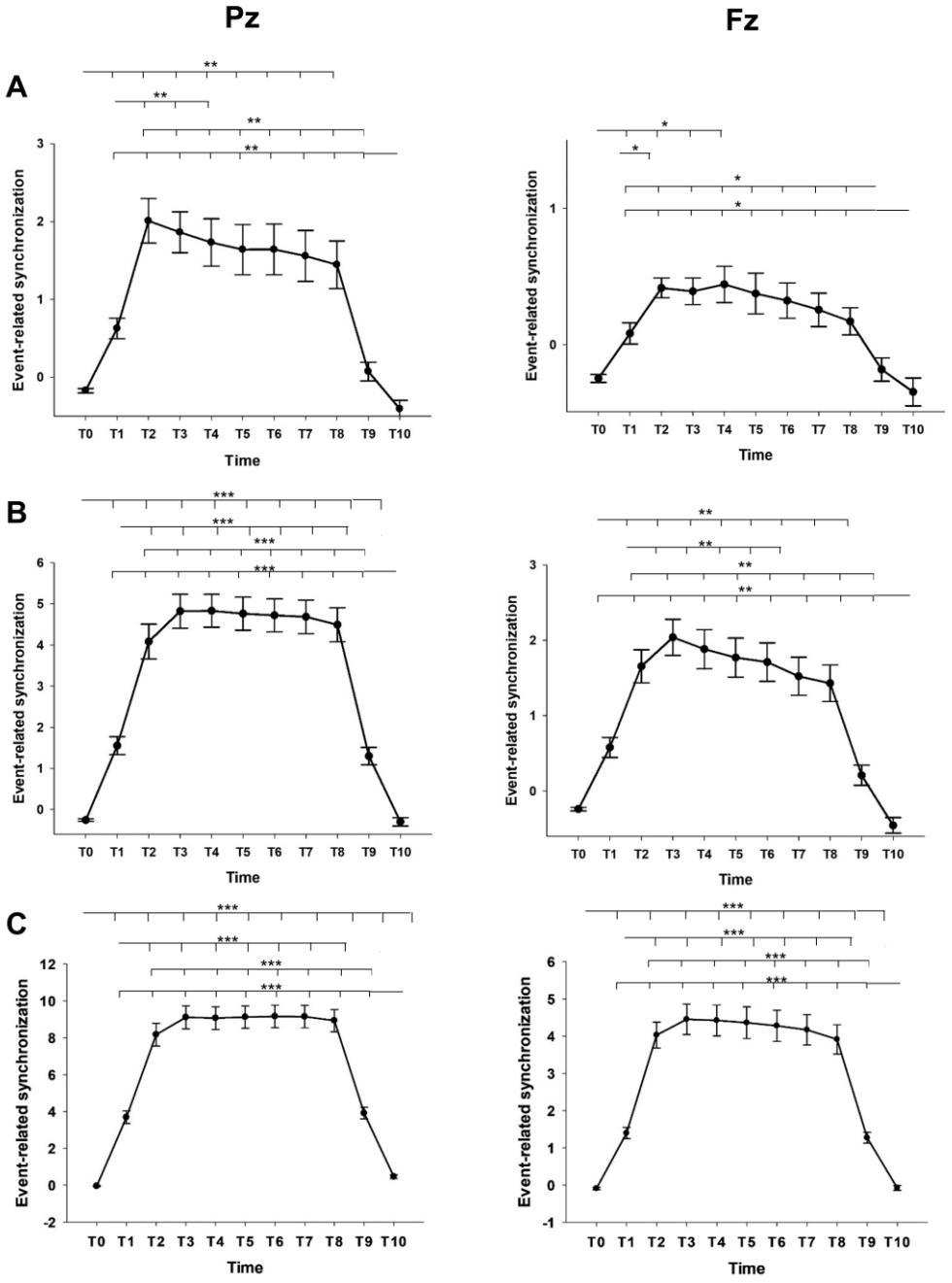

Figure 7. Main effect of the time window on grand-average event related synchronization of steady-state visually evoked potentials induced by flickering light stimulus

T0–T10 indicates 250 ms time windows from 250 ms before the onset of FLS to 500 ms after the offset of FLS. (A), (B), and (C) are the results of the experiment 1 of the sub-study 1, the experiment 2 of the sub-study 1, and the sub-study 2 respectively in the study 1

Error bars indicate standard errors.

$^{*}p < 0.05$, $^{**}p < 0.01$, $^{***}p < 0.001$ by repeated measures analysis of variance with Bonferroni post hoc comparisons

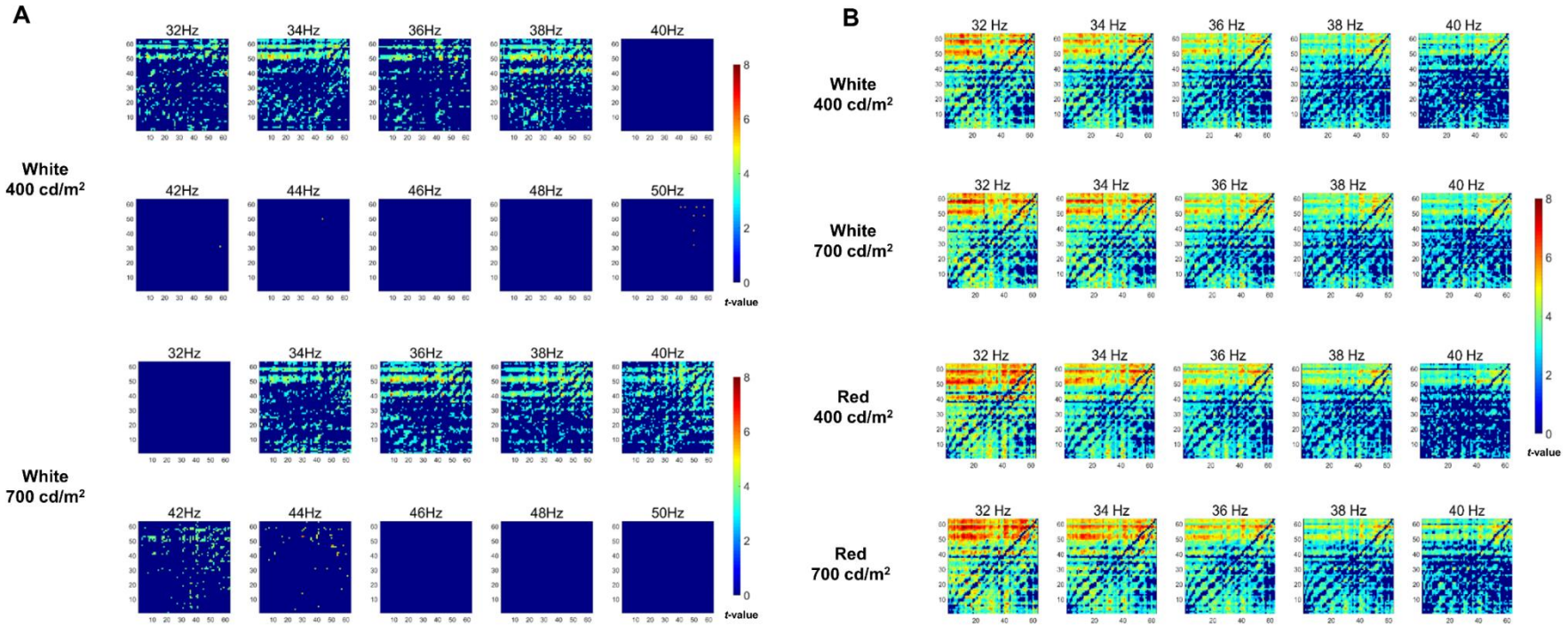

Figure 8. The spectral Granger Causality of entrained gamma rhythm in the experiment 2 of the sub-study 1 (A) and the sub-study 2 (B) of the study 1.

t-values represent the increased spectral Granger causality of the parietooccipital to frontotemporal gamma rhythm connections compared to rsEEG. The left-upper side of each matrix represents the parietooccipital to frontotemporal connections. The electrode numbers from 1 to 63 correspond to Fp1, Fp2, AF7, AF3, AFz, AF4, AF8, F7, F5, F3, F1, Fz, F2, F4, F6, F8, FT9, FT7, FC5, FC3, FC1, FC2, FC4, FC6, FT8, FT10, T7, C5, C3, C1, Cz, C2, C4, C6, T8, TP9, TP7, CP5, CP3, CP1, CPz, CP2, CP4, CP6, TP8, TP10, P7, P5, P3, P1, P2, P4, P6, P8, PO7, PO3, POz, PO4, PO8, O1, Oz, and O2, respectively.

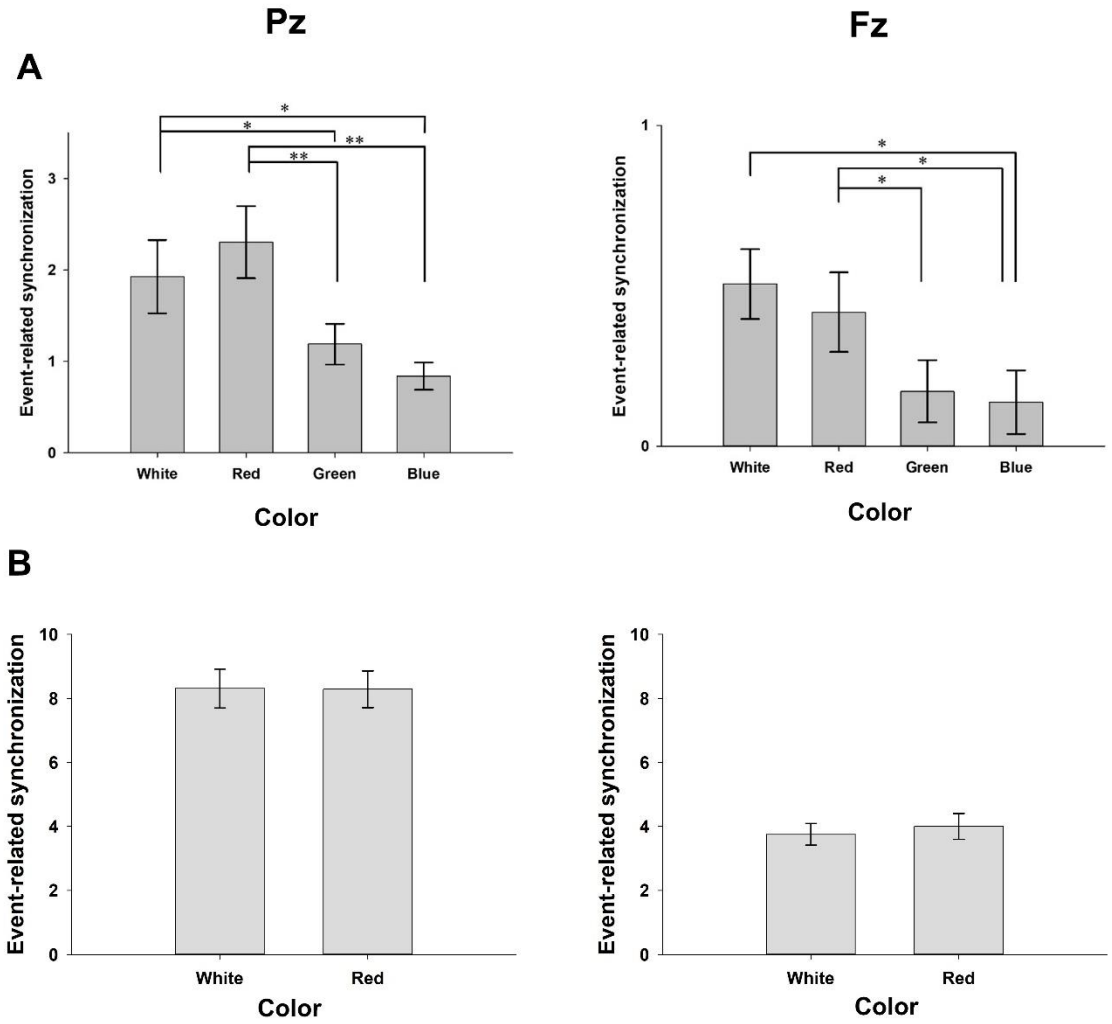

Figure 9. Main effect of color on grand-average event related synchronization of steady-state visually evoked potentials induced by flickering light stimulus in the experiment 1 of the sub-study 1 (A) and the sub-study 2 (B) of the study 1

Error bars indicate standard errors.

$^{*}p < 0.05$, $^{**}p < 0.01$ by repeated measures analysis of variance with Bonferroni post hoc comparisons

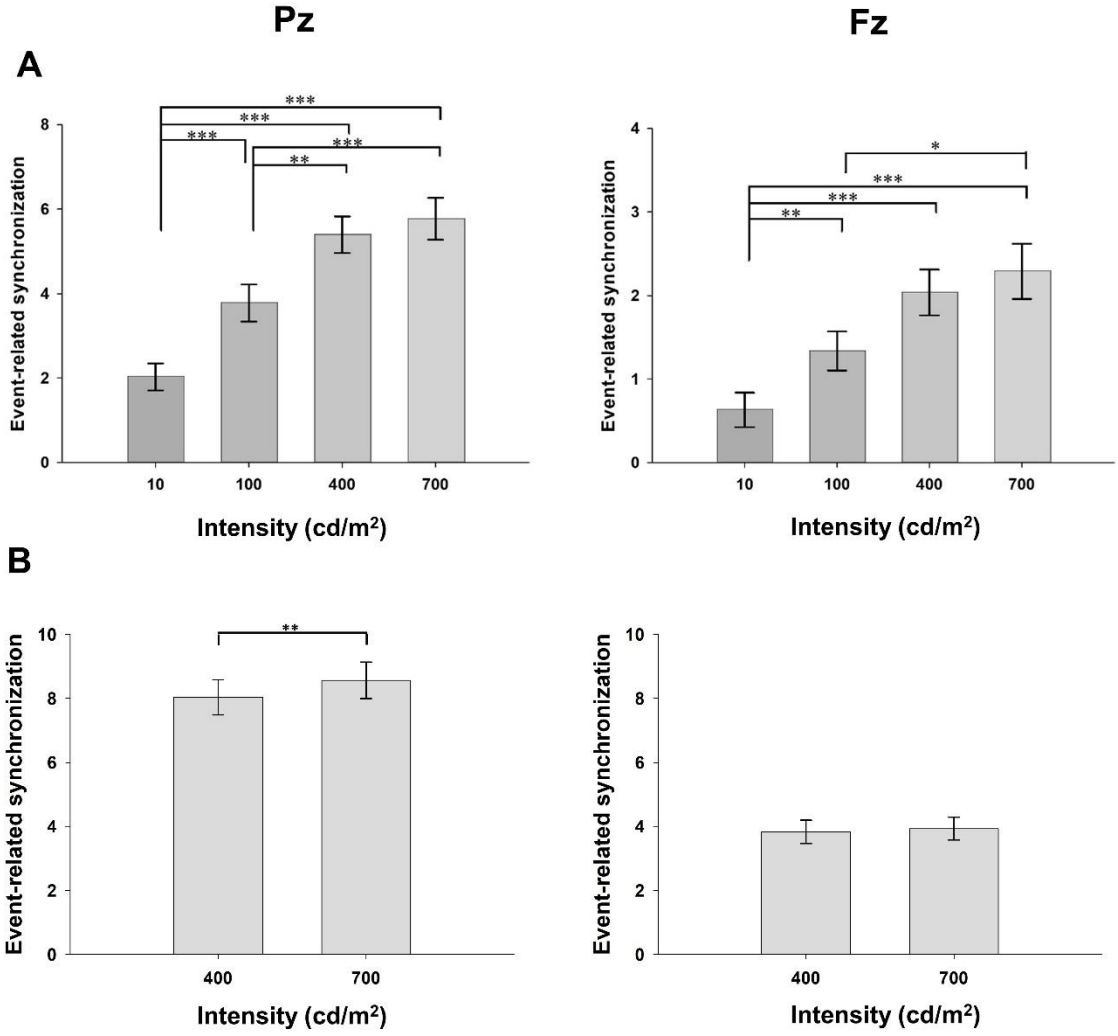

Figure 10. Main effect of luminal intensity on grand-average event related synchronization of steady-state visually evoked potentials induced by flickering light stimulus in the experiment 2 of the sub-study 1 (A) and the sub-study 2 (B) of the study 1

Error bars indicate standard errors.

$^{*}p < 0.05$, $^{**}p < 0.01$, $^{***}p < 0.001$ by repeated measures analysis of variance with Bonferroni post hoc comparisons

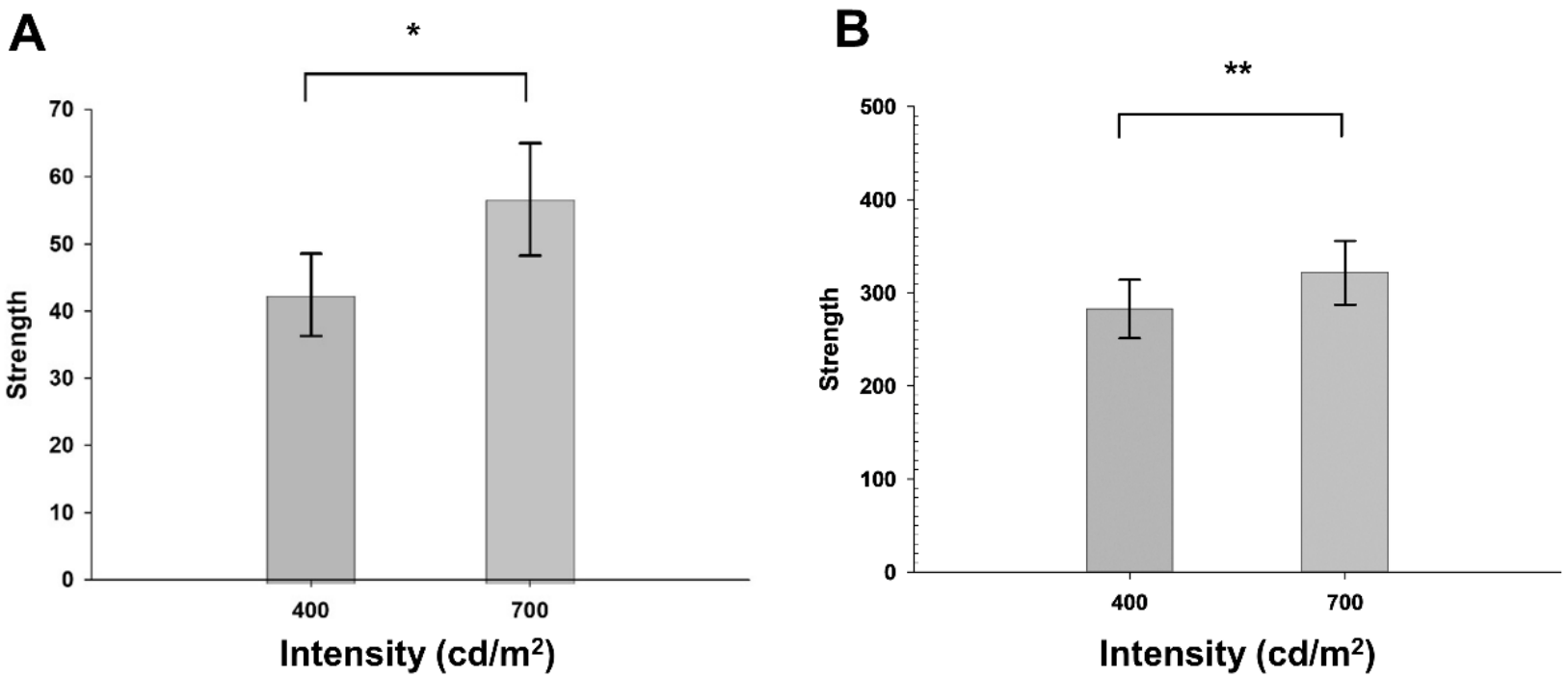

Figure 11. Main effect of luminal intensity on the averaged strength of spectral Granger Causality from parietooccipital to frontotemporal gamma rhythm connections in the experiment 2 of the sub-study 1 (A) and the sub-study 2 (B) of the study 1

Error bars indicate standard errors.

$^{*}p < 0.01$, $^{**}p < 0.001$ by repeated measures analysis of variance with Bonferroni post hoc comparisons

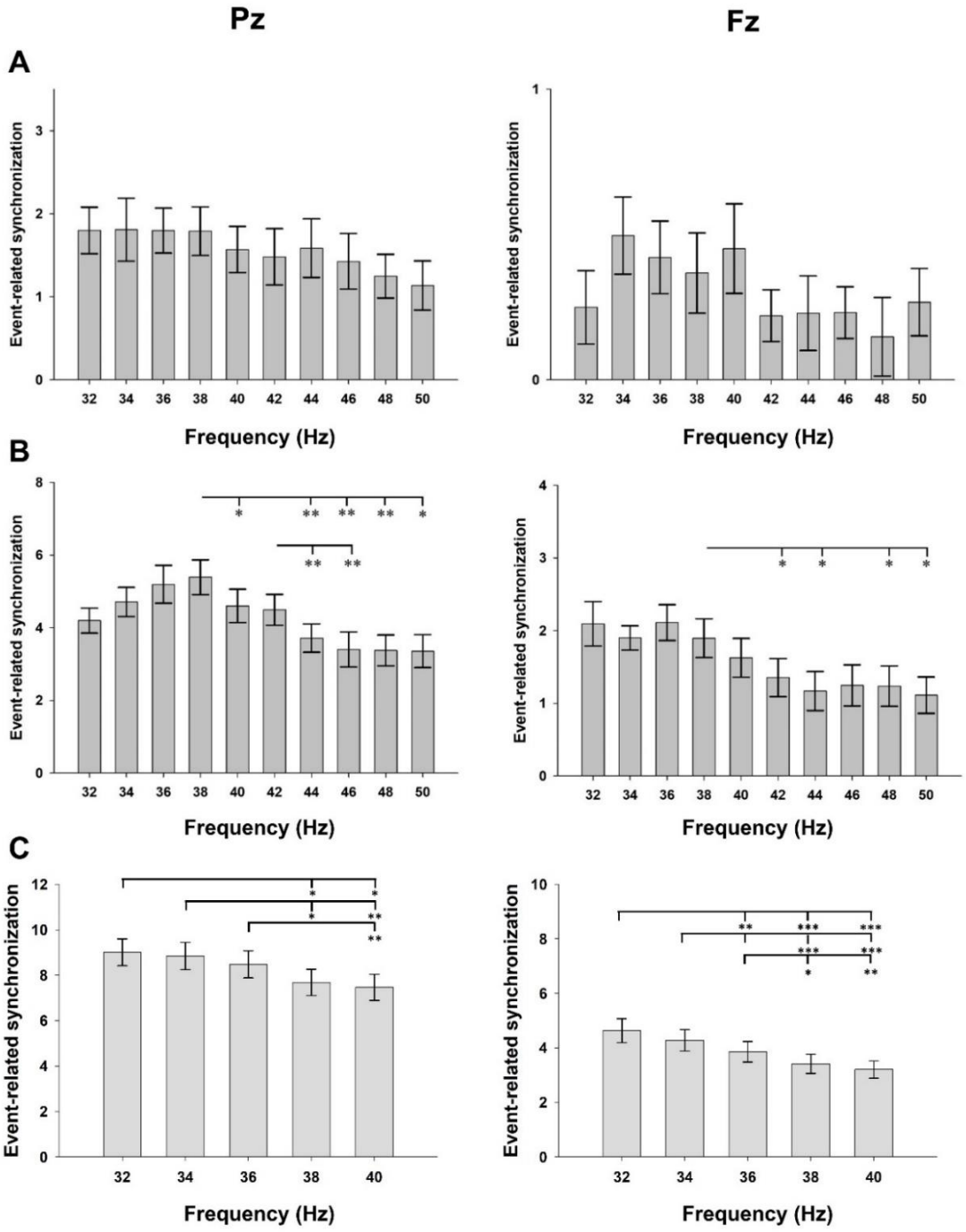

Figure 12. Main effect of flickering frequency on grand-average event related synchronization of steady-state visually evoked potentials induced by flickering light stimulus in the experiment 1 (A) and experiment 2 (B) of the sub-study 1 and the sub-study 2 (C) of the study 1

Error bars indicate standard errors.

$^{*}p < 0.05$, $^{**}p < 0.01$, $^{***}p < 0.001$ by repeated measures analysis of variance with Bonferroni post hoc comparisons

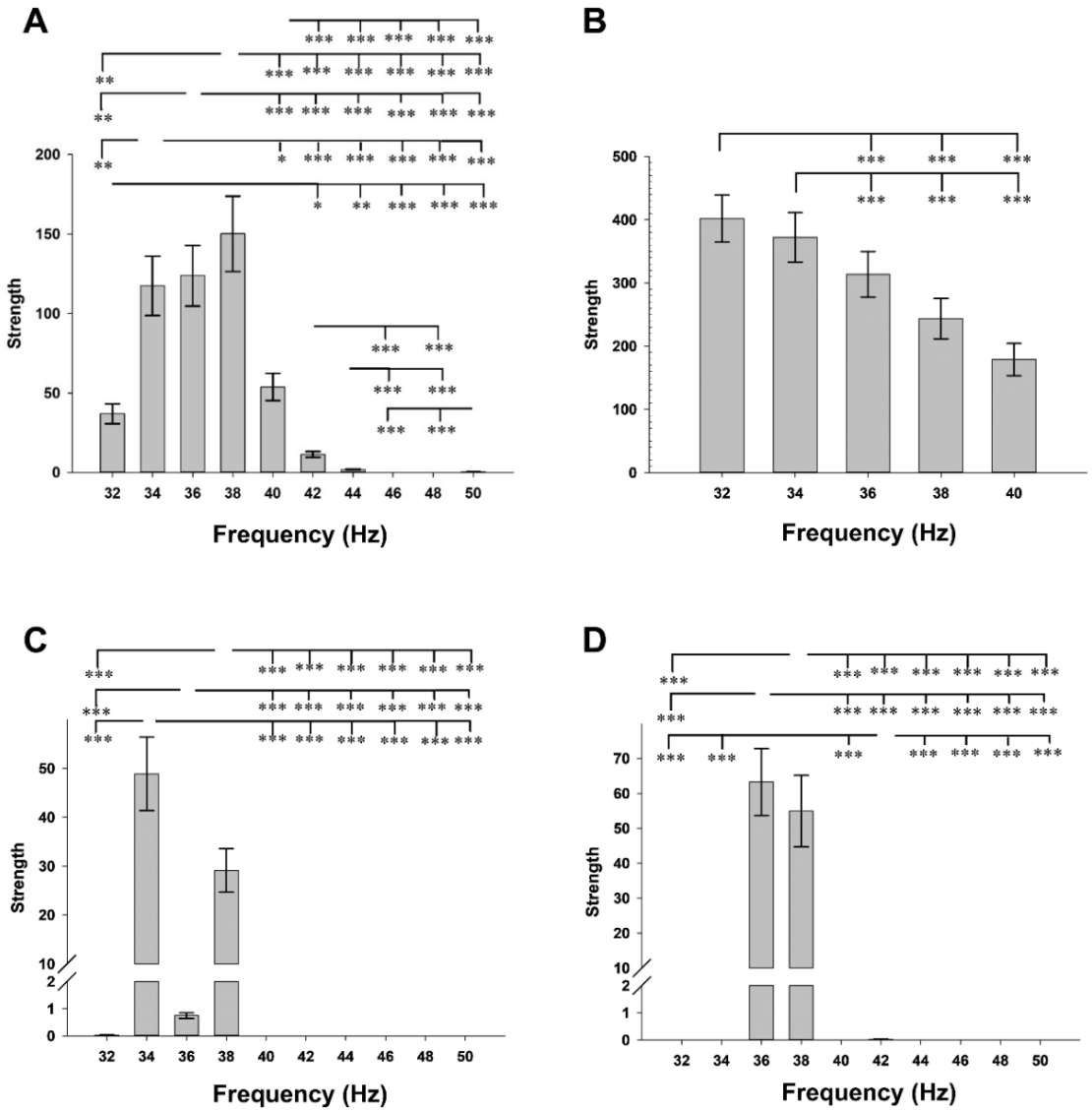

Figure 13. Main effect of flickering frequency and the interaction of flickering frequency with the luminal intensity on the averaged strength of spectral Granger Causality from parietooccipital to frontotemporal gamma rhythm connections. (A) Main effect of flickering frequency in the experiment 2 of the sub-study 1 of the study 1; (B) Main effect of flickering frequency in the sub-study 2 of the study 1; (C) Effect of flickering frequency under 400 cd/m^2 FLS in the experiment 2 of the sub-study 2 of the study 1; (D) Effect of flickering frequency under 700 cd/m^2 FLS in the experiment 2 of the sub-study 2 of the study 1

Error bars indicate standard errors.

$^{*}p < 0.05$, $^{**}p < 0.01$, $^{***}p < 0.001$ by repeated measures analysis of variance with Bonferroni post hoc comparisons

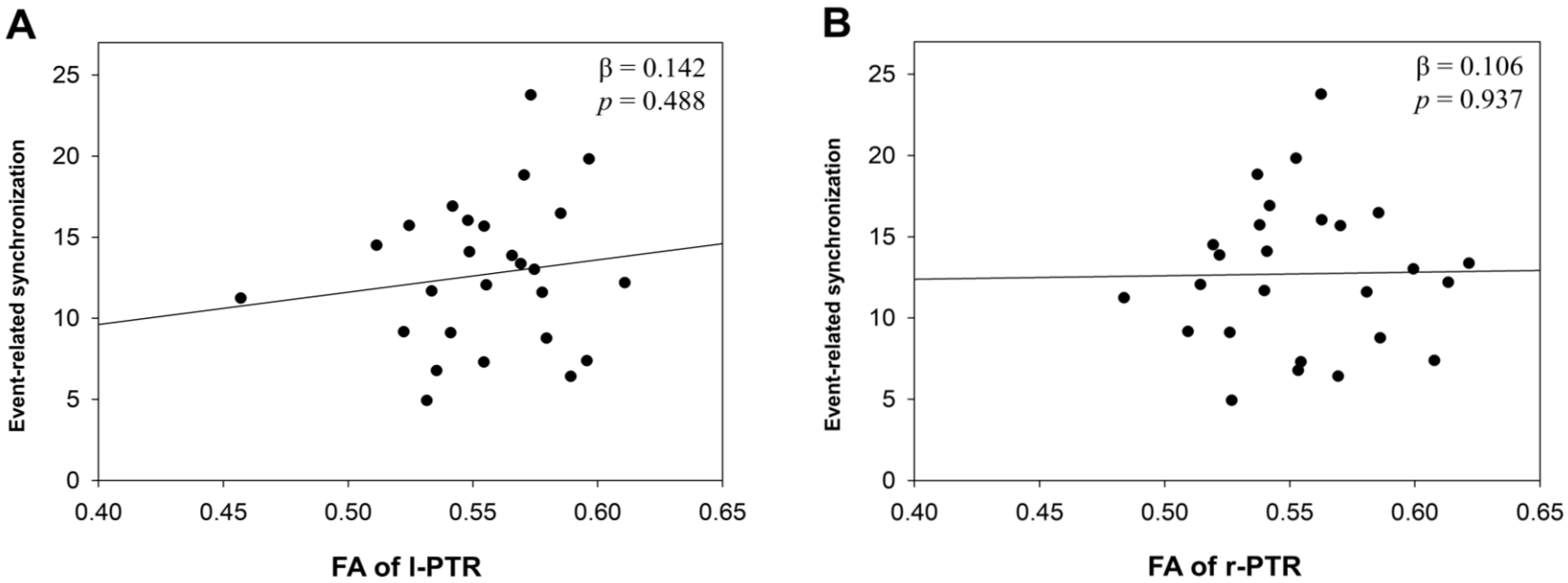

Figure 14. Effect of the fractional anisotropy values of posterior thalamic radiations on the event-related synchronization of gamma rhythms at Oz entrained by flickering visual stimulation in the linear regression analyses

FA, fractional anisotropy; l-PTR, left posterior thalamic radiation; r-PTR, right posterior thalamic radiation

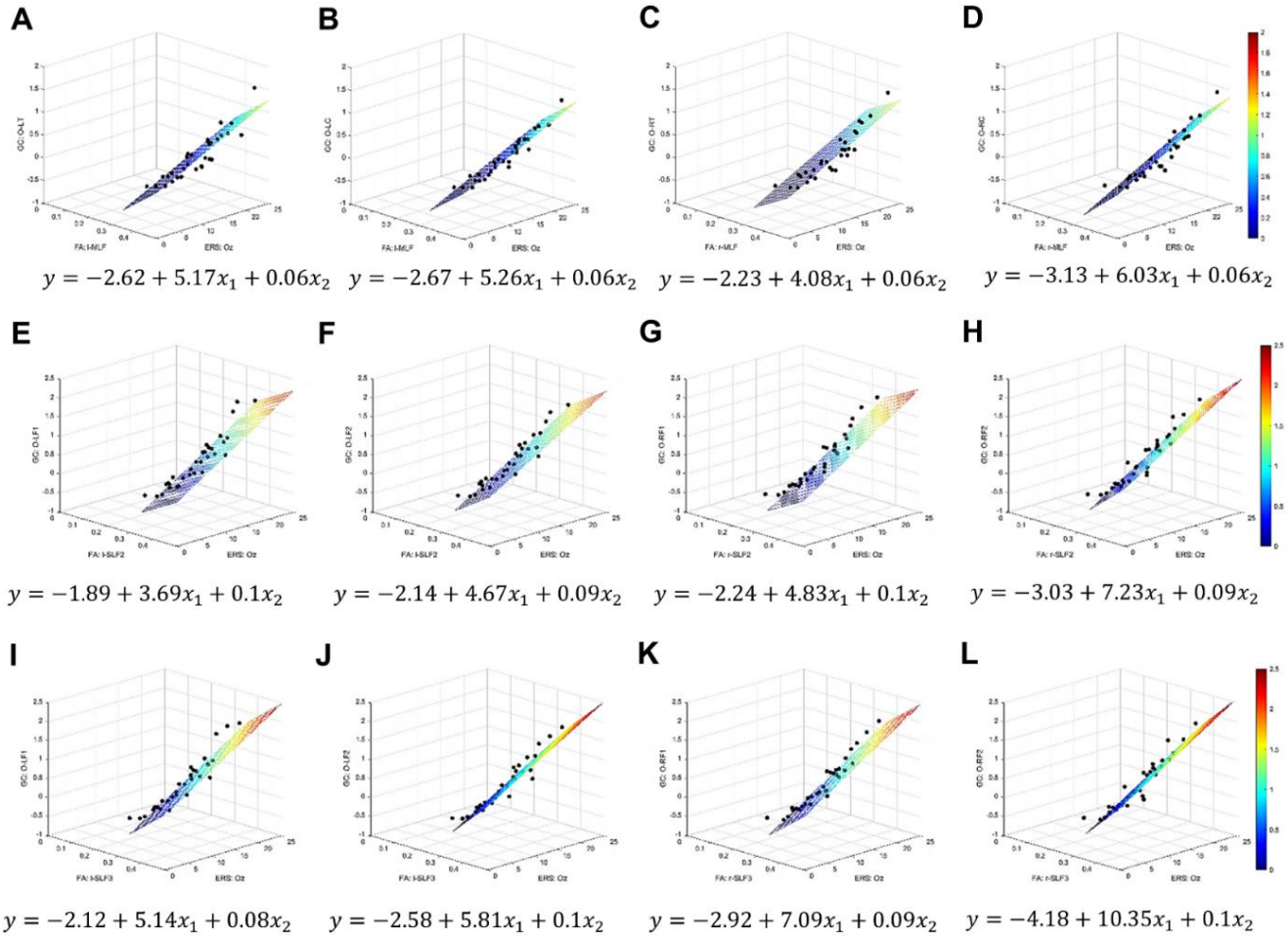

Figure 15. Effect of the fractional anisotropy values of middle and superior longitudinal fasciculi on spectral Granger Causality of the connectivities from visual cortex to other brain regions in the multiple linear regression analyses adjusting ERS at Oz.

(A) left MLF and occipital to left temporal connectivity; (B) left MLF and occipital to left central connectivity; (C) right MLF and occipital to right temporal connectivity; (D) right MLF and occipital to right central connectivity; (E) left SLF2 and parietooccipital to fore of left middle frontal connectivity; (F) left SLF2 and parietooccipital to rear of left middle frontal connectivity; (G) right SLF2 and parietooccipital to fore of right middle frontal connectivity; (H) right SLF2 and parietooccipital to rear of right middle frontal connectivity; (I) left SLF3 and parietooccipital to fore of left inferior frontal connectivity; (J) left SLF3 and parietooccipital to rear of left inferior frontal connectivity; (K) right SLF3 and parietooccipital to fore of right inferior frontal connectivity; (L) right SLF3 and parietooccipital to rear of right inferior frontal connectivity

y, response; x_1, predictor; x_2, predictor; MLF, middle longitudinal fasciculus; SLF, superior longitudinal fasciculus

Bibliography

1. Schomer, D.L. and F.H. Lopes da Silva, *Niedermeyer's ElectroencephalographyBasic Principles, Clinical Applications, and Related Fields: Basic Principles, Clinical Applications, and Related Fields*. 2017: Oxford University Press.
2. Barwick, D., *Clinical Electroencephalography and Topographic Brain Mapping Technology and Practice.* Journal of Neurology, Neurosurgery, and Psychiatry, 1989. **52**(11): p. 1322-1323.
3. *Electrical Neuroimaging*. 2009, Cambridge: Cambridge University Press.
4. Luck, S.J. *An Introduction to the Event-Related Potential Technique*. 2005.
5. Nácher, V., et al., *Coherent delta-band oscillations between cortical areas correlate with decision making*. Proceedings of the National Academy of Sciences, 2013.
6. Abhang, P., B. Gawali, and S. Mehrotra, *Technical Aspects of Brain Rhythms and Speech Parameters*. 2016. p. 51-79.
7. Buzsáki, G., *Theta Oscillations in the Hippocampus.* Neuron, 2002. **33**(3): p. 325-340.
8. Lopes da Silva, F., *Neural mechanisms underlying brain waves: from neural membranes to networks.* Electroencephalography and Clinical Neurophysiology, 1991. **79**(2): p. 81-93.
9. Jensen, O., B. Mathilde, and R. VanRullen, *An oscillatory mechanism for prioritizing salient unattended stimuli.* Trends in cognitive sciences, 2012. **16**: p. 200-6.
10. Jensen, O., et al., *Temporal coding organized by coupled alpha and gamma oscillations prioritize visual processing.* Trends in Neurosciences, 2014. **37**(7): p. 357-369.
11. Pfurtscheller, G., A. Stancák, and C. Neuper, *Event-related synchronization (ERS) in the alpha band — an electrophysiological correlate of cortical idling: A review.* International Journal of Psychophysiology, 1996. **24**(1): p. 39-46.
12. Palva, S. and J.M. Palva, *New vistas for α-frequency band oscillations.* Trends in Neurosciences, 2007. **30**(4): p. 150-158.
13. Makeig, S., *Frontal midline EEG dynamics during working memory.* NeuroImage., 2005. **27**(2): p. 341-356.
14. Rodriguez, E., et al., *Perception's shadow: long-distance synchronization of human brain activity.* Nature, 1999. **397**(6718): p. 430-433.
15. Kucewicz, M.T., et al., *Dissecting gamma frequency activity during human memory processing.* Brain, 2017. **140**(5): p. 1337-1350.
16. Roux, F., et al., *Gamma-Band Activity in Human Prefrontal Cortex Codes for the Number of Relevant Items Maintained in Working Memory.* The Journal of Neuroscience, 2012. **32**(36): p. 12411-12420.
17. Kim, J.S., et al., *Power spectral aspects of the default mode network in schizophrenia: an MEG study.* BMC Neuroscience, 2014. **15**(1): p. 104.

18. Lee, B., et al., *Generators of the gamma-band activities in response to rare and novel stimuli during the auditory oddball paradigm.* Neuroscience letters, 2007. **413**: p. 210-5.
19. Chalk, M., et al., *Attention reduces stimulus-driven gamma frequency oscillations and spike field coherence in V1.* Neuron, 2010. **66**(1): p. 114-125.
20. Schneider, T.R., et al., *Enhanced EEG gamma-band activity reflects multisensory semantic matching in visual-to-auditory object priming*. NeuroImage, 2008. **42**(3): p. 1244-1254.
21. Babiloni, C., et al., *Functional Frontoparietal Connectivity During Short-Term Memory as Revealed by High-Resolution EEG Coherence Analysis.* Behavioral Neuroscience, 2004. **118**(4): p. 687-697.
22. Jeong, J., *EEG dynamics in patients with Alzheimer's disease.* Clinical neurophysiology, 2004. **115**(7): p. 1490-1505.
23. Jelic, V., et al., *Quantitative electroencephalography in mild cognitive impairment: Longitudinal changes and possible prediction of Alzheimer's disease.* Neurobiology of aging, 2000. **21**: p. 533-40.
24. Adler, G., et al., *Prediction of treatment response to rivastigmine in Alzheimer's dementia.* Journal of neurology, neurosurgery, and psychiatry, 2004. **75**(2): p. 292-294.
25. Onofrj, M., et al., *The Effects of a Cholinesterase Inhibitor Are Prominent in Patients With Fluctuating Cognition: A Part 3 Study of the Main Mechanism of Cholinesterase Inhibitors in Dementia.* Clinical Neuropharmacology, 2003. **26**(5).
26. Özbek, Y., E. Fide, and G. Yener, *Resting-state EEG alpha/theta power ratio discriminates early-onset Alzheimer's disease from healthy controls.* Clinical Neurophysiology, 2021. **132**.
27. Ko, J., et al., *Quantitative Electroencephalogram Standardization: A Sex- and Age-Differentiated Normative Database.* Frontiers in Neuroscience, 2021. **15**.
28. Murty, D.V.P.S., et al., *Gamma oscillations weaken with age in healthy elderly in human EEG.* NeuroImage, 2020. **215**: p. 116826.
29. Jabès, A., et al., *Age-Related Differences in Resting-State EEG and Allocentric Spatial Working Memory Performance.* Frontiers in aging neuroscience, 2021. **13**: p. 704362-704362.
30. Sridhar and Manian, *Assessment of Cognitive Aging Using an SSVEP-Based Brain–Computer Interface System.* Big Data and Cognitive Computing, 2019. **3**: p. 29.
31. Rossini, P.M., et al., *Clinical neurophysiology of aging brain: From normal aging to neurodegeneration.* Progress in Neurobiology, 2007. **83**(6): p. 375-400.
32. Güntekin, B. and E. Başar, *Review of evoked and event-related delta responses in the human brain.* International Journal of Psychophysiology, 2016. **103**: p. 43-52.
33. Griskova-Bulanova, I., K. Dapšys, and V. Maciulis, *Does brain ability to synchronize with 40 Hz auditory stimulation change with age?* Acta neurobiologiae experimentalis, 2013. **73**: p. 564-70.
34. Sperling, R.A., et al., *Functional alterations in memory networks in early Alzheimer's disease.* Neuromolecular medicine, 2010. **12**(1): p. 27-43.

35. Pievani, M., et al., *Functional network disruption in the degenerative dementias.* The Lancet. Neurology, 2011. **10**(9): p. 829-843.
36. Soininen, H., et al., *Changes in absolute power values of EEG spectra in the follow-up of Alzheimer's disease.* Acta Neurologica Scandinavica, 1991. **83**.
37. Jelic, V., et al., *Quantitative Electroencephalography Power and Coherence in Alzheimer's Disease and Mild Cognitive Impairment.* Dementia and Geriatric Cognitive Disorders, 1996. **7**(6): p. 314-323.
38. Dierks, T., et al., *Topography of the quantitative electroencephalogram in dementia of the Alzheimer type: Relation to severity of dementia.* Psychiatry Research: Neuroimaging, 1991. **40**(3): p. 181-194.
39. Pozzi, D., et al., *Quantified electroencephalographic correlates of neuropsychological deficits in Alzheimer's disease.* The Journal of neuropsychiatry and clinical neurosciences, 1995. **7**(1): p. 61-67.
40. Babiloni, C., et al., *Measures of resting state EEG rhythms for clinical trials in Alzheimer's disease: Recommendations of an expert panel.* Alzheimer's & Dementia, 2021. **17**(9): p. 1528-1553.
41. Basar, E. and B. Güntekin, *Review of delta, theta, alpha, beta, and gamma response oscillations in neuropsychiatric disorders.* Supplements to Clinical neurophysiology, 2013. **62**: p. 303-41.
42. Başar, E., *A review of gamma oscillations in healthy subjects and in cognitive impairment.* International Journal of Psychophysiology, 2013. **90**(2): p. 99-117.
43. Rossini, P.M., et al., *Conversion from mild cognitive impairment to Alzheimer's disease is predicted by sources and coherence of brain electroencephalography rhythms.* Neuroscience, 2006. **143**(3): p. 793-803.
44. Koenig, T., et al., *Decreased EEG synchronization in Alzheimer's disease and mild cognitive impairment.* Neurobiology of Aging, 2005. **26**(2): p. 165-171.
45. Murty, D.V., et al., *Stimulus-induced gamma rhythms are weaker in human elderly with mild cognitive impairment and Alzheimer's disease.* eLife, 2021. **10**: p. e61666.
46. Gaubert, S., et al., *EEG evidence of compensatory mechanisms in preclinical Alzheimer's disease.* Brain, 2019. **142**(7): p. 2096-2112.
47. Tanaka-Koshiyama, K., et al., *Abnormal Spontaneous Gamma Power Is Associated With Verbal Learning and Memory Dysfunction in Schizophrenia.* Frontiers in Psychiatry, 2020. **11**.
48. Liu, C., et al., *Modulating Gamma Oscillations Promotes Brain Connectivity to Improve Cognitive Impairment.* Cerebral Cortex, 2022. **32**(12): p. 2644-2656.
49. Kwon, J.S., et al., *Gamma frequency-range abnormalities to auditory stimulation in schizophrenia.* Archives of general psychiatry, 1999. **56**(11): p. 1001-1005.
50. Galambos, R., S. Makeig, and P.J. Talmachoff, *A 40-Hz auditory potential recorded from the human scalp.* Proceedings of the National Academy of Sciences of the United States of

America, 1981. **78**(4): p. 2643-2647.

51. Tada, M., et al., *Differential Alterations of Auditory Gamma Oscillatory Responses Between Pre-Onset High-Risk Individuals and First-Episode Schizophrenia.* Cerebral Cortex, 2016. **26**(3): p. 1027-1035.
52. McDermott, B., et al., *Gamma Band Neural Stimulation in Humans and the Promise of a New Modality to Prevent and Treat Alzheimer's Disease.* Journal of Alzheimer's disease : JAD, 2018. **65**(2): p. 363-392.
53. Tao, H.-Y. and X. Tian, *Coherence Characteristics of Gamma-band EEG during rest and cognitive task in MCI and AD.* Conference proceedings : ... Annual International Conference of the IEEE Engineering in Medicine and Biology Society. IEEE Engineering in Medicine and Biology Society. Conference, 2005. **3**: p. 2747-50.
54. van Deursen, J.A., et al., *Increased EEG gamma band activity in Alzheimer's disease and mild cognitive impairment.* Journal of neural transmission (Vienna, Austria : 1996), 2008. **115**(9): p. 1301-1311.
55. Iaccarino, H.F., et al., *Gamma frequency entrainment attenuates amyloid load and modifies microglia.* Nature, 2016. **540**(7632): p. 230.
56. Adaikkan, C., et al., *Gamma Entrainment Binds Higher-Order Brain Regions and Offers Neuroprotection.* Neuron, 2019. **102**(5): p. 929-943.e8.
57. Martorell, A.J., et al., *Multi-sensory Gamma Stimulation Ameliorates Alzheimer's-Associated Pathology and Improves Cognition.* Cell, 2019. **177**(2): p. 256-271.
58. Etter, G., et al., *Optogenetic gamma stimulation rescues memory impairments in an Alzheimer's disease mouse model.* Nature Communications, 2019. **10**.
59. Adaikkan, C. and L.-H. Tsai, *Gamma Entrainment: Impact on Neurocircuits, Glia, and Therapeutic Opportunities.* Trends in Neurosciences, 2020. **43**(1): p. 24-41.
60. Wiesman, A.I., et al., *Visuospatial alpha and gamma oscillations scale with the severity of cognitive dysfunction in patients on the Alzheimer's disease spectrum.* Alzheimer's Research & Therapy, 2021. **13**(1): p. 139.
61. Pastor, M.A., et al., *Human Cerebral Activation during Steady-State Visual-Evoked Responses.* The Journal of Neuroscience, 2003. **23**(37): p. 11621-11627.
62. Vialatte, F.B., et al., *On the synchrony of steady state visual evoked potentials and oscillatory burst events.* Cognitive neurodynamics, 2009. **3**(3): p. 251-261.
63. Ismail, R., et al., *The Effect of 40-Hz Light Therapy on Amyloid Load in Patients with Prodromal and Clinical Alzheimer's Disease.* Int J Alzheimers Dis, 2018. **2018**: p. 6852303.
64. He, Q., et al., *A feasibility trial of gamma sensory flicker for patients with prodromal Alzheimer's disease.* Alzheimer's & Dementia: Translational Research & Clinical Interventions, 2021. **7**(1): p. e12178.
65. Chan, D., et al., *40Hz sensory stimulation induces gamma entrainment and affects brain structure, sleep and cognition in patients with Alzheimer's dementia.* medRxiv, 2021: p.

2021.03.01.21252717.

66. Rager, G.H. and W. Singer, *The response of cat visual cortex to flicker stimuli of variable frequency.* European Journal of Neuroscience, 1998. **10**.
67. Bastos, A.M., et al., *Simultaneous Recordings from the Primary Visual Cortex and Lateral Geniculate Nucleus Reveal Rhythmic Interactions and a Cortical Source for Gamma-Band Oscillations.* The Journal of Neuroscience, 2014. **34**(22): p. 7639.
68. Murty, D.V.P.S., et al., *Large Visual Stimuli Induce Two Distinct Gamma Oscillations in Primate Visual Cortex.* The Journal of Neuroscience, 2018. **38**(11): p. 2730.
69. Perrenoud, Q., C.M.A. Pennartz, and L.J. Gentet, *Membrane Potential Dynamics of Spontaneous and Visually Evoked Gamma Activity in V1 of Awake Mice.* PLoS biology, 2016. **14**(2): p. e1002383-e1002383.
70. Han, H.-B., et al., *Gamma-Band Activities in Mouse Frontal and Visual Cortex Induced by Coherent Dot Motion.* Scientific Reports, 2017. **7**(1): p. 43780.
71. Pastor, M., et al., *Human Cerebral Activation during Steady-State Visual-Evoked Responses.* J Neurosci, 2004. **23**: p. 11621-7.
72. Chen, X., et al., *Effects of stimulation frequency and stimulation waveform on steady-state visual evoked potentials using a computer monitor.* Journal of Neural Engineering, 2019. **16**(6): p. 066007.
73. Herrmann, C., *Human EEG responses to 1–100 Hz flicker: Resonance phenomena in visual cortex and their potential correlation to cognitive phenomena*. Vol. 137. 2001. 346-53.
74. Tsoneva, T., G. Garcia-Molina, and P. Desain, *Neural dynamics during repetitive visual stimulation.* Journal of Neural Engineering, 2015. **12**(6): p. 066017.
75. Horwitz, A., et al., *Visual steady state in relation to age and cognitive function.* PloS one, 2017. **12**(2): p. e0171859.
76. Kutsyr, O., et al., *Gradual Increase in Environmental Light Intensity Induces Oxidative Stress and Inflammation and Accelerates Retinal Neurodegeneration.* Investigative Ophthalmology & Visual Science, 2020. **61**(10): p. 1-1.
77. Peirson, S.N., et al., *Light and the laboratory mouse.* Journal of Neuroscience Methods, 2018. **300**: p. 26-36.
78. Denman, D.J., et al., *Mouse color and wavelength-specific luminance contrast sensitivity are non-uniform across visual space.* eLife, 2018. **7**: p. e31209.
79. Nguyen-Tri, D., O. Overbury, and J. Faubert, *The Role of Lenticular Senescence in Age-Related Color Vision Changes.* Investigative Ophthalmology & Visual Science, 2003. **44**(8): p. 3698-3704.
80. Schneck, M.E., et al., *Comparison of Panel D-15 Tests in a Large Older Population.* Optometry and Vision Science, 2014. **91**(3): p. 284-290.
81. Pfefferbaum, A. and E.V. Sullivan, *Increased brain white matter diffusivity in normal adult aging: relationship to anisotropy and partial voluming.* Magn Reson Med, 2003. **49**(5): p.

953-61.

82. Head, D., et al., *Differential vulnerability of anterior white matter in nondemented aging with minimal acceleration in dementia of the Alzheimer type: evidence from diffusion tensor imaging.* Cereb Cortex, 2004. **14**(4): p. 410-23.
83. Salat, D.H., et al., *Age-related alterations in white matter microstructure measured by diffusion tensor imaging.* Neurobiol Aging, 2005. **26**(8): p. 1215-27.
84. Kim, J.S., et al., *Construction and validation of a cerebral white matter hyperintensity probability map of older Koreans.* NeuroImage: Clinical, 2021. **30**: p. 102607.
85. Kim, K.W., J.R. MacFall, and M.E. Payne, *Classification of white matter lesions on magnetic resonance imaging in elderly persons.* Biological psychiatry, 2008. **64**(4): p. 273-280.
86. Hinault, T., et al., *Disrupted Neural Synchrony Mediates the Relationship between White Matter Integrity and Cognitive Performance in Older Adults.* Cereb Cortex, 2020. **30**(10): p. 5570-5582.
87. Hinault, T., et al., *Age-related differences in network structure and dynamic synchrony of cognitive control.* Neuroimage, 2021. **236**: p. 118070.
88. Babaeeghazvini, P., et al., *Brain Structural and Functional Connectivity: A Review of Combined Works of Diffusion Magnetic Resonance Imaging and Electro-Encephalography.* Frontiers in Human Neuroscience, 2021. **15**.
89. Babaeeghazvini, P., et al., *A combined diffusion-weighted and electroencephalography study on age-related differences in connectivity in the motor network during bimanual performance.* Human brain mapping, 2019. **40**(6): p. 1799-1813.
90. Douglas, P.K. and D.B. Douglas. *Reconsidering Spatial Priors In EEG Source Estimation : Does White Matter Contribute to EEG Rhythms?* in *2019 7th International Winter Conference on Brain-Computer Interface (BCI)*. 2019.
91. Rojas, D.C., et al., *Transient and steady-state auditory gamma-band responses in first-degree relatives of people with autism spectrum disorder.* Molecular autism, 2011. **2**: p. 11-11.
92. Ross, B., A.T. Herdman, and C. Pantev, *Stimulus induced desynchronization of human auditory 40-Hz steady-state responses.* J Neurophysiol, 2005. **94**(6): p. 4082-93.
93. Ross, B., *A novel type of auditory responses: temporal dynamics of 40-Hz steady-state responses induced by changes in sound localization.* J Neurophysiol, 2008. **100**(3): p. 1265-77.
94. Parciauskaite, V., et al., *40-Hz auditory steady-state responses and the complex information processing: An exploratory study in healthy young males.* PLOS ONE, 2019. **14**(10): p. e0223127.
95. Pastor, M.A., et al., *Activation of Human Cerebral and Cerebellar Cortex by Auditory Stimulation at 40 Hz.* The Journal of Neuroscience, 2002. **22**(23): p. 10501.
96. Ladouce, S., et al., *Improving user experience of SSVEP BCI through low amplitude depth and high frequency stimuli design.* Scientific Reports, 2022. **12**(1): p. 8865.

97. Muthukumaraswamy, S.D., et al., *Visual gamma oscillations and evoked responses: Variability, repeatability and structural MRI correlates.* NeuroImage, 2010. **49**(4): p. 3349-3357.
98. Kim, D.-W., et al., *Classification of selective attention to auditory stimuli: Toward vision-free brain–computer interfacing.* Journal of Neuroscience Methods, 2011. **197**(1): p. 180-185.
99. Sakowitz, O.W., et al., *Bisensory stimulation increases gamma-responses over multiple cortical regions.* Cognitive Brain Research, 2001. **11**(2): p. 267-279.
100. Grimes, A.M., et al., *Central auditory function in Alzheimer's disease.* Neurology, 1985. **35**(3): p. 352.
101. Häggström, J., et al., *A Longitudinal Study of Peripheral and Central Auditory Function in Alzheimer's Disease and in Mild Cognitive Impairment.* Dementia and Geriatric Cognitive Disorders Extra, 2018. **8**(3): p. 393-401.
102. Chen, X., et al., *High-speed spelling with a noninvasive brain–computer interface.* Proceedings of the National Academy of Sciences, 2015. **112**(44): p. E6058-E6067.
103. Chen, J., et al., *Application of a single-flicker online SSVEP BCI for spatial navigation.* PLOS ONE, 2017. **12**(5): p. e0178385.
104. Choi, G.-Y., et al., *A multi-day and multi-band dataset for a steady-state visual-evoked potential–based brain-computer interface.* GigaScience, 2019. **8**(11): p. giz133.
105. Kim, D.-W., et al., *Can Anodal Transcranial Direct Current Stimulation Increase Steady-State Visual Evoked Potential Responses?* jkms, 2019. **34**(43): p. 0-0.
106. Guger, C., et al., *How Many People Could Use an SSVEP BCI?* Frontiers in Neuroscience, 2012. **6**.
107. Lee, J.H., et al., *Development of the Korean Version of the Consortium to Establish a Registry for Alzheimer's Disease Assessment Packet (CERAD-K): Clinical and Neuropsychological Assessment Batteries.* The Journals of Gerontology: Series B, 2002. **57**(1): p. P47-P53.
108. Yoo, S.W., Y. Kim, and J.S. Noh, *Validity of Korean version of the mini-international neuropsychiatric interview.* Anxiety Mood, 2006. **2**: p. 50-55.
109. Delorme, A. and S. Makeig, *EEGLAB: an open source toolbox for analysis of single-trial EEG dynamics including independent component analysis.* Journal of Neuroscience Methods, 2004. **134**(1): p. 9-21.
110. Cui, J., et al., *BSMART: a Matlab/C toolbox for analysis of multichannel neural time series.* Neural Networks, 2008. **21**(8): p. 1094-1104.
111. Tsoneva, T., G. Garcia-Molina, and P. Desain, *SSVEP phase synchronies and propagation during repetitive visual stimulation at high frequencies.* Scientific Reports, 2021. **11**(1): p. 4975.
112. Cohen, M.X., *Analyzing neural time series data: theory and practice*. 2014: MIT press.
113. Rubinov, M. and O. Sporns, *Complex network measures of brain connectivity: uses and interpretations.* Neuroimage, 2010. **52**(3): p. 1059-69.
114. Boccaletti, S., et al., *Complex networks: Structure and dynamics.* Physics Reports, 2006. **424**(4):

p. 175-308.
115. Heo, J. and G. Yoon, *EEG Studies on Physical Discomforts Induced by Virtual Reality Gaming.* Journal of Electrical Engineering & Technology, 2020. **15**(3): p. 1323-1329.
116. Azizollahi, H., A. Aarabi, and F. Wallois, *Effects of uncertainty in head tissue conductivity and complexity on EEG forward modeling in neonates.* Human brain mapping, 2016. **37**.
117. Neoh, M., et al., *Disapproval from romantic partners, friends and parents: Source of criticism regulates prefrontal cortex activity.* PloS one, 2020. **15**: p. e0229316.
118. Tsuzuki, D., et al., *Macroanatomical Landmarks Featuring Junctions of Major Sulci and Fissures and Scalp Landmarks Based on the International 10–10 System for Analyzing Lateral Cortical Development of Infants.* Frontiers in Neuroscience, 2017. **11**.
119. Luck, S.J., *An Introduction to the Event-Related Potential Technique, second edition*. 2014: MIT Press.
120. Smith, S.M., et al., *Advances in functional and structural MR image analysis and implementation as FSL.* NeuroImage, 2004. **23**: p. S208-S219.
121. Hua, K., et al., *Tract probability maps in stereotaxic spaces: analyses of white matter anatomy and tract-specific quantification.* NeuroImage, 2008. **39**(1): p. 336-347.
122. McCrea, M., et al., *An Integrated Review of Recovery after Mild Traumatic Brain Injury (MTBI): Implications for Clinical Management.* The Clinical neuropsychologist, 2009. **23**: p. 1368-90.
123. Wakana, S., et al., *Reproducibility of quantitative tractography methods applied to cerebral white matter.* NeuroImage, 2007. **36**(3): p. 630-644.
124. Warrington, S., et al., *XTRACT - Standardised protocols for automated tractography in the human and macaque brain.* NeuroImage, 2020. **217**: p. 116923.
125. Arrigo, A., et al., *New Insights in the Optic Radiations Connectivity in the Human Brain.* Investigative Ophthalmology & Visual Science, 2016. **57**(1): p. 1-5.
126. Garza, K.M., et al., *Gamma Visual Stimulation Induces a Neuroimmune Signaling Profile Distinct from Acute Neuroinflammation.* The Journal of Neuroscience, 2020. **40**(6): p. 1211.
127. Huang, M.-X., et al., *Marked Increases in Resting-State MEG Gamma-Band Activity in Combat-Related Mild Traumatic Brain Injury.* Cerebral cortex (New York, N.Y. : 1991), 2019. **30**.
128. Hamid, B., et al., *Abnormalities of Quantitative Electroencephalography in Children with Asperger Disorder Using Spectrogram andCoherence Values.* Iranian Journal of Psychiatry, 1970. **3**(2).
129. Popova, P., et al., *The impact of cognitive training on spontaneous gamma oscillations in schizophrenia.* Psychophysiology, 2017. **55**.
130. Benasich, A.A., et al., *Early cognitive and language skills are linked to resting frontal gamma power across the first 3 years.* Behavioural brain research, 2008. **195**(2): p. 215-222.
131. Herrmann, C.S. and T. Demiralp, *Human EEG gamma oscillations in neuropsychiatric disorders.* Clinical Neurophysiology, 2005. **116**(12): p. 2719-2733.

132. Rochart, R., et al., *Compromised Behavior and Gamma Power During Working Memory in Cognitively Healthy Individuals With Abnormal CSF Amyloid/Tau.* Frontiers in Aging Neuroscience, 2020. **12**.
133. Pointer, J.S. and R.F. Hess, *The contrast sensitivity gradient across the human visual field: With emphasis on the low spatial frequency range.* Vision Research, 1989. **29**(9): p. 1133-1151.
134. Rider, A.T., G.B. Henning, and A. Stockman, *Light adaptation controls visual sensitivity by adjusting the speed and gain of the response to light.* PLOS ONE, 2019. **14**(8): p. e0220358.
135. Umino, Y., R. Pasquale, and E. Solessio, *Visual Temporal Contrast Sensitivity in the Behaving Mouse Shares Fundamental Properties with Human Psychophysics.* eNeuro, 2018. **5**(4): p. ENEURO.0181-18.2018.
136. Jia, X., D. Xing, and A. Kohn, *No consistent relationship between gamma power and peak frequency in macaque primary visual cortex.* J Neurosci, 2013. **33**(1): p. 17-25.
137. Hadjipapas, A., et al., *Parametric variation of gamma frequency and power with luminance contrast: A comparative study of human MEG and monkey LFP and spike responses.* Neuroimage, 2015. **112**: p. 327-340.
138. Lowet, E., et al., *Input-dependent frequency modulation of cortical gamma oscillations shapes spatial synchronization and enables phase coding.* PLoS Comput Biol, 2015. **11**(2): p. e1004072.
139. Roberts, M.J., et al., *Robust gamma coherence between macaque V1 and V2 by dynamic frequency matching.* Neuron, 2013. **78**(3): p. 523-36.
140. Eckhorn, R., et al., *Coherent oscillations: A mechanism of feature linking in the visual cortex?* Biological Cybernetics, 1988. **60**(2): p. 121-130.
141. Friedman-Hill, S., P.E. Maldonado, and C.M. Gray, *Dynamics of Striate Cortical Activity in the Alert Macaque: I. Incidence and Stimulus-dependence of Gamma-band Neuronal Oscillations.* Cerebral Cortex, 2000. **10**(11): p. 1105-1116.
142. Ross, J.E., D.D. Clarke, and A.J. Bron, *Effect of age on contrast sensitivity function: uniocular and binocular findings.* The British journal of ophthalmology, 1985. **69**(1): p. 51-56.
143. Robson, S.E., et al., *Structural and neurochemical correlates of individual differences in gamma frequency oscillations in human visual cortex.* Journal of Anatomy, 2015. **227**(4): p. 409-417.
144. Edden, R.A.E., et al., *Orientation Discrimination Performance Is Predicted by GABA Concentration and Gamma Oscillation Frequency in Human Primary Visual Cortex.* The Journal of Neuroscience, 2009. **29**(50): p. 15721.
145. Ferando, I. and I. Mody, *In vitro gamma oscillations following partial and complete ablation of delta subunit-containing GABAA receptors from parvalbumin interneurons.* Neuropharmacology, 2015. **88**: p. 91-8.
146. Mann, E.O. and I. Mody, *Control of hippocampal gamma oscillation frequency by tonic*

inhibition and excitation of interneurons. Nat Neurosci, 2010. **13**(2): p. 205-12.

147. Cardin, J.A., et al., *Driving fast-spiking cells induces gamma rhythm and controls sensory responses.* Nature, 2009. **459**(7247): p. 663-7.
148. Carlen, M., et al., *A critical role for NMDA receptors in parvalbumin interneurons for gamma rhythm induction and behavior.* Mol Psychiatry, 2012. **17**(5): p. 537-48.
149. Gulyas, A.I., et al., *Parvalbumin-containing fast-spiking basket cells generate the field potential oscillations induced by cholinergic receptor activation in the hippocampus.* J Neurosci, 2010. **30**(45): p. 15134-45.
150. Sohal, V.S., et al., *Parvalbumin neurons and gamma rhythms enhance cortical circuit performance.* Nature, 2009. **459**(7247): p. 698-702.
151. Gaetz, W., et al., *Relating MEG measured motor cortical oscillations to resting gamma-aminobutyric acid (GABA) concentration.* Neuroimage, 2011. **55**(2): p. 616-21.
152. Gold, J.R. and V.M. Bajo, *Insult-induced adaptive plasticity of the auditory system.* Frontiers in Neuroscience, 2014. **8**.
153. Sundman-Eriksson, I. and P. Allard, *Age-correlated decline in [3H]tiagabine binding to GAT-1 in human frontal cortex.* Aging Clinical and Experimental Research, 2006. **18**(3): p. 257-260.
154. McQuail, J., C. Frazier, and J. Bizon, *Molecular aspects of age-related cognitive decline: The role of GABA signaling.* Trends in molecular medicine, 2015. **21**.
155. Torrey, E.F., et al., *Neurochemical markers for schizophrenia, bipolar disorder, and major depression in postmortem brains.* Biological Psychiatry, 2005. **57**: p. 252-260.
156. Muthukumaraswamy, S.D. and K.D. Singh, *Spatiotemporal frequency tuning of BOLD and gamma band MEG responses compared in primary visual cortex.* Neuroimage, 2008. **40**(4): p. 1552-60.
157. Grachev, I.D. and A.V. Apkarian, *Aging alters regional multichemical profile of the human brain: an in vivo1H-MRS study of young versus middle-aged subjects.* Journal of Neurochemistry, 2001. **76**(2): p. 582-593.
158. Betts, L.R., et al., *Aging reduces center-surround antagonism in visual motion processing.* Neuron, 2005. **45**(3): p. 361-6.
159. Schmolesky, M.T., et al., *Degradation of stimulus selectivity of visual cortical cells in senescent rhesus monkeys.* Nature Neuroscience, 2000. **3**(4): p. 384-390.
160. Bennett, P.J., R. Sekuler, and A.B. Sekuler, *The effects of aging on motion detection and direction identification.* Vision Res, 2007. **47**(6): p. 799-809.
161. Leventhal, A.G., et al., *GABA and its agonists improved visual cortical function in senescent monkeys.* Science, 2003. **300**(5620): p. 812-5.
162. Regan, D., *An Effect of Stimulus Colour on Average Steady-state Potentials evoked in Man.* Nature, 1966. **210**(5040): p. 1056-1057.
163. Tello, R.J.M.G., et al., *Comparison of the influence of stimuli color on Steady-State Visual*

Evoked Potentials. Research on Biomedical Engineering, 2015. **31**: p. 218-231.

164. Roorda, A. and D.R. Williams, *The arrangement of the three cone classes in the living human eye.* Nature, 1999. **397**(6719): p. 520-522.
165. Roorda, A., et al., *Packing arrangement of the three cone classes in primate retina.* Vision Research, 2001. **41**(10): p. 1291-1306.
166. Bieger, J., G.G. Molina, and D. Zhu. *Effects of stimulation properties in steady-state visual evoked potential based brain-computer interfaces*. in *Proceedings of 32nd Annual International Conference of the IEEE Engineering in Medicine and Biology Society*. 2010. Engineering in Medicine and Biology Society.
167. Sloane, M.E., C. Owsley, and S.L. Alvarez, *Aging, senile miosis and spatial contrast sensitivity at low luminance.* Vision Research, 1988. **28**(11): p. 1235-1246.
168. Winn, B., et al., *Factors affecting light-adapted pupil size in normal human subjects.* Investigative ophthalmology & visual science, 1994. **35**: p. 1132-7.
169. Wijk, H., et al., *Color discrimination, color naming and color preferences in 80-year olds.* Aging Clinical and Experimental Research, 1999. **11**(3): p. 176-185.
170. Binnie, C.D., et al., *Colour and photosensitive epilepsy.* Electroencephalography and Clinical Neurophysiology, 1984. **58**(5): p. 387-391.
171. Notbohm, A. and C.S. Herrmann, *Flicker Regularity Is Crucial for Entrainment of Alpha Oscillations.* Frontiers in Human Neuroscience, 2016. **10**(503).
172. Notbohm, A., J. Kurths, and C.S. Herrmann, *Modification of Brain Oscillations via Rhythmic Light Stimulation Provides Evidence for Entrainment but Not for Superposition of Event-Related Responses.* Frontiers in Human Neuroscience, 2016. **10**(10).
173. Andersen, S.K., M.M. Müller, and J. Martinovic, *Bottom-Up Biases in Feature-Selective Attention.* The Journal of Neuroscience, 2012. **32**(47): p. 16953-16958.
174. Mouli, S. and R. Palaniappan. *Eliciting higher SSVEP response from LED visual stimulus with varying luminosity levels*. in *2016 International Conference for Students on Applied Engineering (ICSAE)*. 2016.
175. Jones, M., et al., *Gamma Band Light Stimulation in Human Case Studies: Groundwork for Potential Alzheimer's Disease Treatment.* J Alzheimers Dis, 2019.
176. Christina, J., *Human retinal circuitry and physiology.* Psychology & Neuroscience, 2008. **1**.
177. Wu, J. and Y.C. Okada, *Physiological bases of the synchronized population spikes and slow wave of the magnetic field generated by a guinea-pig longitudinal CA3 slice preparation.* Electroencephalography and Clinical Neurophysiology, 1998. **107**(5): p. 361-373.
178. Murakami, S. and Y. Okada, *Contributions of principal neocortical neurons to magnetoencephalography and electroencephalography signals.* The Journal of physiology, 2006. **575**: p. 925-36.
179. Teipel, S.J., et al., *Regional networks underlying interhemispheric connectivity: an EEG and DTI study in healthy ageing and amnestic mild cognitive impairment.* Human brain mapping,

2009. **30**(7): p. 2098-2119.

180. Sponheim, S.R., et al., *Evidence of disrupted functional connectivity in the brain after combat-related blast injury.* NeuroImage, 2011. **54**: p. S21-S29.
181. Wang, C., et al., *Disrupted Gamma Synchrony after Mild Traumatic Brain Injury and Its Correlation with White Matter Abnormality.* Frontiers in Neurology, 2017. **8**.
182. Cohen, M.X., *Error-related medial frontal theta activity predicts cingulate-related structural connectivity.* NeuroImage, 2011. **55**(3): p. 1373-1383.
183. Steinmann, S., et al., *The role of functional and structural interhemispheric auditory connectivity for language lateralization - A combined EEG and DTI study.* Scientific Reports, 2018. **8**.
184. Scrascia, F., et al., *Relationship among Diffusion Tensor Imaging, EEG Activity, and Cognitive Status in Mild Cognitive Impairment and Alzheimer's Disease Patients.* Journal of Alzheimer's disease : JAD, 2013. **38**.
185. Nunez, P., R. Srinivasan, and R. Fields, *EEG functional connectivity, axon delays and white matter disease.* Clinical neurophysiology : official journal of the International Federation of Clinical Neurophysiology, 2014. **126**.
186. Buzsáki, G., *Rhythms of the brain*. Rhythms of the brain. 2006, New York, NY, US: Oxford University Press. xv, 448-xv, 448.
187. Friston, K. and G. Buzsáki, *The Functional Anatomy of Time: What and When in the Brain.* Trends in Cognitive Sciences, 2016. **20**(7): p. 500-511.
188. Nie, J., et al., *Axonal Fiber Terminations Concentrate on Gyri.* Cerebral Cortex, 2012. **22**(12): p. 2831-2839.
189. Liewald, D., et al., *Distribution of axon diameters in cortical white matter: an electron-microscopic study on three human brains and a macaque.* Biological Cybernetics, 2014. **108**(5): p. 541-557.
190. Sullivan, E.V. and A. Pfefferbaum, *Diffusion tensor imaging and aging.* Neuroscience & Biobehavioral Reviews, 2006. **30**(6): p. 749-761.
191. Kamali, A., et al., *Distinguishing and quantification of the human visual pathways using high-spatial-resolution diffusion tensor tractography.* Magnetic resonance imaging, 2014. **32**(7): p. 796-803.
192. Kammen, A., et al., *Automated retinofugal visual pathway reconstruction with multi-shell HARDI and FOD-based analysis.* Neuroimage, 2016. **125**: p. 767-779.
193. Baldwin, M.K.L., et al., *Cortical and subcortical connections of V1 and V2 in early postnatal macaque monkeys.* The Journal of comparative neurology, 2012. **520**(3): p. 544-569.
194. Kharazia, V.N. and R.J. Weinberg, *Glutamate in thalamic fibers terminating in layer IV of primary sensory cortex.* The Journal of neuroscience : the official journal of the Society for Neuroscience, 1994. **14**(10): p. 6021-6032.
195. Bassi, L., et al., *Probabilistic diffusion tractography of the optic radiations and visual function*

in preterm infants at term equivalent age. Brain, 2008. **131**(2): p. 573-582.

196. Webb, C.E., et al., *Age-related degradation of optic radiation white matter connectivity differentially predicts visual and non-visual executive functions.* bioRxiv, 2020: p. 2020.11.04.368423.
197. Hans, J., M. Lammens, and A. Hori, *Clinical neuroembryology: development and developmental disorders of the human central nervous system*. 2014: Springer.
198. de Gervai, P.D., et al., *Tractography of Meyer's Loop asymmetries.* Epilepsy research, 2014. **108**(5): p. 872-882.
199. Falk, D., et al., *Human cortical asymmetries determined with 3D MR technology.* Journal of Neuroscience Methods, 1991. **39**(2): p. 185-191.
200. Alvarez, I., D.S. Schwarzkopf, and C.A. Clark, *Extrastriate projections in human optic radiation revealed by fMRI-informed tractography.* Brain structure & function, 2015. **220**(5): p. 2519-2532.
201. Kommerell, G., et al., *Ocular prevalence versus ocular dominance.* Vision Research, 2003. **43**(12): p. 1397-1403.
202. Bürgel, U., et al., *Mapping of Histologically Identified Long Fiber Tracts in Human Cerebral Hemispheres to the MRI Volume of a Reference Brain: Position and Spatial Variability of the Optic Radiation.* NeuroImage, 1999. **10**(5): p. 489-499.
203. Hellige, J.B., *Hemispheric asymmetry for visual information processing.* 1999(0065-1400 (Print)).
204. Piazza, E.A. and M.A. Silver, *Relative Spatial Frequency Processing Drives Hemispheric Asymmetry in Conscious Awareness.* Frontiers in Psychology, 2017. **8**.
205. Kitterle, F.L., S. Christman, and J.B. Hellige, *Hemispheric differences are found in the identification, but not the detection, of low versus high spatial frequencies.* Perception & Psychophysics, 1990. **48**(4): p. 297-306.
206. Piazza, E.A. and M.A. Silver, *Persistent hemispheric differences in the perceptual selection of spatial frequencies.* Journal of cognitive neuroscience, 2014. **26**(9): p. 2021-2027.
207. Kalyvas, A., et al., *Mapping the human middle longitudinal fasciculus through a focused anatomo-imaging study: shifting the paradigm of its segmentation and connectivity pattern.* Brain Structure and Function, 2020. **225**(1): p. 85-119.
208. Janelle, F., et al., *Superior Longitudinal Fasciculus: A Review of the Anatomical Descriptions With Functional Correlates.* Frontiers in Neurology, 2022. **13**.
209. Chu, C.J., et al., *EEG functional connectivity is partially predicted by underlying white matter connectivity.* NeuroImage, 2015. **108**: p. 23-33.
210. Sun, Y., et al., *Disrupted Functional Brain Connectivity and Its Association to Structural Connectivity in Amnestic Mild Cognitive Impairment and Alzheimer's Disease.* PLOS ONE, 2014. **9**(5): p. e96505.
211. Blinowska, K.J., et al., *Functional and effective brain connectivity for discrimination between*

Alzheimer's patients and healthy individuals: A study on resting state EEG rhythms. Clinical Neurophysiology, 2017. **128**(4): p. 667-680.

212. Volosyak, I., et al., *BCI demographics II: how many (and what kinds of) people can use a high-frequency SSVEP BCI?* IEEE Transactions on Neural Systems and Rehabilitation Engineering, 2011. **19**: p. 232-239.
213. Butler, P.D. and D.C. Javitt, *Early-stage visual processing deficits in schizophrenia.* Current opinion in psychiatry, 2005. **18**(2): p. 151-157.
214. Gates, G.A., et al., *Central Auditory Dysfunction May Precede the Onset of Clinical Dementia in People with Probable Alzheimer's Disease.* Journal of the American Geriatrics Society, 2002. **50**(3): p. 482-488.
215. Prettyman, R., P. Bitsios, and E. Szabadi, *Altered pupillary size and darkness and light reflexes in Alzheimer's disease.* Journal of neurology, neurosurgery, and psychiatry, 1997. **62**: p. 665-8.
216. Chougule, P.S., et al., *Light-Induced Pupillary Responses in Alzheimer's Disease.* Frontiers in Neurology, 2019. **10**: p. 360.
217. Goldstein, L.E., et al., *Cytosolic β-amyloid deposition and supranuclear cataracts in lenses from people with Alzheimer's disease.* The Lancet, 2003. **361**(9365): p. 1258-1265.
218. Armstrong, R.A., *Alzheimer's Disease and the Eye.* Journal of Optometry, 2009. **2**(3): p. 103-111.
219. Fründ, I., et al., *EEG oscillations in the gamma and alpha range respond differently to spatial frequency.* Vision Research, 2007. **47**(15): p. 2086-2098.
220. Corbett, J.J., *Chapter 9 - The Pupil*, in *Peripheral Neuropathy (Fourth Edition)*, P.J. Dyck and P.K. Thomas, Editors. 2005, W.B. Saunders: Philadelphia. p. 203-215.
221. Pierscionek, B.K. and R.A. Weale, *The optics of the eye-lens and lenticular senescence.* Documenta Ophthalmologica, 1995. **89**(4): p. 321-335.
222. Kehler, L., et al. *The effect of transcranial alternating current stimulation (tACS) on cognitive function in older adults with dementia*. in *2020 42nd Annual International Conference of the IEEE Engineering in Medicine & Biology Society (EMBC)*. 2020.
223. Benussi, A., et al., *Exposure to gamma tACS in Alzheimer's disease: A randomized, double-blind, sham-controlled, crossover, pilot study.* Brain Stimulation, 2021. **14**(3): p. 531-540.
224. Noda, Y., et al., *Photobiological Neuromodulation of Resting-State EEG and Steady-State Visual-Evoked Potentials by 40 Hz Violet Light Optical Stimulation in Healthy Individuals.* Journal of Personalized Medicine, 2021. **11**(6).
225. Agger, M.P., et al., *Novel Invisible Spectral Flicker Induces 40 Hz Neural Entrainment with Similar Spatial Distribution as 40 Hz Stroboscopic Light.* Journal of Alzheimer's Disease, 2022. **88**: p. 335-344.
226. Stauch, B.J., et al., *Human visual gamma for color stimuli.* eLife, 2022. **11**: p. e75897.
227. Zibrandtsen, I.C., M. Agger, and T.W. Kjaer, *Gamma Entrainment in a Large Retrospective*

Cohort: Implications for Photic Stimulation Therapy for Alzheimer's Disease. Journal of Alzheimer's Disease, 2020. **75**: p. 1181-1190.

228. Sharpe, R.L.S., et al., *Gamma entrainment frequency affects mood, memory and cognition: an exploratory pilot study.* Brain Informatics, 2020. **7**(1): p. 17.

국문 초록

서울대학교 대학원

뇌인지과학과

박예승

연구배경 및 목적: 40Hz 점멸광자극 (flickering light stimulation, FLS)을 사용한 감마뇌파동조는 알츠하이머병 (Alzheimer's disease, AD) 모델 쥐에서 병리를 감소시키고 인지 기능을 향상시키는 데 효과적이었지만 알츠하이머병 환자에서는 그 효능에 대해 논란이 있다. 알츠하이머병 환자의 상충되는 결과는 몇 가지 주요 요인에 기인할 수 있다. 첫째, 감마뇌파동조를 위한 FLS의 최적 매개변수는 일주 동물인 인간과 야행성 동물인 쥐 간에 다를 수 있다. 둘째, 최적의 FLS에 대한 반응은 백질 (white matter, WM) 섬유 다발 미세 구조적 무결성의 개인 간 차이로 인해 알츠하이머병 환자 간에 다를 수 있다. 이 연구는 일주 동물인 인간에서 감마뇌파를 동반하기 위한 FLS의 최적 매개변수 (색상, 밝기 및 점멸 주파수)를 찾고 감마뇌파의 동반 및 전파에 대한 백질 섬유 다발의 확산비등방성 (fractional anisotropy, FA)의 영향을 조사하는 것을 목표로 했다.

연구방법: 인지기능이 정상인 젊은 성인 16명과 노인 35명을 대상으로, 시각피질에 감마뇌파동조를 유도하고, 동조 된 시각피질의 감마뇌파를 다른 뇌 영역으로의 전파시킬 수 있는 FLS의 최적 색상 (백색, 적색, 녹색 및 청색), 밝기 (10 cd/m^2, 100 cd/m^2, 400 cd/m^2 및 700 cd/m^2) 및 점멸 주파수 (32-50 Hz)를 사건 관련 비 동기화/사건 관련 동기화 (event-related desynchronization/event-related synchronization, ERD/ERS)와 스펙트럼 그랜저 인과성 (spectral Granger Causality, sGC) 분석을 이용하여 조사했다. 아울러 젊은 성인과 노인에서 FLS의 부작용을 조사했다. 이어서 감마뇌파가 FLS에 의해 시각피질에 적절하게 동조 된 인지기능이 정상인 노인 26명을 대상으로, 시각피질에서 동조 된 감마뇌파의 ERS와

시각피질과 측두 및 전두 영역들 간 연결성인 sGC에 후방시상방사와 중간 및 상부 세로다발들의 확산비등방성이 미치는 영향을 회귀분석과 분산분석을 이용하여 조사했다.

연구결과: 사람에서는 백색 ($p < 0.05$) 및 적색 ($p < 0.01$)과 같은 장파장 FLS가 녹색 및 청색과 같은 단파장 FLS보다 감마뇌파동조를 더 강하게 유발하고, 동조 된 감마뇌파를 더 넓은 뇌 영역으로 전파시켰다. 또 700 cd/m^2 ($p < 0.001$) 및 400 cd/m^2 ($p < 0.01$)와 같은 강한 휘도 FLS는 100 cd/m^2 및 10 cd/m^{2}와 같은 약한 휘도 FLS보다 감마뇌파동조를 더 강하게 유발하고, 동조 된 감마뇌파를 더 넓은 뇌 영역으로 전파시켰다. 34-38 Hz에서 점멸하는 FLS는 젊은 성인에서 감마뇌파를 동반하고 전파하는 데 가장 효과적이었고 (Pz에서 동반: $p < 0.05$, 전파: $p < 0.05$) 32-34 Hz에서 점멸하는 FLS는 노인에게 가장 효과적이었다 (Pz에서 동반: $p < 0.05$, 전파: $p < 0.001$). 노인에서 32-34 Hz에서 점멸하는 700 cd/m^{2}의 백색 FLS는 시각 피질에서 가장 강하게 감마뇌파를 동반하고 ($p < 0.05$) 다른 뇌 영역으로 가장 널리 전파했다 ($p < 0.05$).

32 Hz에서 점멸하는 700 cd/m^{2}의 FLS는 좌후시상방사선의 FA가 낮지 않은 노인보다 낮은 노인에서 감마뇌파가 시각피질에 덜 동반된다 ($p < 0.05$). 또한, 시각피질에서 측두엽 및 전두엽 영역으로의 감마뇌파 sGC는 중간 및 상부 세로 다발의 FA와 유의하게 연관되었다 ($p < 0.05$). 젊은 성인은 더 짧은 파장과 더 약한 강도를 가진 FLS에 비하여 더 긴 파장 (백색과 적색)과 더 강한 휘도 (700 cd/m^2)의 FLS에 더 많은 부작용을 보였다 (파장 $p < 0.05$ 및 휘도 $p < 0.01$). 그러나 노인은 700 cd/m^{2}에서 400 cd/m^2 사이, 백색과 적색 FLS 사이에서 유사한 수준의 부작용을 보였고 ($p > 0.05$), 부작용의 심각성은 젊은 성인보다 경미했다.

결론: 주행성인 인간에서 감마 동조를 위한 최적의 점멸 주파수는 야행성 쥐보다 약 20% 낮았다. 더 강한 휘도와 더 긴 파장의 FLS가 감마뇌파를 더 잘 동조 시킬 수 있지만 더

크고 심각한 부작용을 초래할 수 있다. 노인의 경우 32-34 Hz에서 점멸하는 700 cd/m^2의 백색 또는 적색 FLS가 감마뇌파를 동조하고 전파하는 데 최적일 수 있다. 감마뇌파는 백질 섬유 다발의 미세 구조적 무결성이 손상된 노인에서는 최적의 FLS에 의해 적절하게 동조 되지 않았기 때문에, 감마뇌파의 동조 및 전파와 관련된 백질 영역의 무결성은 시각적 자극을 사용하여 감마뇌파동조 적용을 결정할 때 측정되고 고려되어야 한다.

주요어: 감마뇌파, 동조, 전파, 점멸광자극, 백질 미세 구조 무결성, 인간, 노인

학번: 2017-26326